



Wissenschaftszentrum Weihenstephan für Ernährung,
Landnutzung und Umwelt

Lehrstuhl für Ernährungsphysiologie

Effects of diet-induced obesity on intestinal barrier integrity and enteroendocrine secretion

Veronika Maria Müller

Vollständiger Abdruck der von der Fakultät Wissenschaftszentrum Weihenstephan für Ernährung, Landnutzung und Umwelt der Technischen Universität München zur Erlangung des akademischen Grades eines

Doktors der Naturwissenschaften

genehmigten Dissertation.

Vorsitzender:

Univ.-Prof. Dr. Dirk Haller

Prüfer der Dissertation:

1. Univ.-Prof. Dr. Hannelore Daniel

2. Univ.-Prof. Dr. Martin Klingenspor

Die Dissertation wurde am 30.09.2015 bei der Technischen Universität München eingereicht und ist durch die Fakultät Wissenschaftszentrum Weihenstephan für Ernährung, Landnutzung und Umwelt am 08.02.2016 angenommen.

Eine Arbeit wie diese kann nie ohne die Hilfe und Unterstützung von weiteren Personen gelingen und daher gilt mein besonderer DANK:

Frau Prof. Dr. Daniel, die am Schülertag 2004 der TU München mein Interesse und meine Leidenschaft für die Ernährungswissenschaft weckte. Vielen Dank, dass Sie mir dieses spannende Thema überließen und Ihr Vertrauen in mich setzten. Darüber hinaus möchte ich mich für Ihre Betreuung und Unterstützung in Form von fachlichen Diskussionen, Ratschlägen und Anregungen bedanken.

Herrn Prof. Dr. Klingenspor für die Erstellung des Gutachtens und Herrn Prof. Dr. Haller für die Übernahme des Prüfungsvorsitzes.

Tamara für die Betreuung. Danke für deinen Einsatz und deine motivierenden Worte.

Herrn Kottra und Mena, die mich in die Elektrophysiologie einführten.

Helene für unzählige Puffer, aufgespannte Gewebe und Gummibärchen. Herzlichen Dank.

Alex, Beate, Irmgard, Jarlei, Julia, Kerstin, Kurt, Margot, Marina und Sebastian für die gute Zusammenarbeit und tatkräftige Unterstützung im Labor.

Juli, Pia und Katrin, die immer eine offene Tür für mich in ihrem Würfel hatten und Ronny, Manu und Rosalie für die gute Bürogesellschaft.

Brigitte und Cordula für die uneingeschränkte Hilfsbereitschaft. Herzlichen Dank.

ALLEN Mitgliedern des Lehrstuhls für eine schöne Zeit am Institut.

Caro, Valentina und Lisa für die freundschaftliche Zusammenarbeit im BMBF Projekt.

Silvia für die Freundschaft und die unzähligen Gespräche und Diskussionen.

Franz für die Liebe, die Geduld, die Unterstützung und die vielen gefahrenen Kilometer.

Ein besonderer Dank gilt meinen Eltern. Danke für euren Glauben an mich und Unterstützung, ohne die diese Arbeit niemals möglich gewesen wäre. DANKE für ALLES.

Table of content

Summary	1
Zusammenfassung	2
1 Introduction.....	4
1.1 Intestinal barrier.....	4
1.2 Intestinal sensing and gut hormone secretion	9
1.3 Gut microbiota	12
1.4 Bile acids	13
1.5 Metabolic endotoxemia.....	18
1.6 Aim of the project.....	19
2 Materials and Methods	20
2.1 Materials.....	20
2.1.1 Equipment and software applications	20
2.1.2 Chemicals, media and consumables	21
2.1.3 Buffers and solutions	23
2.1.4 Kits, antibodies and primers.....	26
2.2 Methods.....	28
2.2.1 Mice, husbandry and diets	28
2.2.2 Electrophysiological measurements.....	31
2.2.3 Molecular biological methods.....	34
2.2.4 Histology	38
2.2.5 Immunohistochemistry	40
2.2.6 LC-MS/MS measurements.....	41
2.2.7 High-throughput 16S ribosomal RNA gene sequencing (carried out by Dr. Thomas Clavel, TUM).....	42
2.2.8 Plasma analysis	43
2.2.9 Primary colonic cell cultures.....	44

CONTENT

2.2.10	Statistical analysis	46
3	Results	47
3.1	Gut barrier integrity	47
3.1.1	Impact of different high-fat diets on gut barrier integrity in mice.....	47
3.1.1.1	Plant-based high-fat diets.....	47
3.1.1.2	Animal-based high-fat diets.....	51
3.1.2	Impairments in mice fed the beef tallow-based high-fat diet	55
3.1.2.1	Inflammation markers in adipose tissue and liver.....	55
3.1.2.2	Body mass and intestinal morphology	57
3.1.2.3	Tight junction and scaffold proteins	59
3.1.2.4	Gut microbiota.....	62
3.1.2.5	Bile acids in cecal content	64
3.2	Intestinal sensing and hormone secretion	67
3.2.1	Effect of high-fat diet feeding on hormone secretion in vivo.....	68
3.2.2	Effect of high-fat diet treatment on bile acid metabolism.....	70
3.2.3	Microbial products of metabolism can induce GLP-1 secretion in vitro .	75
3.2.3.1	Bile acid-mediated GLP-1 secretion	76
3.2.3.2	Short-chain fatty acids-mediated GLP-1 secretion	79
4	Discussion	80
4.1	Gut barrier integrity depends on housing conditions.....	80
4.1.1	Determinants of gut barrier impairment.....	80
4.1.2	Intestinal microbial colonization and intestinal barrier function.....	81
4.2	GLP-1 secretion can be affected by microbial products	86
4.2.1	Bile acid homeostasis is slightly altered by feeding a high-fat diet.....	86
4.2.2	Incretin hormone secretion is altered in high-fat diet condition	87
4.2.3	GLP-1 secretion upon stimulation by bile acid- and short-chain fatty acid is enhanced in primary colonic cell cultures from animals fed a high-fat diet	88
5	Conclusions.....	92

6	Appendix	94
6.1	Figures and tables.....	94
6.2	List of abbreviations.....	97
6.3	References	99
6.4	List of publications.....	114

Summary

Obesity is a worldwide escalating problem promoted by changes in the lifestyle with lack of physical activity and high-calorie diets rich in fat. Being obese is a major risk factor for the development of metabolic disorders such as type 2 diabetes mellitus. Recent studies have suggested that the consumption of such high-fat diets may cause changes in intestinal permeability resulting in a metabolic endotoxemia and low-grade inflammation. Moreover, high-fat diets influence the intestinal microbiota composition. Products of metabolism by host and microbiota such as bile acids or short-chain fatty acids are potent stimulants for the secretion of the gastrointestinal hormones like GLP-1 and GLP-2 from enteroendocrine cells. The intestinal barrier and glucose homeostasis are in turn modulated by GLP-1/2. The aim of the present study was to elucidate the impact of feeding a high-fat diet in mice on gut barrier integrity and on gastrointestinal endocrine secretion.

Taking advantage of AKR/J, C57BL/6 and SWR/J mice, the influence of diet induced-obesity, dietary fat content and source, duration of the feeding period as well as hygienic status of the animal facility on gut barrier integrity was investigated. Intestinal barrier function in small and large intestine was evaluated in Ussing chambers by electrical resistance and permeability measurements. As the most striking finding, we demonstrate that the housing conditions and associated changes in gut bacterial colonization are pivotal for the maintenance of gut barrier integrity in diet-induced obese mice. This result may also explain the discrepancies in outcomes of high-fat feeding trials seen in different laboratories.

Secretion of the GLP-1/2 upon bile acid and short-chain fatty acid stimulation was assessed in primary colonic cell cultures derived from mice that were fed different diets. GLP-1 release in response to the secondary bile acid deoxycholic acid and the short-chain fatty acid propionate was increased in primary colonic cell cultures prepared from diet-induced obese mice.

In summary, studies described here provide a comprehensive analysis of parameters influencing gut barrier integrity and enteroendocrine secretion in response to a high-fat diet in mice and pull microbial colonization, intestinal hormone secretion and gut barrier integrity together.

Zusammenfassung

Übergewicht ist ein Problem, das weltweit auftritt und Veränderungen der Lebensgewohnheiten hinzu geringerer körperlicher Aktivität und hochkalorischer Ernährung widerspiegelt. Übergewicht ist dabei ein Hauptrisikofaktor für die Entwicklung von metabolischen Erkrankungen wie Typ 2 Diabetes mellitus. Tierexperimentelle Befunde haben einen Zusammenhang zwischen einer hochkalorischen und fettreichen Ernährungsweise und einer Erhöhung der intestinalen Permeabilität aufgezeigt. Dies hat die Darmbarriere in den Fokus gerückt. Als Folge einer erhöhten intestinalen Permeabilität gilt beispielsweise die metabolische Endotoxämie, die mit einem niedrig-gradigen Entzündungsstatus einhergeht. Zusätzlich beeinflusst eine hochkalorische und fettreiche Ernährungsweise die Zusammensetzung der intestinalen Mikrobiota. Stoffwechselprodukte des Wirts und der Mikrobiota, wie z.B. Gallensäuren oder kurzkettige Fettsäuren, sind wirkungsvolle Stimulantien für die Ausschüttung der gastrointestinalen Hormone GLP-1 und GLP-2 aus enteroendokrinen Zellen. Während GLP-1 an Regulation der Glukosehomöostase beteiligt ist, beeinflusst GLP-2 u.a. die intestinale Barrierefunktion. Das Ziel der vorliegenden Studien war es, den Einfluss fettreicher Ernährung auf die Darmbarriere und die gastrointestinale endokrine Sekretion im Mausmodell zu untersuchen.

An AKR/J, C57BL/6 und SWR/J Mäusen wurde der Einfluss der Fettmenge und -quelle, der Fütterungsdauer, der Suszeptibilität für Übergewicht und der Hygienestatus der Tierstallung auf die Darmbarriere untersucht. Die Barrierefunktion des Dün- und Dickdarms wurde anhand des transepithelialen Widerstands und der Permeabilität von Markern in Ussing-Kammern beurteilt. Als wichtigster Befund der experimentellen Studien kann gelten, dass die Aufrechterhaltung einer intakten Darmbarriere in ernährungsbedingt übergewichtigen Mäusen abhängig ist vom Hygienestatus der Tierstallung und somit von der intestinalen mikrobiellen Besiedlung. Dieser Befund erklärt möglicherweise auch die extrem widersprüchlichen Ergebnisse zum Einfluss von Diäten und Übergewicht auf die intestinale Barrierefunktion.

Darüber hinaus wurde die Sekretion von GLP-1/2 an intestinalen Primärkulturen untersucht. Interessanterweise war die, durch die sekundäre Gallensäure Deoxycholsäure und die kurzkettige Fettsäure Propionat ausgelöste Ausschüttung

von GLP-1 in Primärkulturen, die aus ernährungsbedingt übergewichtigen Mäusen generiert wurden, erhöht.

Die vorliegende Studie ist die Erste, die eine systematische und umfassende Analyse von alimentären Faktoren auf die Darmbarriere und Sekretionsleistung in ernährungsbedingt übergewichtigen Mäusen vornahm und die einen Zusammenhang zwischen der mikrobiellen Besiedlung, der intestinalen Hormonsekretion und der Aufrechterhaltung der Darmbarriere bei fettreicher Ernährung aufzeigt.

1 Introduction

During the last decades overweight and obesity became a global problem. According to the World Health Organization, between 1980 and 2014 the prevalence of obesity reduplicated worldwide with 1.9 billion adults being overweight – and around 600 million classified as obese in 2014 [1]. Changes in lifestyle with lack of physical activity and a diet rich in energy and high in fat are the main factors underlying this development.

In 2007, Cani *et al.* reported a change in microbiota composition after four weeks of high-fat diet (HFD) intervention associated with an increased intestinal permeability in a mouse feeding study [2]. This impairment of the gut barrier was proposed to cause a metabolic endotoxemia and low-grade inflammation as promoting factors for cardiovascular diseases and type 2 diabetes mellitus [3]. In the present study we tested by using different mouse strains and diets of different fat quantity and quality whether these findings can be reproduced and to which extent they depend on the feeding regimens.

1.1 Intestinal barrier

In the small intestine nutrients derived from the digestion of food are absorbed, whereas in the large intestine mainly electrolytes and water are absorbed. To facilitate nutrient digestion and absorption the surface area of the small intestine is enlarged by protrusions such as circular folds, villi and microvilli. Between the villi so-called crypts of Lieberkühn are found containing the intestinal stem cells essential for the renewal of the epithelium. The surface area of the large intestine is far less enlarged and villus structures are lacking. The intestinal lineage consists of multiple cell types such as absorptive enterocytes, mucus-producing goblet cells, hormone-secreting enteroendocrine cells, paneth cells, tuft cells and microfold cells [4].

The intestinal barrier is a semi-permeable barrier allowing the vectorial transport of nutrients, electrolytes and water but preventing the permeation of antigens or microorganisms from the luminal environment into circulation [5]. There are two main routes for passage through the intestinal barrier: the transcellular and the paracellular pathway. The transcellular route passes through the cells either by active transport or transcytosis. In contrast, the paracellular route takes course between adjacent cells and is regulated by junctional complexes [6]. The intestinal barrier is subdivided into

three layers: The intestinal mucus layer, the underlying intestinal epithelium and the immune system (Figure 1).

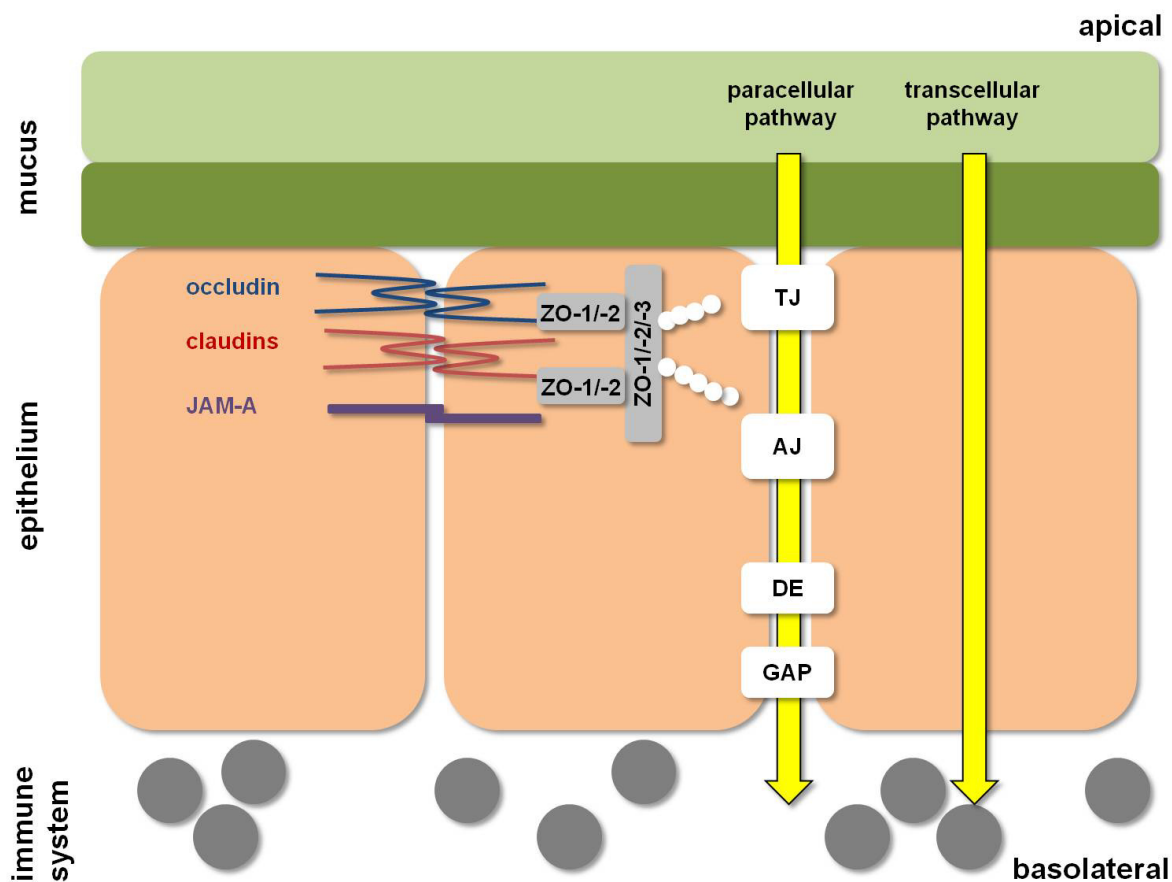


Figure 1: The intestinal barrier consists of three layers of defense. The first defense line is the mucus layer. The second layer is the intestinal epithelium. Neighboring epithelial cells are connected at the lateral side by intercellular junctional protein complexes consisting of tight junctions (TJ), adherens junctions (AJ), desmosomes (DE) and gap junctions (GAP). Tight junction proteins such as occludin, claudins or junctional adhesion molecule A (JAM-A) are linked to the cytoskeleton *via* zonula occludens (ZO) proteins. The third layer of defense is formed by the mucosal immune response. Figure modified from [7].

Intestinal mucus layer

In the gastrointestinal tract, the mucus forms the first defense line protecting the epithelium of the host from microbiota present in the intestinal lumen [8, 9]. Mucus consists of mucins characterized by at least one O-glycosylated PTS domain rich in the amino acids proline, threonine and serine [10]. There are two types of mucins: the gel-forming and the transmembrane mucins. Gel-forming mucins are large polymers (>100 MDa) secreted by goblet cells. In the intestine, MUC2 is the most abundant gel-forming mucin. MUC3, MUC12 and MUC17 are intestinal transmembrane mucins comprising a cytoplasmic tail and an extracellular mucin domain (1-10 MDa). The transmembrane mucins form the so-called glycocalyx covering the apical surface of

the enterocytes [10]. The intestinal mucus composition varies between small and large intestine [11]. The mucus in the small intestine is not attached to the epithelium and is penetrable to bacteria. However, several mechanisms such as movement of the mucus *via* peristaltic waves, continuous mucus production by goblet cells and secretion of antimicrobial compounds from paneth cells prevent the penetration of bacteria into the epithelium of the small intestine [8, 9]. The mucus of the large intestine is two-layered. The outer layer is loose and colonized by bacteria, whereas the inner layer is attached to the epithelium and is free of bacteria. In colonic tissue of mice lacking the *Muc2* gene, bacteria reach the epithelial surface. Beyond that, *Muc2*-deficient mice suffer from colitis at the age of seven weeks [12]. Thus, mucins are important to maintain the intestinal homeostasis and gut barrier integrity.

Tight junctions as regulators of the epithelium

Neighboring epithelial cells are connected at the lateral side by intercellular junctional complexes consisting of tight junctions, adherens junctions, desmosomes and gap junctions [7]. Tight junctions have two functions, a fence and a gate function [13]. The fence function of the tight junctions is achieved by dividing the membrane into an apical and a basolateral zone, whereas their gate function is important for the transepithelial barrier, namely the permeability *via* the paracellular pathway [14].

Tight junction proteins are transmembrane proteins and their classification was revised in 2010 [15, 16]. Since then the four-transmembrane domain proteins are grouped into tight junction-associated MARVEL proteins (TAMPs) and in claudins. Aside of these two families, the junctional adhesion molecule (JAM) family should be considered as well. The classical members of the JAM family are JAM-A, JAM-B and JAM-C, but only JAM-A is involved in the tight junction formation [17]. Mice lacking JAM-A display a normal epithelial architecture, but the mucosal permeability is increased [18]. The TAMPs family comprises the tight junction proteins occludin [19], tricellulin [20] and marveld3 [21]. In 1993, the first member of the TAMPs family, the 60 kDa protein occludin was discovered. A few years later a mouse lacking the occludin gene was generated. Interestingly, this knockout mouse had a normal gut barrier function [22]. The reason for a lack of an effect remains unexplained, but the loss of occludin might be compensated by the two other family members [21]. Regarding the tight junction family of claudins, in mammals 24 members are reported with molecular weights ranging from 20 to 27 kDa. Most of the claudins were either

shown to tighten the epithelium or to form paracellular channels. In the murine intestine the barrier builders claudin-1, -3, -4, -5 and -8 are found [23]. A high expression of these claudins results in a decreased paracellular permeability, whereas a high expression of the pore-forming claudin-2 increases paracellular permeability [14]. In patients suffering from Crohn`s disease pore-forming claudin-2 is up-regulated [24, 25]. Additionally, the barrier-tightening claudin-5 or -8 are down-regulated and redistributed [24].

Tight junction proteins are linked to the cytoskeleton *via* zonula occludens (ZO) proteins. ZO-1, ZO-2 and ZO-3 belong to these scaffold proteins and are important for the structural organization of the intercellular junctional complex and/or involved in signal transduction pathways [26]. In the past tight junctions were considered to be a static, but now there is evidence that their assembly and disassembly is dynamic and respond to physiological or pathophysiological stimuli [27]. Several signaling pathways *via* enzymes such as protein kinase C, mitogen-activated protein kinases, myosin light chain kinase and Rho GTPases are involved. Tight junction structure and function is modified by protein phosphorylation or rearrangements resulting in changes of barrier function [7].

Mucosal immune responses

As soon as microbes penetrate through the mucus and the intestinal epithelial cell layer, a mucosal immune response is provoked. The mucosa-associated lymphoid tissue in the intestine, also referred to as gut-associated lymphoid tissue (GALT), comprises organized lymphoid tissues such as Payer`s patches or single lymphoid cells and lymphoid cells distributed throughout the epithelium or the lamina propria [28]. The lamina propria is based underneath the epithelium and as soon as bacteria infiltrate, they are recognized and attacked by macrophages. On the surface of macrophages specific receptors are expressed such as toll-like receptors (TLR) and nucleotide binding oligomerization domain (NOD) proteins which are activated by bacterial cell wall constituents, in particular lipopolysaccharide (LPS) or proteoglycans [29, 30]. In the response, the transcription of nuclear factor- κ B initiates the expression of pro-inflammatory cytokines including interleukine-1 β (IL-1 β), interleukine-6 (IL-6), interleukine-12 (IL-12) or tumor necrosis factor (TNF) [31]. Moreover, the GALT is involved in the formation and secretion of secretory immunoglobulin A (SIgA) into the intestinal lumen. SIgA anticipates pro-inflammatory

responses and maintains the epithelial barrier by coating commensal bacteria and by forming complexes with commensal or pathogenic bacteria [32].

Assessment of gut barrier integrity

There are numerous *in* and *ex vivo* approaches to determine gut barrier integrity. Amongst others, urinary excretion assays of marker compounds, bacteria-related tests, histological and electrophysiological approaches are common [33].

For assessment *in vivo* most commonly the urinary excretion of orally administered molecular probes is determined (Table 1). These probes should be water-soluble, nontoxic, nonmetabolizable and not naturally present in the urine but easily detectable [34]. Sucrose in the urine is considered to reflect the permeability of the stomach, lactulose and mannitol may mark the permeability of the small intestine and sucralose may provide a permeability measure of the large intestine. ^{51}Cr -EDTA or a mixture of polyethylene glycols ranging in mass from 400 to 4000 Da are frequently used as permeability markers for all intestinal regions [33]. Bacterial-related assays include measurement of LPS or circulating endotoxin core antibodies. Useful histological approaches are the determination of the expression and distribution of tight junction proteins or of bacteria in the inner mucus layer.

Table 1: Commonly used probes for assessment of intestinal barrier integrity. Modified from [35].

	Probe
<i>Lower molecular weight (Molecular weight <200Da)</i>	
Monosaccharides	L-rhamnose, L-arabinose
Sugar alcohols	D-mannitol
<i>Higher molecular weight (Molecular weight >300Da)</i>	
Oligosaccharides	lactose, lactulose, sucrose, sucralose, raffinose, cellobiose
Ethylene glycol polymers	PEG-400, PEG-1500, PEG-3000
Non-degraded radiolabeled chelates	^{51}Cr -EDTA, $^{99\text{m}}\text{Tc}$ -DTPA
Contrast media	iohexol, iodixanol

Gut barrier integrity *ex vivo* is mainly studied using Ussing chambers (2.2.2) which allow measurements of the transepithelial resistance and the permeability of the intestine under controlled conditions. Intestinal tissue explants are mounted as flat sheets into a chamber enabling separation of the luminal from the serosal side. Intestinal permeability is determined by diffusion of fluorescent probes e.g. fluorescein (0.38 kDa), fluorescein isothiocyanate–dextran (FITC-dextran, 4-20 kDa) or horseradish peroxidase (44 kDa) from the luminal to the serosal side. Additionally, electrodes measure the spontaneous transepithelial potential and defined current

pulses are supplied to the tissue. According to the Ohm's law, transepithelial resistance as a marker of intestinal integrity can be calculated.

1.2 Intestinal sensing and gut hormone secretion

The nutrient composition of an ingested meal is sensed in specialized enteroendocrine cells (EECs) throughout the intestine and as a result different peptide hormones regulating for example gastrointestinal motility, glucose homeostasis, energy expenditure, appetite and satiety are secreted [36].

EECs represent less than 1% of all enterocytes and are found throughout the intestine with characteristic distributions. Most of the EECs have a conical shape and an open type structure with a small apical surface reaching the gut lumen [37]. On this surface sensory transporters and receptors are located (Table 2). They are activated by luminal nutrient or non-nutrient stimuli and consequently gut hormones are released into circulation. For instance, the uptake of glucose by sodium-dependent glucose transporter 1 (SGLT1) and of di- or tripeptides by proton-coupled peptide transporter 1 (PEPT1) elicit the release of peptide hormones [38-41], whereas certain G protein-coupled receptors (GPCR) are activated by long-/medium-chain fatty acids, fiber-derived short-chain fatty acids, or bile acids [42-49]

Table 2: Intestinal sensor proteins for nutrient and non-nutrient stimuli.

Stimuli	Activator	Sensor	Reference
<i>Nutrient</i>			
Carbohydrates	glucose	SGLT1	[38-40]
Proteins	di-/tripeptides	PEPT1	[41]
Lipids	long-chain fatty acids	GPR40, GPR119, GPR120	[42-44]
<i>Non-nutrient</i>			
Fibers	short-chain fatty acids	FFAR2, FFAR3	[45-47]
Bile acids	bile acids	TGR5	[48, 49]

Once released into circulation, gut hormones act in different ways: (1) endocrine signaling after release into the circulation by targeting the hormone receptors in different tissues, (2) paracrine signaling to neighboring EECs and enterocytes or (3) activation of neuronal afferents [36]. Traditionally, EECs were considered as distinct cell subtypes assigned to certain hormones such as I cells secreting cholecystokinin (CCK), K cells secreting glucose-dependent insulinotropic peptide (GIP) and L cells secreting glucagon-like peptide-1 (GLP-1), glucagon-like peptide-2 (GLP-2) and peptide YY (PYY) [50]. Recently, this classification according to cell

subtype was revised and unique expression patterns of gut hormones depending on the location within the gastrointestinal tract were described. GIP is expressed primarily in the duodenum, CCK in duodenum and jejunum and PYY in the distal ileum and colon. GLP-1 expression increases from jejunum to colon [51-53]. GIP and GLP-1 are so-called incretins acting on pancreatic β cells mediating the incretin effect. It describes the observation that oral glucose administration elicits a substantial greater insulin response compared to the same amount of glucose applied intravenously [54, 55]. Both, GIP and GLP-1 are inactivated by dipeptidyl peptidase 4 (DPP4).

Bile acid-induced TGR5 signaling and metabolic consequences

In the beginning of the 21st century two independent groups identified the $G\alpha_s$ protein-coupled receptor TGR5 also called G protein-coupled bile acid receptor 1 (GP-BAR1) or membrane-type receptor for bile acids (M-BAR) [56, 57]. TGR5 consists of 333 amino acids forming seven transmembrane domains, three extracellular loops and three intracellular loops [58]. The receptor is activated dose-dependently by bile acids and their glyco- or tauro-conjugates. The most potent agonists are lithocholic acid and deoxycholic acid followed by chenodeoxycholic acid and cholic acid [56, 57]. Binding of bile acids to TGR5 activates cyclic adenosine monophosphate (cAMP) formation *via* adenylyl cyclase. Exocytosis of hormone-containing vesicles from enteroendocrine L cells is activated by Epac and phospholipase C- ϵ inducing an intracellular Ca^{2+} increase [59]. TGR5 expression is widely scattered throughout different organs of the body varying in the magnitude of expression [60]. In the intestine, TGR5 is mainly located in the ileum and colon [61]. In addition, the receptor is expressed in the enteric nervous system [62], gall bladder [63], spleen [61], monocytes [57], brown and white adipose tissue and skeletal muscle [61]. Depending on the organ, activation of TGR5 is involved in anti-inflammatory effects, intestinal motility and secretion, energy and whole body glucose homeostasis [60]. In brown adipose tissue the induction of the TGR5/cAMP pathway increases energy expenditure by activation of type 2 iodothyronine deiodinase converting the inactive thyroxine to active 3,5,3'-triiodothyronine. A supplementation of 0.5% cholic acid to a HFD prevented C57BL/6J mice from diet-induced obesity (DIO) by increasing energy expenditure [64, 65]. Moreover, activation of TGR5 reduces the production of pro-inflammatory cytokines such as IL-1, IL-6 and TNF in monocytes [66]. Further evidence for a down-regulation of the immune response by

TGR5 is based on the observation that LPS-induced stimulation of macrophages isolated from TGR5^{-/-} mice provoke a higher TNF expression compared to macrophages derived from TGR5^{+/+} mice [67]. In addition, there is evidence that TGR5 is involved in systemic glucose homeostasis since TGR5 is expressed in pancreatic β cells and bile acid-induced stimulation of β cells leads to insulin secretion [68]. In EECs, however, the activation of TGR5 by bile acids induces the release of the incretin hormone GLP-1 which in turn amplifies insulin output [48, 49].

Model systems for the investigation of GLP-1 secretion

Different model systems are used to investigate the underlying mechanisms linking intestinal sensing to GLP-1 secretion from EEC. Most often used to study GLP-1 secretion *in vitro* are immortalized cell lines derived from tumor cells such as GLUTag, STC-1 or NCI-H716 cells [69-71]. These cell lines consist of one single cell type and differ in the responsiveness to nutrient and non-nutrient stimuli. In 2008, Reimann *et al.* reported the generation of mixed primary intestinal cultures from adult mouse intestine releasing GLP-1 upon nutrient and non-nutrient stimuli [41, 49, 72]. These primary intestinal cultures conserve the interplay of different cell types and enable investigation of GLP-1 output depending on the genetic background, but they are inappropriate for long-term cultivation. The most promising but high-priced model systems are three-dimensional intestinal crypt cultures also called intestinal organoids or mini-guts [73, 74]. They derive from individual Lgr5⁺ crypt base columnar cells and provide long-term cultures from adult tissues [74]. Recently it was shown, that these organoids possess GLP-1 producing L cells [75] and can thus be used to study L cell development and GLP-1 secretion in response to nutrients or pharmaceuticals [76].

1.3 Gut microbiota

The term gut microbiota includes the entity of bacteria, archaea, viruses, fungi and protozoa in the gastrointestinal tract. The gut microbiota is dominated by anaerobic bacteria; the most abundant phyla are *Firmicutes* and *Bacteroidetes* [77]. Within the gastrointestinal tract the microbial density and diversity increases from the stomach over small to large intestine. Humans harbor 10^7 cells per gram content in the stomach, 10^7 cells per gram content in the ileum and up to 10^{12} cells per gram content in the colon [78]. The composition of the microbiota is influenced by the host's diet, lifestyle, hygiene or by antibiotics and other drugs [77].

Gut microbiota and obesity

In an obese state, the composition, diversity and function of the gut microbiome is altered. Obese humans harbor more *Firmicutes* and fewer *Bacteroidetes* compared to lean individuals [79]. A genetically obese animal model is the ob/ob mouse carrying a mutation in the gene encoding the hormone leptin. On a standard control diet, homozygous ob/ob mice exhibit increased levels of *Firmicutes* and decreased levels of *Bacteroidetes* compared to their lean littermates [80]. The same changes in *Firmicutes* and *Bacteroidetes* are observed in mice fed a HFD [81-83]. Moreover, in DIO mice the gut bacterial diversity is decreased [81, 84]. Apart from the microbiota composition and diversity, the role of the microbiota in energy homeostasis needs to be considered in the context of obesity. Transplantation of microbiota from ob/ob or lean mice into germ-free wild-type mice results in an increased body fat content in animals receiving the ob/ob microbiota [85]. This finding suggests an increased energy harvest capacity in an obesity-associated gut microbiome. Moreover, the absence of microbes in the intestine is discussed to be protective against DIO [86], although the data are ambiguous [83].

Microbial impact on host physiology and metabolism

The gut microbiota influences numerous physiological parameters of the host including bone-mass density [87], fat-storage [88], intestinal angiogenesis [89] and development of the immune system [90]. In addition, the microbiota affects host metabolism through diet-dependent mechanisms [91]. For example, the microbiota ferments polysaccharides and transforms cholesterol-derived primary bile acids into secondary bile acids (for detail see 1.4). The fermentation of non-digestible carbohydrates provides short-chain fatty acids such as acetate, propionate and

butyrate and allows microbial growth. Butyrate is an energy substrate for the colonic epithelium, whereas acetate and propionate are substrates for hepatic lipogenesis and gluconeogenesis. Additionally, short-chain fatty acids regulate colonic gene expression and glucose homeostasis through the G-protein-coupled receptors FFAR2 and FFAR3 (see also 1.2) [91]. Moreover, components of the bacterial cell wall activate pro-inflammatory signaling cascades (for detail see 1.5).

1.4 Bile acids

Biosynthesis

There is a variety of naturally occurring bile acids in mammals and other vertebrate species [92]. Bile acids are amphipathic molecules, synthesized from cholesterol in the liver. For the synthesis at least 17 enzymes are required and the firsthand products of this four-stage process are termed primary bile acids. In brief, the synthesis is initiated by 7 α -hydroxylation of cholesterol, followed by further modifications of the ring structure, side-chain shortening and finally the conjugation to an amino acid such as glycine and taurine [93]. In mice, 75% of the bile acids are formed *via* this pathway and the remaining 25% *via* the acidic pathway [94]. The first and rate-limiting step of the classic pathway is the hydroxylation of cholesterol at the C₇ position by the cholesterol 7 α -hydroxylase (CYP7A1) in the endoplasmic reticulum of hepatocytes. In contrast, the acidic pathway is initiated by the hydroxylation of the cholesterol side-chain through the mitochondrial sterol 27-hydroxylase (CYP27A1) followed by the hydroxylation of the C₇ position by the oxysterol 7 α -hydroxylase (CYP7B1) in the endoplasmic reticulum of the hepatocytes [93]. These pathways deliver the primary bile acids cholic acid (CA) and chenodeoxycholic acid (CDCA) as shown in Figure 2. In rodents, at minimum two additional primary bile acids occur, α -muricholic acid (α MCA) and β -muricholic acid (β MCA) [95]. For higher hydrophilicity, primary bile acids are conjugated to either glycine or taurine. Together with cholesterol, phospholipids, fatty acids and bilirubin, these conjugated bile acids are part of the bile, which is concentrated and stored in the gall bladder. Upon dietary intake contraction of the gall bladder is elicited by CCK and the bile is discharged into the proximal small intestine [96].

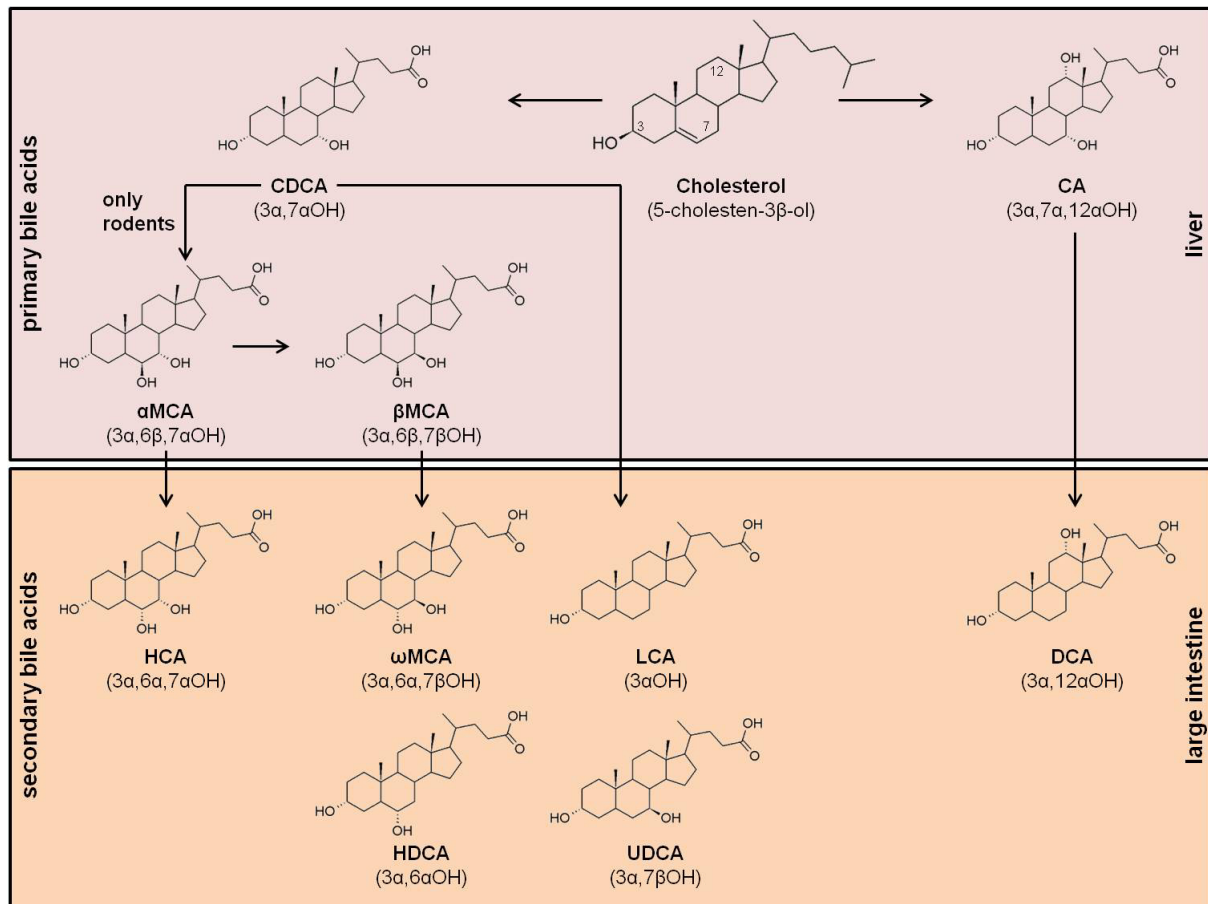


Figure 2: Overview of primary and secondary bile acids. The primary bile acids (CA, 3 α ,7 α ,12 α trihydroxy-5 β -cholanoic acid) and chenodeoxycholic acid (CDCA, 3 α ,7 α -dihydroxy-5 β -cholanoic acid) are synthesized from cholesterol in the liver. In rodents at least two additional bile acids, α -muricholic acid (α MCA, 3 α ,6 β ,7 α -trihydroxy-5 β -cholanoic acid) and β -muricholic acid (β MCA, 3 α ,6 β ,7 β -trihydroxy-5 β -cholanoic acid), are formed. Primary bile acids are transformed by microbiota to secondary bile acids such as deoxycholic acid (DCA, 3 α ,12 α -dihydroxy-5 β -cholanoic acid), lithocholic acid (LCA, 3 α -hydroxy-5 β -cholanoic acid), ursodeoxycholic acid (UDCA, 3 α ,7 β -dihydroxy-5 β -cholanoic acid), hyocholic acid (HCA, 3 α ,6 α ,7 α -trihydroxy-5 β -cholanoic acid) and hyodeoxycholic acid (HDCA, 3 α ,6 α -dihydroxy-5 β -cholanoic acid). Figure modified from [95, 97].

Enterohepatic circulation

In the terminal ileum bile acids are actively absorbed by the ileal bile acid transporter (IBAT). Inside the enterocyte bile acids are bound to the ileal bile acid binding protein (IBABP) which shuttles them to the basolateral membrane. They exit the cell *via* the heterodimeric organic solute transporter OST α / β and return *via* the portal system to the liver. Hepatocytes take up unconjugated or sulphated bile acids by members of the organic anion transporting polypeptide (OATP) family, whereas conjugated bile acids are taken up by the sodium-taurocholate cotransporting polypeptide (NTCP) [98]. In the hepatocyte bile acids are again conjugated and resecreted into the bile *via* the bile salt export pump (BSEP). This shuttling of bile acids between intestine and liver is termed enterohepatic circulation (Figure 3). As a consequence of the

enterohepatic circulation a pool of bile acids, dynamic in pool size and composition, accumulates [95]. The bile acid pool size add up to 4 mg in mice and 2-4 g in humans [98].

Microbial transformations of bile acids

Primary bile acids that are not absorbed at the terminal ileum (<10%) and thus are delivered by spill over to the large intestine where they are converted by microbial transformation (Figure 2) [98]. In a first step, bile acids are deconjugated by bile salt hydrolases. After this enzymatic hydrolysis of the amide bond linking bile acids to taurine or glycine, bile acids pass through other transformations such as epimerization, oxidation, reduction, hydroxylation and dehydroxylation [99]. The primary bile acids CA and CDCA are converted by 7 α -dehydroxylation into the secondary bile acids deoxycholic acid (DCA) and lithocholic acid (LCA) [100]. Another possible transformation of CDCA is the epimerization at the C₃ hydroxy group resulting in the secondary bile acid ursodeoxycholic acid (UDCA) [99]. Additional secondary bile acids are ω -muricholic acid (ω MCA), hyocholic acid (HCA) and hyodeoxycholic acid (HDCA) [95]. Due to their hydrophobicity, secondary bile acids undergo facilitated diffusion across the colonic epithelium. Bile acids remaining in the colonic lumen are excreted *via* feces [101]. The gut microbiota thus influences the composition of the bile acid pool substantially. Due to their detergent properties, bile acids can also show antimicrobial activity with inhibition of bacterial growth which in turn changes the composition of the microbiota [102].

Metabolic modulation by bile acids

Given the fact that bile acids are detergents, they facilitate the intestinal absorption of dietary fat and fat-soluble vitamins by forming micelles. Second, the biosynthesis of bile acids from cholesterol is an important way to eliminate cholesterol from the body [96, 101]. Initiated by the discovery of two receptors responsive to bile acids, namely the farnesoid receptor X (FXR) in 1999 [103-105] and the bile acid receptor 1 TGR5 in 2002 [56], research turned towards the relevance of bile acids as signaling molecules. In addition, bile acids can also activate the pregnane X receptor, vitamin D receptor, sphingosine-1-phosphate receptor and muscarinic receptors [106].

FXR is a nuclear receptor present in a number of organs including liver, intestine and adipose tissue [107]. Depending on the site of expression, FXR affects lipid and lipoprotein metabolism, influences glucose homeostasis and regulates enterohepatic

circulation and bile acid synthesis [101]. Bile acid synthesis by CYP7A1 is either regulated *via* the FXR-SHP pathway or the FXR-FGF15 pathway (Figure 3). In the former pathway, bile acids induce FXR-mediated expression of the small heterodimer partner (SHP) which in turn represses the transcription of CYP7A1 [101]. In the latter pathway, bile acids induce *via* FXR the expression of fibroblast growth factor 15 (FGF15 in rodents, FGF19 in humans) in the distal ileum and subsequently, FGF15 is secreted into portal circulation. Upon binding to fibroblast growth factor receptor 4 (FGFR4) and its accessory protein β klotho, CYP7A1 expression is inhibited [108]. The importance of FXR for blood glucose homeostasis is reflected by impaired glucose tolerance, decreased insulin sensitivity and disordered insulin signaling in FXR^{-/-} mice [109]. In addition, there is an FXR-independent mechanism of metabolic regulation by bile acids *via* TGR5 (for detail 1.2).

Influence of dietary fat

In humans a HFD (source: animal fat) results in a higher fecal bile acid excretion compared to a CD [110, 111]. Similar observations were reported when mice were fed a diet enriched in cholesterol. Here, the bile acid pool size was increased and more fecal bile acids were excreted [112, 113]. In 2012, *Devkota et al.* described a connection between dietary fat intake and immune-mediated diseases mediated by bile acids. Consuming a diet high in saturated fats causes changes in the bile acid pool which can result in a microbial imbalance and effects on the host immune system [114].

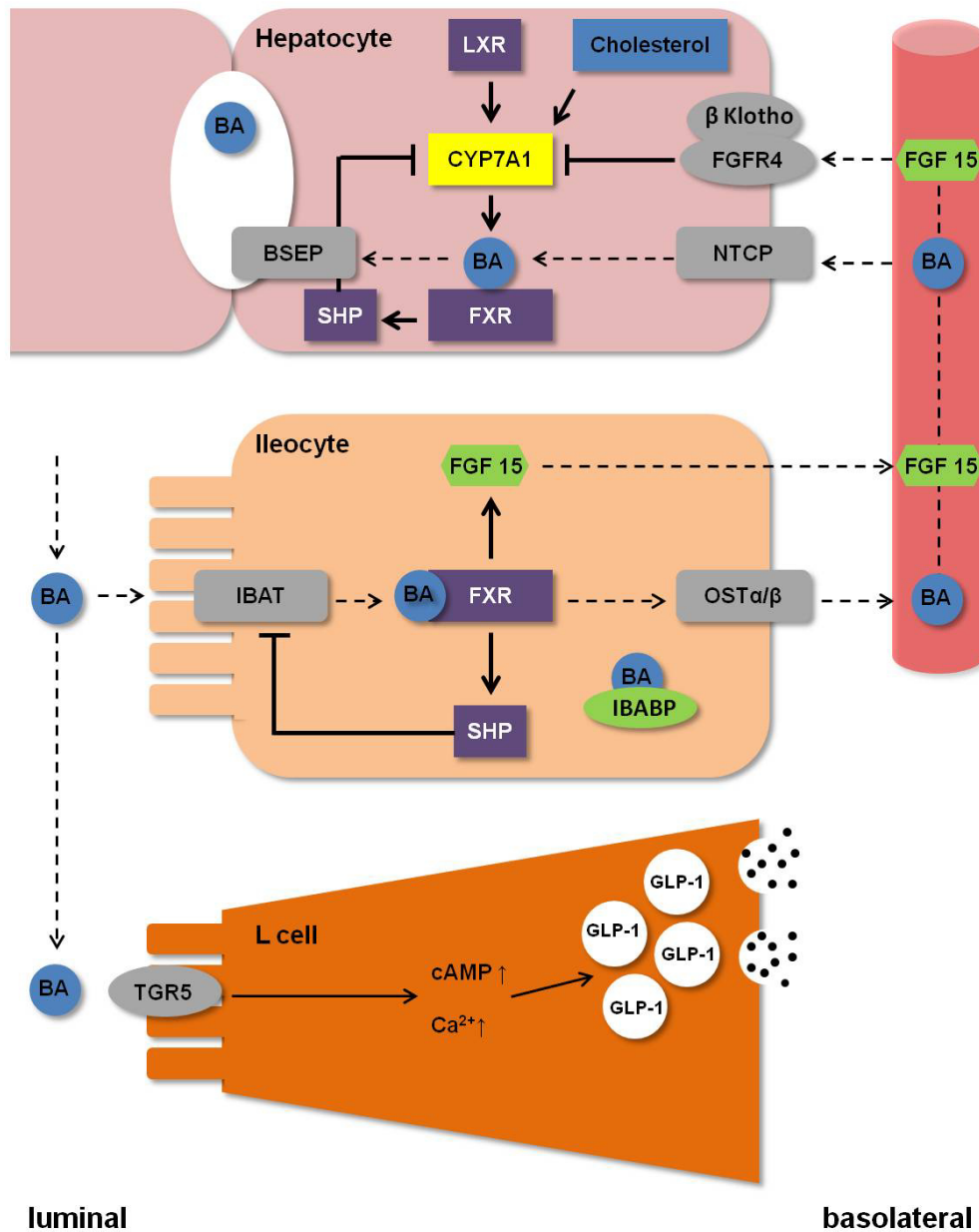


Figure 3: Enterohepatic circulation and metabolic regulation by bile acids. Bile acids are synthesized in the liver from cholesterol, stored in the gall bladder and released into the duodenum. At the terminal ileum they are absorbed, exit the ileocyte at the basolateral membrane and return to the liver *via* the portal system. The shuttling of bile acids between intestine and liver is termed enterohepatic circulation. Bile acids have the ability to regulate their own biosynthesis by the FXR-SHP or the FXR-FGF15-FGFR4 pathway. Moreover, bile acids modulate glucose metabolism by inducing GLP-1 secretion from enteroendocrine L cells *via* TGR5 activation. Abbreviations: BA, bile acid; BSEP, bile salt export pump; CYP7A1, cholesterol 7 α -hydroxylase; FGF15, fibroblast growth factor 15; FGFR4, fibroblast growth factor receptor 4; FXR, farnesoid receptor X; GLP-1, glucagon-like peptide-1; IBABP, ileal bile acid binding protein; IBAT, ileal bile acid transporter; LXR, liver X receptor; NTCP, sodium-taurocholate cotransporting polypeptide; OST α/β , organic solute transporter α/β ; SHP, small heterodimer partner; TGR5, G protein-coupled bile acid receptor 1. Figure modified from [95].

1.5 Metabolic endotoxemia

LPS is a component of the outer cell wall of Gram-negative bacteria and continuously released into the gut lumen when Gram-negative bacteria disaggregate. It is composed of an O-antigen, a core region and the lipid A region which is responsible for the action as an endotoxin [115]. Cani *et al.* demonstrated a two- to threefold increase of plasma LPS after four weeks of HFD intervention in mice. They termed this moderate elevation of LPS 'metabolic endotoxemia', as LPS levels are 10 to 15 times lower than during a septic shock [2]. Apart from HFD interventions in wild type mice [2, 3, 116-119], such a metabolic endotoxemia was also observed in genetically obese mice [3, 120]. How LPS penetrates from the gut lumen into the body and how dietary fat facilitates this process is not clear, yet. One possible mechanism is a TLR4-mediated absorption of LPS [121, 122]. Inside the epithelial cell, LPS is transported to the Golgi compartment where chylomicrons containing apolipoproteins, cholesterol, phospholipids and triglycerides are assembled. Chylomicrons have a high affinity for LPS and most likely both, chylomicrons and LPS are released into circulation at the same time [123]. This assumption is supported by human studies indicating increased plasma endotoxin levels after HFD consumption [124-127]. In brief, dietary fat absorption is accompanied by increased chylomicron formation promoting translocation of LPS from the gut lumen into circulation. However, since lipid absorption takes place in the small intestine which has a far lower bacterial density than colon, this route of LPS translocation within chylomicrons may not be so important after all. Within body fluids LPS is bound to LPS-binding protein (LBP). This LPS:LBP complex transfers LPS to CD14 being expressed predominantly on the surface of monocytes and macrophages. In return, the LPS:CD14 complex activates pro-inflammatory cytokine secretion *via* TLR4 and MD-2 [115]. It has been reported that metabolic endotoxemia induced by four weeks of HFD intervention or by subcutaneous chronic LPS infusion, elevates plasma levels of cytokines such as TNF, IL-1 and IL-6 in liver, adipose tissue and muscle [2]. Taken together, a metabolic endotoxemia is considered to deteriorate the inflammatory tone of the host.

1.6 Aim of the project

The aim of the present study was to investigate in mice the impact of feeding diets with increasing fat content on gut barrier integrity and gastrointestinal hormone secretion. Special emphasis was given to the dietary fat content and fat source, the length of the feeding period and housing conditions. Permeability features of the gut were assessed *via* electrophysiological measurements in Ussing chambers. In addition, inflammatory markers, microbiota composition and bile acid production were studied in particular in a trial assessing the effects of two different housing conditions. Furthermore, the influence of a HFD intervention on enteroendocrine secretion was assessed *in vivo* and *in vitro*. In particular, bile acid- and short-chain fatty acid-induced GLP-1 secretion from murine primary colonic cell cultures was investigated including intracellular calcium signaling and gene expression analysis.

2 Materials and Methods

2.1 Materials

2.1.1 Equipment and software applications

Table 3: Equipment

Equipment	Type	Company
Confocal microscope	FLUOVIEW FV10i	Olympus, Tokyo, Japan
Digital microscope	M8	PreciPoint, Freising, Germany
Disperser	Kinematica Polytron™ PT 1600E	Thermo Fisher Scientific, Waltham, USA
Electrophoresis chamber	Mini-PROTEAN® 3 cell	BioRad, Hercules, USA
Embedding station	AP280	Microm, Walldorf, Germany
Evaporator	SPD111V SpeedVac	Thermo Fisher Scientific, USA
Freeze Dryer	Christ Alpha 1-4 LD	SciQuip, Newtown, UK
Glucometer	FreeStyleLite	Abbott Laboratories, Illinois, USA
Infrared imaging system	Odyssey®	LI-COR, Lincoln, USA
Incubator	CO ₂ -Incubator	Binder, Tuttlingen, Germany
Inverted contrasting microscope	Leica DM IL	Leica, Solms, Germany
Laminar flow hood	Heraeus® HERAsafe® KS	Thermo Fisher Scientific, USA
LC System	1260 Infinity	Agilent Technologies, Santa Clara, USA
LC Column	Luna® 5 µm C18(2) 100 Å, 250 x 4.6 mm	Phenomenex, Torrance, USA
	Luna® 5 µm C18(2) 100 Å, 150 x 4.6 mm	Phenomenex, Torrance, USA
Live cell imaging perfusion system	POC-R2	PeCon, Erbach, Germany
Mass spectrometer	QTRAP® 5500 System	AB Sciex, Framingham, USA
Microplate reader	Varioskan™ Flash Multimode Reader	Thermo Fisher Scientific, Waltham, USA
Microwave	Micromat 15	AEG, Frankfurt, Germany
Mixing instrument	Thermomix compact	Eppendorf, Hamburg, Germany
Multichannel voltage-current-clamp	VCC MC6,	Physiologic Instruments, California, USA
Multistainer	ST5020	Leica, Solms, Germany
Spectrophotometer	Ultrospec 3100 pro	GE Healthcare, Buckinghamshire, UK
	NanoDrop 1000,	peqLab, Erlangen, Germany
Tissue processor	TP1020	Leica, Solms, Germany
Thermal cycler	Light cycler480	Roche, Basel, Switzerland
	Mastercycler ep realplex	Eppendorf, Hamburg, Germany
	TPersonal	Biometra, Goettingen, Germany
Ultrasonic power	UP200S	Hielscher, Teltow, Germany
Voltage-sensing electrodes	DRIREF-5SH	World Precision Instruments, Florida, USA
Water Bath	WCB-11H	Witeg, Wertheim, Germany
Rotary microtome	HM 355 S	Microm, Walldorf, Germany

MATERIALS AND METHODS

Table 4: Software applications

Software packages	Company
Acquire and Analyze 2.3	Physiological Instruments, San Diego, USA
Analyst [®]	AB Sciex, Framingham, USA
FV10-ASW 4.1 Viewer	Olympus, Tokyo, Japan
GraphPad Prism 6	GraphPad Software, San Diego, USA
Image studio [™] lite	LI-COR, Lincoln, USA
LAS AF lite	Leica, Solms, Germany
LightCycler [®] 480	Roche, Basel, Switzerland
Microsoft Excel	Microsoft, Redmond, USA
Microsoft Word	Microsoft, Redmond, USA

2.1.2 Chemicals, media and consumables

Table 5: Chemicals and reagents

Chemical	Company
5 PRIME [™] Isol-RNA lysis reagent	Thermo Fisher Scientific, Waltham, USA
Acetonitrile	Sigma-Aldrich, St.Louis, USA
Agarose	Lonza, Basel, Schweiz
Ammonium acetate	Sigma-Aldrich, St.Louis, USA
Ammonium persulfate (APS)	Carl Roth, Karlsruhe, Germany
Bovine serum albumin (BSA) Fraction V	AppliChem, Darmstadt, Germany
Bromphenolblue	GE Healthcare, Buckinghamshire, UK
CaCl ₂	Carl Roth, Karlsruhe, Germany
Carbogen gas	Linde, Munich, Germany
Citric acid	Carl Roth, Karlsruhe, Germany
Chenodeoxycholic acid	Sigma-Aldrich, St.Louis, USA
Chloroform	Carl Roth, Karlsruhe, Germany
Cholic acid	Sigma-Aldrich, St.Louis, USA
Collagenase from <i>Clostridium histolyticum</i>	Sigma-Aldrich, St.Louis, USA
cOmplete, Mini, EDTA-free	Roche, Basel, Switzerland
4',6-diamidino-2-phenylindole (DAPI)	Sigma-Aldrich, St.Louis, USA
Deoxycholic acid	Sigma-Aldrich, St.Louis, USA
Dithiothreitol (DTT)	AppliChem, Darmstadt, Germany
Ethanol	Merck Millipore, Darmstadt, Germany
Ethylenediaminetetraacetic acid (EDTA)	Carl Roth, Karlsruhe, Germany
Ethylene glycol-bis(2-aminoethylether)-N,N,N',N'-tetraacetic acid (EGTA)	Carl Roth, Karlsruhe, Germany
Eserine	Sigma-Aldrich, St.Louis, USA
Fluorescein, sodium salt	Sigma-Aldrich, St.Louis, USA
Fluorescein isothiocyanate-dextran	Sigma-Aldrich, St.Louis, USA
Formaldehyde solution 37 %	Carl Roth, Karlsruhe, Germany
Forskolin	Sigma-Aldrich, St.Louis, USA
Formic acid	Sigma-Aldrich, St.Louis, USA
Fura-2, AM	Thermo Fisher Scientific, Waltham, USA
Glucose	Carl Roth, Karlsruhe, Germany
Glycine	Merck Millipore, Darmstadt, Germany
Glycerol	Merck Millipore, Darmstadt, Germany

Hexane	Sigma-Aldrich, St.Louis, USA
Igepal CA-630	Sigma-Aldrich, St.Louis, USA
Ionomycin	Sigma-Aldrich, St.Louis, USA
3-isobutyl-1-methylxanthine (IBMX)	Sigma-Aldrich, St.Louis, USA
Isoflurane	Baxter, Deerfield, USA
Isopropyl alcohol	Sigma-Aldrich, St.Louis, USA
KCl	Carl Roth, Karlsruhe, Germany
KH ₂ PO ₄	Merck Millipore, Darmstadt, Germany
Lithocholic acid	Sigma-Aldrich, St.Louis, USA
Matrigel® Basement Membrane Matrix	Corning, Corning, USA
4-(2-hydroxyethyl)-1-piperazineethanesulfonic acid (HEPES)	Carl Roth, Karlsruhe, Germany
β-Mercaptoethanol	Merck Millipore, Darmstadt, Germany
Methanol	Merck Millipore, Darmstadt, Germany
MgCl ₂	Carl Roth, Karlsruhe, Germany
NaCl	Merck Millipore, Darmstadt, Germany
NaHCO ₃	Carl Roth, Karlsruhe, Germany
NaH ₂ PO ₄	Carl Roth, Karlsruhe, Germany
Na ₂ HPO ₄	Carl Roth, Karlsruhe, Germany
Paraplast X-TRA®	Sigma-Aldrich, St.Louis, USA
Phenylmethanesulfonyl fluoride (PMSF)	Carl Roth, Karlsruhe, Germany
Pluronic F127	Sigma-Aldrich, St.Louis, USA
Protein assay dye reagent concentrat	BioRad, Hercules, USA
PYROSPERSE™ Dispersing Agent	Lonza, Basel, Schweiz
Roti®-Mount FluorCare	Carl Roth, Karlsruhe, Germany
Rotiphorese®Gel 30	Carl Roth, Karlsruhe, Germany
Saponin	Sigma-Aldrich, St.Louis, USA
Sodium dodecyl sulphate (SDS)	SERVA Electrophoresis, Heidelberg, Germany
N,N,N',N'-Tetramethylethylenediamine (TEMED)	Carl Roth, Karlsruhe, Germany
Tri-Natriumcitrat Dihydrat	Carl Roth, Karlsruhe, Germany
Tris(hydroxymethyl)aminomethane (Tris)	Merck Millipore, Darmstadt, Germany
Tween®20	SERVA Electrophoresis, Heidelberg, Germany
Water, LC-MS Reagent	J.T. Baker, Center Valley, USA
Xylene	Carl Roth, Karlsruhe, Germany

Table 6: Commercial media and solutions for cell culture

Medium	Company
Dulbecco's Modified Eagle's Medium – high glucose	Sigma-Aldrich, St.Louis, USA
Dulbecco's Phosphate Buffered Saline	Sigma-Aldrich, St.Louis, USA
Fetal calf serum	Merck Millipore, Darmstadt, Germany
L-glutamin	Sigma-Aldrich, St.Louis, USA
Penicillin/streptomycin	Sigma-Aldrich, St.Louis, USA

MATERIALS AND METHODS

Table 7: Consumables

Consumables	Type	Company
Fine forceps	Dumont #5	FST, Heidelberg, Germany
Insect pin	Minutien (0.15 x 12mm)	Bioform, Nürnberg Germany
Microcentrifuge tube	TubeOne®	Starlab, Hamburg, Germany
Microscope slides	SuperFrost Ultra Plus®	Menzel-Gläser, Braunschweig, Germany
Micropestles		Eppendorf, Hamburg, Germany
Microvette 500	Potassium-EGTA	Sarstedt, Nümbrecht, Germany
Nitrocellulose membrane	Whatman™10401196 Protran™ BA85	GE Healthcare, Buckinghamshire, UK
Plastic paraffin film	Parafilm®	Brand, Werheim, Germany
Tissue culture dish	ø 54 mm	TPP, Trasadingen, Switzerland
Tissue culture test plates	6-well	TPP, Trasadingen, Switzerland
Tissue culture test plates	24-well	TPP, Trasadingen, Switzerland

2.1.3 Buffers and solutions

Table 8: Krebs buffer (carbogen-gassed, pH 7.4)

Chemical	Concentration
NaCl	114 mM
NaHCO ₃	21 mM
KCl	5.4 mM
Na ₂ HPO ₄	2.4 mM
CaCl ₂	1.2 mM
MgCl ₂	1.2 mM
NaH ₂ PO ₄	0.6 mM
Glucose	10 mM

Table 9: 10xPhosphate buffered saline (pH 7.4)

Chemical	Concentration
NaCl	1.37 M
KCl	27 mM
Na ₂ HPO ₄	100 mM
KH ₂ PO ₄	18 mM

Table 10: Lysis buffer for western blotting (pH 7.4)

Chemical	Concentration
Tris	100 mM
NaCl	200 mM
EDTA	2 µM
Glycerol	8 %
DTT	1.25 µM

Table 11: 4xLaemmli buffer (pH 6.8)

Chemical	Concentration
SDS	8 %
Glycerol	20 %
β -Mercaptoethanol	20 %
Bromphenolblue	0.4 %
Tris	250 mM

Table 12: 3xResolving gel buffer (pH 8.8)

Chemical	Concentration
Tris	1.12 M
SDS	0.3 %

Table 13: 1xStacking gel buffer (pH 6.8)

Chemical	Concentration
Tris	0.14 M
SDS	0.1 %

Table 14: 1xRunning buffer

Chemical	Concentration
Tris	125 mM
Glycine	960 mM
SDS	5 %

Table 15: Transfer buffer

Chemical	Concentration
Tris	20 mM
Glycine	150 mM
Methanol	20 %
SDS	0.02 %

Table 16: Citrate buffer (pH 6.0)

Chemical	Concentration
Citric acid	1.8 mM
Tri-Natriumcitrat Dihydrat	8.2 mM

Table 17: 138 Buffer (pH 7.4)

Chemical	Concentration
KCl	4.5 mM
NaCl	138 mM
NaHCO ₃	4.2 mM
NaH ₂ PO ₄	1.2 mM
CaCl ₂	2.6 mM
MgCl ₂	1.2 mM
HEPES	10 mM

MATERIALS AND METHODS

Table 18: Lysis buffer for primary cell cultures

Chemical	Concentration
Deoxycholic acid	12 mM
Igepal CA-630	1 %
Tris	50 mM
NaCl	150 mM
cOmplete, Mini, EDTA-free	1 tablet/50 ml

Table 19: Bile acid standard mix in MetOH: water (1:1)

Chemical	Company	Concentration
Chenodeoxycholic acid	Sigma-Aldrich, St.Louis, USA	100 nm
Cholic acid	Sigma-Aldrich, St.Louis, USA	100 nm
Dehydrocholic acid	Sigma-Aldrich, St.Louis, USA	100 nm
Deoxycholic acid	Sigma-Aldrich, St.Louis, USA	100 nm
Sodium glycochenodeoxycholate	Sigma-Aldrich, St.Louis, USA	100 nm
Glycocholic acid hydrate	Sigma-Aldrich, St.Louis, USA	100 nm
Sodium glycodeoxycholate	Calbiochem, Sandhausen, Germany	100 nm
Sodium glyoursodeoxycholates	Calbiochem, Sandhausen, Germany	100 nm
Lithocholic acid	Sigma-Aldrich, St.Louis, USA	100 nm
ω -Muricholic acid	Steraloids, Newport, USA	100 nm
Sodium tauroolithocholate	Sigma-Aldrich, St.Louis, USA	100 nm
Ursodeoxycholic acid	Sigma-Aldrich, St.Louis, USA	100 nm
Sodium taurochenodeoxycholate	Sigma-Aldrich, St.Louis, USA	100 nm
Sodium taurocholic acid hydrate	Sigma-Aldrich, St.Louis, USA	100 nm
Sodium taurodeoxycholate hydrate	Sigma-Aldrich, St.Louis, USA	100 nm
Tauro muricholic acid	Steraloids, Newport, USA	100 nm
Sodium tauroursodeoxycholates	Calbiochem, Sandhausen, Germany	100 nm

Table 20: Bile acids internal standard mix in methanol: water (1:1)

Chemical	Company	Concentration
d4-Deoxycholic acid	C/D/N Isotopes, Quebec, Canada	1 μ M
d4-Cholic Acid	Campro Scientifi, Berlin; Germany	1 μ M
d4-Glyoursodeoxycholic acid	C/D/N Isotopes, Quebec, Canada	1 μ M
d4-Glycodeoxycholic acid	C/D/N Isotopes, Quebec, Canada	1 μ M
d4-Glycocholic acid	C/D/N Isotopes, Quebec, Canada	1 μ M
d5-Taurocholic acid	C/D/N Isotopes, Quebec, Canada	1 μ M

2.1.4 Kits, antibodies and primers

Table 21: Commercial kits and enzymes

Kits and enzymes	Company
Cholesterol liquicolor mono	Human Gesellschaft für Biochemica und Diagnostica mbH, Wiesbaden, Germany
DPP IV Inhibitor	Roche, Basel, Switzerland
dNTP Mix	Bioline, London, UK
Glucagon Like Peptide-1 (Active) ELISA	Merck Millipore, Darmstadt, Germany
LightCycler 480 Probes Master	Roche, Basel, Switzerland
Limulus ameocyte lysate chromogenic endpoint assay	Hycult® biotech, Plymouth Meeting, USA
M-MLV Reverse Transcriptase	Promega, Madison, USA
Mouse GLP-2 ELISA	BioVendor R&D, Brno, Czech Republic
Mouse IL-6 Kit V-PLEX	Meso Scale Discovery, Rockville, USA
Mouse/Rat Total Active GLP-1, Insulin, Glucagon Kit	Meso Scale Discovery, Rockville, USA
PageRuler™ Prestained Protein Ladder	Thermo Fisher Scientific, Waltham, USA
QIAshredder	Qiagen, Venlo, Netherlands
QuantiTect SYBR® Green RT-PCR Kit	Qiagen, Venlo, Netherlands
Rat/Mouse GIP (total) ELISA	Merck Millipore, Darmstadt, Germany
Rnasin® Ribonuclease Inhibitor	Promega, Madison, USA
Rneasy Protect Mini Kit	Qiagen, Venlo, Netherlands
SensiMix™ SYBR® No-ROX Kit	Bioline, London, UK
Triglycerides liquicolor mono	Human Gesellschaft für Biochemica und Diagnostica mbH, Wiesbaden, Germany

Table 22: Primary antibodies for western blotting (WB) and immunohistochemistry (IHC)

Raised against	Host species	Dilution	Application	Company
anti-β-actin	goat	1:4000	WB	Santa Cruz Biotechnology, Dallas, USA
anti-claudin-2	rabbit	1:200	WB	Immuno-Biological Laboratories
anti-claudin-3	rabbit	1:400	WB	Invitrogen TM , Carlsbad, USA
		1:150	IHC	
anti-claudin-5	rabbit	1:500	WB	Invitrogen TM , Carlsbad, USA
		1:150	IHC	
Anti-GIP	goat	1:200	IHC	Santa Cruz Biotechnology, Dallas, USA
Anti-GLP-1	goat	1:200	IHC	Santa Cruz Biotechnology, Dallas, USA
anti-JAM-A	rat	1:200	WB	Santa Cruz Biotechnology, Dallas, USA
anti-occludin	rabbit	1:500	WB	Invitrogen TM , Carlsbad, USA
anti-ZO-1	rabbit	1:500	WB	Invitrogen TM , Carlsbad, USA

Table 23: Secondary antibodies for western blotting (WB) and immunohistochemistry (IHC)

Raised against	Host species	Dilution	Fluorophore	Application	Company
anti-goat IgG	donkey	1:12000	IRDye® 800CW	WB	LI-COR, Lincoln, USA
anti-rabbit IgG	donkey	1:12000	IRDye® 680	WB	LI-COR, Lincoln, USA
anti-rat IgG	donkey	1:10000	IRDye® 800CW	WB	LI-COR, Lincoln, USA
Anti-goat IgG	donkey	1:500	Cy3	IHC	Jackson ImmunoResearch, West Grove, USA

MATERIALS AND METHODS

Table 24: Primer sequences

Gene	Name	Forward sequence (5'- 3')	Reverse sequence (5'- 3')
Abcb11		TGGTAGAGAAGAGGCGACAAT	TGAGGTAGCCATGTCCAGAA
Actin		ATTGTTACCAACTGGGACGA	GAGCATAGCCCTCGTAGATG
β Klotho		AACAGCTGTCTACACTGTGGG	ATGGAGTGCTGGCAGTTGATC
Cyp7a1		AGCAACTAAACAACCTGCCAG	GTCCGGATATTCAAGGATGCA
Cyp27a1		TACACCAATGTGAATCTGGC	TAACCTCGTTTAAGGCATCC
Dpp4		AGGATCACATCGACAGGAGA	ATCCACACTGTCTTGGGGTA
Fabp6	IBABP	CAAGGCTACCGTGAAGATGGA	CCCACGACCTCCGAAGTCT
Fgf15		AGACGATTGCCATCAAGGACG	GTACTGGTTGTAGCCTAAACAG
Fgfr4		CAGAGGCCTTTGGTATGGAT	AGGTCTGCCAATCCTTGTC
Gapdh		CCTGGAGAAACCTGCCAAGTATG	GAGTGGGAGTTGCTGTTGAAGTC
Gcg		TGCTTATAATGCTGGTGCAA	TTGGTGTTTCAACCACTG
Gip		GTGGCCTTTGAAGACCTGCTC	AAGTCCCCTCTGCGTACCTT
Gpbar1	TGR5	CCCTGGCAAGCCTCATCGTC	TGTGAGCAGCCCGGCTAGTA
Nr1h2	LXR- β	GCAACATGATCTCAATGGTG	AGCCCAAAGTCACGCCC
Nr1h3	LXR- α	TGTTTCTCCTGATTCTGCAA	TGACTCCAACCCTATCCCT
Nr1h4	FXR	GCAGGGAGAAAACGGAAC	TCTGTACATGACTGGTTGCC
Ntcp		GCCACACTATGTACCCTACGTC	TTTAGTCGGAAGAGAGCAGAGA
Shp		CGATCCTCTTCAACCCAGATG	AGGGCTCCAAGACTTCACACA
Slc10a2	ASBT	TGGGTTTCTTCTGGCTAGACT	TGTTCTGCATTCCAGTTTCAA
Slc51a	Ost- α	TACAAGAACACCCTTTGCC	CGAGGAATCCAGAGACCAAA
Slc51b	Ost- β	GTATTTTCGTGCAGAAGATGCG	TTTCTGTTTGCCAGGATGCTC

Table 25: Primer sequences and probes using the Universal Probe Library (UPL)

Name	UPL number	Forward sequence (5'- 3')	Reverse sequence (5'- 3')
Gapdh	#9	TCCACTCATGGCAAATTCOA	TTTGATGTTAGTGGGGTCTCG
Saa3	#26	ATGCTCGGGGGAACACTATGAT	ACAGCCTCTCTGGCATCG
Tnf	#49	TGCCTATGTCTCAGCCTCTTC	GAGGCCATTTGGGAACCTTCT
Mcp1	#62	CATCCACGTGTTGGCTCA	GATCATCTTGCTGGTGAATGAGT
Il1 β	#78	TGTAATGAAAGACGGCACACC	TCTTCTTTGGGTATTGCTTGG
Hprt	#95	TCCTCCTCAGACCGCTTTT	CCTGGTTCATCATCGCTAATC

2.2 Methods

2.2.1 Mice, husbandry and diets

AKR/J, C57BL/6J, C57BL/6N and SWR/J mice were bred in the specific pathogen-free (SPF) animal facility at the WZW School of Life Sciences of the Technische Universität München in Freising-Weihenstephan (Germany). Depending on the experimental setting, mice were housed in the SPF animal facility or were transferred to the conventional (CV) animal facility at the Kleintierforschungszentrum WZW. The SPF and the CV husbandry conditions are compiled in Table 26. For health monitoring, animals in the two husbandries were monitored following the Federation of European Laboratory Animal Science Associations (FELASA) recommendations [128, 129]. All animal experiments were performed in compliance to the recommendations of the FELASA and to the Animal Welfare Act (District Government of Upper Bavaria). All diets (Table 27) used for this work were either ordered from Ssniff (Soest, Germany) or from SAFE diets (Augy, France).

Table 26: Parameters for the husbandry in the conventional (CV) and the specific pathogen-free (SPF) animal facility

Parameter	CV	SPF
Temperature	22±2 °C	22±2 °C
Humidity	50±5 %	55 ±5 %
Light: dark cycle	12 h:12 h	12 h:12 h
Caging system	open type	individually ventilated
Experimental diet	irradiated	irradiated
Water	deionized	deionized and autoclaved
Bedding	not autoclaved	autoclaved
Access		
• Clothing and shoes	one change	two changes
• Mask, gloves and hairnet	yes	yes
• Air shower	no	yes

Experimental setting 1: Plant-based high-fat diet and mouse strains with different susceptibility to diet-induced obesity

Male 8-week old SWR/J, C57BL/6J or AKR/J mice received a plant-based control diet (pCD, 13 kJ% fat based on soy oil, S5745-E720, Ssniff) for 4 weeks. At the age of 12 weeks the diet was either switched to plant-based high-fat diet (pHFD48, 48 kJ% fat based on soy and palm oil, S5745-E722, Ssniff) or mice were fed the pCD for 4 more weeks. This dietary intervention was conducted in the SPF animal facility.

Experimental setting 2: Plant-based high-fat diet intervention differing in feeding period and fat content

At the age of 8 weeks, male C57BL/6J mice were exposed to the pCD for 4 weeks. At the age of 12 weeks the diet was either switched to the pHFD48 for 1, 4, 8, 12 or 24 weeks. Control groups were continuously fed the pCD for the respective feeding periods. The 4 and 12 weeks feeding trials were conducted with an increased fat content of 61 kJ% in the high-fat diet (pHFD61, 61 kJ% fat based on soy and palm oil, S5745-E714, Ssniff) as well. All feeding trails of this experiment were conducted in the SPF husbandry.

Experimental setting 3: Lard-based high-fat diets with increasing fat proportion

At the age of 8 weeks, 24 male C57BL/6J mice were fed a lard/corn oil-based control diet (ICD, 13 kJ% fat, S5745-E707, Ssniff) for 4 weeks. Afterwards, 6 mice per group remained on ICD or were switched to lard/corn oil-based high-fat diets with increasing fat contents: IHFD48 (48 kJ% fat, S5745-E717, Ssniff), IHFD75 (75 kJ% fat, S5745-E727, Ssniff), IHFD78^{cf} (78 kJ% fat and carbohydrate-free, 236 HF U8954V1, SAFE). As a control, 8-weeks old C57BL/6J mice were fed the pCD used in the former experimental settings. The whole experiment was conducted in the SPF animal facility.

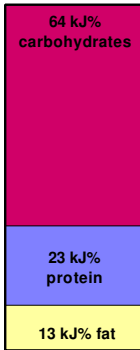
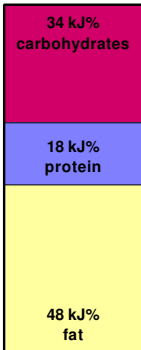

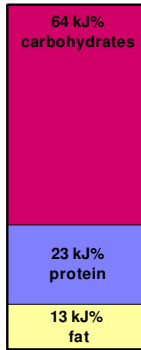

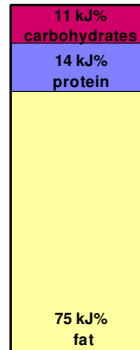
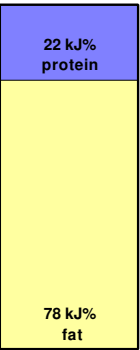
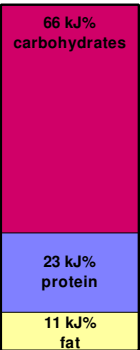
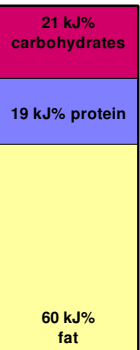
Experimental setting 4: Beef tallow-based high-fat diets in different animal facilities

Male 10-week old C57BL/6N mice were fed either a control diet (CD, 11 kJ% fat based on soy oil, E15000-04, Ssniff) or a beef tallow-based high-fat diet (HFD, 60 kJ% fat based on soy oil and beef tallow, E15741-34, Ssniff) for 12 weeks. This experiment was performed in both, the SPF and the CV animal facility.

Experimental setting 5: Short-term beef tallow-based high-fat diet intervention

Male 6-week old C57BL/6N mice were fed either a control diet (CD, 11 kJ% fat based on soy oil, E15000-04, Ssniff) or a beef tallow-based high-fat diet (HFD, 60 kJ% fat based on soy oil and beef tallow, E15741-34, Ssniff) for 4 weeks. This experiment was conducted in the CV animal husbandry.

Table 27: Composition of the diets

	pCD	pHFD48	pHFD61	ICD	IHFD48	IHFD75	IHFD78 ^{ct}	CD	HFD
Order number	S5745-E720	S5745-E722	S5745-E714	S5745-E707	S5745-E717	S5745-E727	236 HF U8954V1	E15000-04	E15741-34
Company	Ssniff	Ssniff	Ssniff	Ssniff	Ssniff	Ssniff	SAFE	Ssniff	Ssniff
Composition [kJ%]									
Protein	23	18	16	23	18	14	22	23	19
Fat	13	48	61	13	48	75	78	11	60
Carbohydrates	64	34	23	64	34	11	0	66	21
									
Source [kg%]									
Protein	Casein	24	24	24	24	24	37	24	27.7
Fat	Beef tallow								31.5
	Lard			1.5	17.7	35	35		
	Corn oil			3.5	7.3	14.5	14.5		
	Palm oil		20	30					
	Soybean oil	5	5	5				4	3.1
Carbohydrates	Corn starch	47.8	27.8	3.3	47.8	27.8	3.3	30	
	Glucose							10	
	Maltodextrin	5.6	5.6	5.6	5.6	5.6	5.6	19.6	15.7
	Sucrose	5	5	5	5	5	5		8

2.2.2 Electrophysiological measurements

Ussing chamber

The Ussing chamber was developed in the 1950s by Hans Ussing and his colleague Zerahn. They isolated frog skin and studied the active transport of sodium as the source of the electric current [130]. Since then, this method has been adapted to examine different epithelial tissues such as respiratory, ocular and particularly intestinal tissue [131]. In the gut, the transcellular transport of ions, nutrients and drugs across the epithelium or the passive movement through the paracellular route are analyzed.

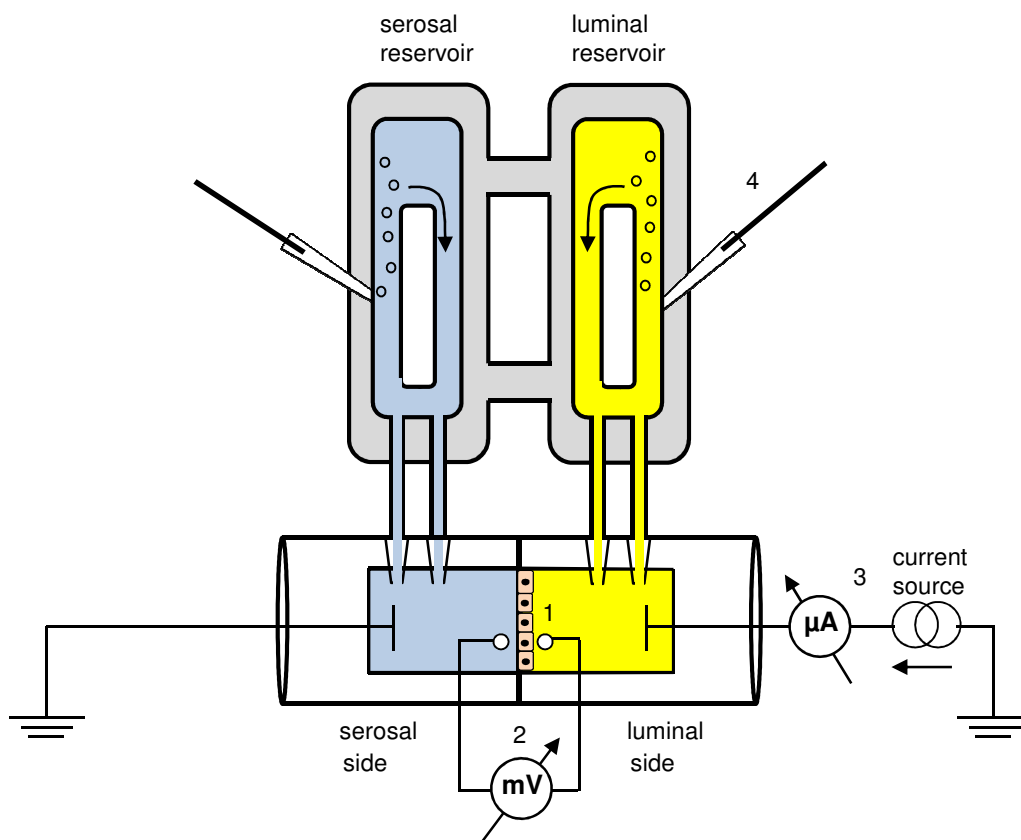


Figure 4: Experimental setup of an Ussing chamber. (1) In the chamber, the epithelium separates the luminal (yellow) from the serosal side (blue). A fluorescent permeability marker is added to the luminal side. (2) Agar bridges connected to voltage-sensing electrodes are placed at the epithelium, whereas (3) current (Ag/AgCl) electrodes apply defined pulses to the tissue. The water jacket (grey) heats the Krebs buffer to 37°C. (4) Carbogen gas induces circulation of the Krebs buffer.

The Ussing chambers used (Figure 4) consisted of two chamber parts. Between these two parts the intestinal tissue was mounted vertically as a flat sheet and it divided in this way the chamber into a luminal and a serosal halve. The chamber halves were connected to the circulation reservoirs. They were filled with ‘Krebs buffer’ (Table 8) which was warmed-up to 37°C (Table 3) and bubbled with carbogen

gas (gas mixture of 95% O₂ and 5% CO₂, Table 5). The transepithelial potential difference (PD_t) was measured by a multichannel voltage-current-clamp (Table 3). Therefore, 3.5% agar bridges were placed next to the tissue and connected to voltage-sensing electrodes (Table 3) *via* a 3 M KCl solution. Additionally, current Ag/AgCl electrodes were placed at the outer end of each chamber half. They were connected to the clamp device as well and thus it was possible to apply defined current pulses to the tissue. The area of the mounted tissue had a surface of 0.287 cm²

Tissue preparation

Mice were sacrificed by an overdose of Isoflurane (Table 5); the intestine was dissected and placed in ice-cold carbogen-gassed 'Krebs buffer' (Table 8). 1.5 cm pieces of the jejunum (centre of the small intestine), distal ileum (end of the small intestine) and proximal or distal colon (beginning and end of the colon) were placed in Sylgard[®] plates filled with ice-cold Krebs puffer. Intestinal tissue samples were opened along the mesenteric border, pinned with insect pins (Table 7) on a piece of Parafilm[®] (Table 7) using fine forceps (Table 7). Finally, the tissues were mounted as flat sheets in the chambers.

Bath correction and zeroing of voltage-sensing electrodes

The 'Krebs buffer' (also called bath solution) influences the transepithelial resistance (TER) *per se*. Therefore, as a control, Ussing chambers were operated solely with bath solution (no tissue). All measurements were corrected by subtraction of the average blank value recorded. Prior to each measurement, the voltage-sensing electrodes were referenced and set to 0 mV.

Transepithelial resistance

TER is a valuable parameter for assessing the integrity of the intestine. After mounting, the chambers were inserted into the gripping devices and connected to the reservoirs. Luminal and serosal sides of the Ussing chambers were filled simultaneously with preheated carbogen-gassed Krebs puffer (pH 7.4). During the measurement both sides of the chambers were continuously bubbled with carbogen gas and the temperature was maintained by a water jacket at 37°C. Tissues were equilibrated for 45 min and the TER at the end of the equilibration period was used for further analysis. At the end of the experiment, 50 µl of 1 M EGTA solution were

added on both sides of the chamber to induce a break of the intestinal barrier; the remaining TER was determined as well.

During the whole experiment, the chambers were operated in the current-clamp configuration; thereby the transepithelial potential difference (ΔPD_t) was measured. In order to calculate the TER (R_t), defined current pulses (ΔI) were applied to the tissues (20 μA for 500 ms every 20 sec). The resulting temporary changes of the transepithelial potential differences (ΔPD_t) allowed computing the transepithelial resistance (R_t) according to the Ohm's law:

$$R = \frac{U}{I}$$

R	resistance	[Ω]
U	voltage	[V]
I	current	[A]

$$R_t = \frac{\Delta PD_t}{\Delta I}$$

R_t	transepithelial resistance	[k Ω cm ²]
ΔPD_t	transepithelial potential difference	[mV]
ΔI	current	[μA cm ⁻²]

The TER was given as Ω cm² tissue. All experiments were recorded and analyzed using the 'Acquire and Analyze 2.3' software (Table 4).

Flux and permeability of paracellular markers

Beside the TER, paracellular permeability was determined to evaluate the integrity of the intestinal tissue. The paracellular permeability can be estimated using the flux of paracellular markers. Tissues were equilibrated for 45 min in the presence of 62.5 μM fluorescein (MW 332 g/mol) or 62.5 μM FITC-dextran (average MW 3,000-5,000 g/mol) on the luminal side. At the end of the equilibration period at time points 45 min (t_1) and 60 min (t_2) samples were collected from the serosal bath. The fluorescence intensity was measured at 485/520 nm in a microplate reader (Table 3), the concentration of the paracellular marker was computed and the flux (J) was calculated according to the following equation:

$$J = \frac{(c_2 - c_1) \cdot V}{(t_2 - t_1) \cdot A}$$

J:	flux
c ₁ , c ₂ :	concentration on the serosal side at time point 1 respectively 2
V	volume of the chamber
t ₁ , t ₂	time point 1 respectively 2
A	tissue area exposed to fluorescence marker

The permeability of a paracellular marker was calculated by dividing the flux (J) by the difference of concentration of the paracellular marker between the luminal bath and the serosal bath in the beginning of the experiment.

$$P = \frac{J}{c}$$

P	permeability
J	flux
c	difference of permeability marker concentration between luminal and serosal sides at time point 0 min

2.2.3 Molecular biological methods

RNA isolation from tissue

For ribonucleic acid (RNA) isolation, the commercial 'RNeasy Protect Mini Kit' (Table 21) was used. 20 mg of ground frozen tissue (right lobe of the liver or the right epididymal adipose tissue) were thawed in 650 µl 'RTL lysis puffer' containing 10 mM DTT and homogenized with micropestles (Table 7). Adipose tissue was homogenized using a syringe with a 24 G cannula, whereas 400 µl of liver homogenates were transferred to QIAshredder (Table 21) and centrifuged at 20000 x g for 2 min.

For RNA isolation from intestinal tissue, 30 mg of ground, frozen tissue were homogenized with 1 ml '5 PRIME™ Isol-RNA lysis reagent' (Table 5). Samples were centrifuged at 2500 x g for 5 min at 4°C and transferred to new tubes. To each tube 200 µl of chloroform were added and mixed thoroughly for 15 sec. After incubation for 5 min at room temperature, samples were centrifuged at 12000 x g for 15 min at 4°C. The aqueous phase was transferred to a new tube and 500 µl of 75% ice-cold ethanol added. Subsequently, RNA was isolated according to the manufacturer's instruction. Yield and quality of the isolated RNAs were verified spectrophotometrically (Table 3).

MATERIALS AND METHODS

RNA isolation from primary colonic cell cultures

Primary colonic cell cultures were cultivated as described in 2.2.9. After 24 h cells were washed three times with '138 Buffer' (Table 17). After adding 200 µl of '5 PRIME™ Isol-RNA lysis reagent' (Table 5) to each well, cultures were harvested using cell scrapers and subsequently lysed by pipetting up and down. The lysates of three wells were pooled in one tube and stored at -80°C until further processing. To each tube 120 µl of chloroform were added and a vigorous shake was given for 15 sec. After 5 min of incubation, samples were centrifuged at 12000 x g for 15 min at 4°C. The aqueous phase was removed, transferred to a new tube and one volume of 100% ice-cold ethanol was added and mixed by pipetting up and down. The RNA-ethanol mix was transferred to the columns of the 'RNeasy Protect Mini Kit' (Table 21). Subsequently, RNA isolation was performed according to manufacturer's instruction. Yield and quality of the isolated RNAs were determined spectrophotometrically (Table 3).

One-step real-time reverse transcription PCR

For simultaneous amplification and quantification of target genes the 'QuantiTect SYBR® Green RT-PCR Kit' (Table 21) was used. 10 ng of mRNA, 0.5 µM forward and reverse primers (Table 24), 10 µl of 'QuantiTect SYBR Green RT-PCR Master Mix', 0.2 µl of 'QuantiTect RT Mix' and 7.8 µl of PCR water were pipetted in a cooled 96-well plate. Afterwards, the plate was sealed and centrifuged at 300 g for 1 min. The one step reverse transcription PCR was performed in the 'Mastercycler ep realplex' (Table 3) according to the program given in Table 28. Relative mRNA expression was calculated using the $2^{-\Delta\Delta Cq}$ method and normalized for the expression of the housekeeping genes *Gapdh* and *β-Actin*. Data were expressed as fold change (mice on control diet set to 1).

Table 28: Programme for one-step real-time RT-PCR

Step	Temperature [°C]	Time [sec]	Cycles
Reverse transcription	50	1800	
Initialization	95	900	
Denaturation	95	15	
Primer Annealing	60	30	40
Elongation	72	30	
Melting curve	60 to 95	1200	

Two-Step-PCR

Reverse transcription PCR

For cDNA synthesis 1 µg RNA and 200 ng hexanucleotide primers were used and adjusted to a final volume of 14 µl with RNase-free water and incubated at 70°C in a thermal cycler (Table 3) for 5 min. Afterwards, samples were immediately placed on ice for 5 min. Then ‘1 µl M-MLV Reverse Transcriptase’ (Table 21), 5.0 µl ‘M-MLV RT 5x Reaction buffer’, 25 U ‘Recombinant RNAsin’ (Table 21), 0.5 mM ‘dNTP Mix’ (Table 21) were added and the volume was adjusted to 25 µl with RNase-free water. Samples were incubated for 50 min at 48°C and then for 15 min at 70°C. The cDNA was stored at -20°C.

Quantitative real-time PCR for analysis of gene expression of inflammatory markers

Quantification of gene expression was conducted using mono color hydrolysis probes from the Universal Probe Library (UPL, Roche). 1 µg of cDNA, 8 nM forward and reverse primers (Table 25), 4 nM of the probe (Table 25), 5 µl of ‘LightCycler 480 Probes Master Mix’ (Table 21) were filled up with PCR water to 10 µl and pipetted in a cooled 96-well. Afterwards, the plate was sealed and briefly centrifuged. The qPCR was performed in a ‘LightCycler 480’ (Table 29). Relative mRNA expression was calculated using the equation $2^{-\Delta\Delta Cq}$ and normalized to expression of the housekeeping genes *Gapdh* and *Hprt*. Data were expressed as fold changes versus mice on CD housed in the SPF facility.

Table 29: qRT-PCR program for analysis of gene expression of inflammatory markers

Step	Temperature [°C]	Time [s]	Cycles
Initial denaturation	95	180	
2 step cycle	95	5	45
	60°C	10	
Cooling	40°C	30	

Quantitative real-time PCR for analysis of gene expression in enterohepatic circulation and gut hormones

Gene expression in the enterohepatic circulation and gut hormones was analyzed using the fluorescence dye SYBR Green. Therefore, 1 µg cDNA, 1µl of forward and reverse primers (2.5 µM, Table 24), 5µl of ‘SensiMix™ SYBR® No-ROX’ (Table 21) were filled up with PCR water to 10 µl and pipetted into a 384-well plate. The plate was sealed and centrifuged for a few seconds. The analysis was recorded in a ‘LightCycler 480’ (Table 29). At the end of the run, a melting curve analysis was

MATERIALS AND METHODS

generated to assess primer specificity and interfering side products. Relative mRNA expression was calculated using the $2^{-\Delta\Delta Cq}$ method and normalized to expression of the housekeeping gene *Gapdh*. Data were expressed as fold changes vs. mice on CD.

Table 30: qRT-PCR program for analysis of gene expression in the enterohepatic circulation and gut hormones

Step	Temperature [°C]	Time [s]	Cycles
Initial denaturation	95	420	
Denaturation	95	10	
Primer Annealing	60	15	45
Elongation	72	15	
Melting curve	60 to 95	600	

Protein extraction from tissue

Frozen intestinal tissues of the jejunum and colon were ground and 40 mg portions were homogenized in 500 μ l of 'Lysis buffer' containing 2 mM PMSF (Table 10) three times for 20 sec by a disperser (Table 3). Subsequently, the homogenates were treated five times by ultrasound (Table 3). Afterwards, samples were centrifuged at 660 x g for 5 min at 4°C. For further purification supernatants containing (total) cellular proteins were centrifuged at 20000 x g for 1 h at 4°C. The supernatant was collected for analysis of cytosolic proteins while the sediment containing membrane proteins was dissolved in 100 μ l 'Lysis buffer' with 10 mM PMSF and homogenized by using a 24 G cannula. Concentrations of total, cytosolic and membrane proteins were quantified according to the Bradford method. For sodium dodecyl sulphate polyacrylamide gel electrophoresis (SDS-PAGE) 30 μ g of total or membrane protein were mixed with '4xLaemmli buffer' (Table 11) and heated for 5 min at 95°C.

Bradford assay

Protein concentrations were determined by Bradford assay. At first a standard curve was defined. 200 μ l 'Protein assay dye reagent concentrate' (Table 5), 200 μ l H₂O and 1 μ l standard (100, 250, 500, 750, 1000, 1250 and 500 μ g/ml bovine serum albumin) were mixed in a cuvette and incubated for 10 min. Finally, absorbance at 595 nm was measured in a spectrophotometer (Table 3). The same procedure was applied to the samples.

SDS PAGE and Western blot

After preparing the gel casting module (Table 3), either 8.5% resolving gel for the detection of large proteins (ZO-1) or 10% resolving gel for the detection of smaller proteins (claudin-2, claudin-3, claudin-5, JAM-A or occludin) were cast. On the top of each resolving gel a 5% stacking gel was placed. Afterwards, the gels were put in a vertical electrophoresis system; the chamber was filled with 'Running buffer' (Table 14) and samples as well as a molecular weight standard (Table 21) were loaded. Electrophoresis was carried out for 20 min at 120 V followed by 40 min at 160 V. After SDS-PAGE, gels were wet blotted in a tank filled with 'Transfer buffer' (Table 15) onto a nitrocellulose membrane (Table 7). For detection of small proteins gels were blotted for 20 min at 360 mA and for detection of large proteins for 2 h at 200 mA.

8.5% resolving gel	3.45 ml 1x resolving gel puffer (Table 12) , 3 ml H ₂ O, 2.55 ml Rotiphorese@Gel 30, 100µl APS, 5µl TEMED
10% resolving gel	3 ml 1xresolving gel puffer (Table 12), 3 ml H ₂ O, 3 ml Rotiphorese@Gel 30, 100µl APS, 5µl TEMED
5% stacking gel	3.2 ml 1xstacking gel puffer (Table 13), 0.6 ml Rotiphorese@Gel 30, 25µl APS, 5µl TEMED

After blotting, the membranes were washed three times with PBS (Table 9) and blocked with 1% bovine serum albumin in PBS for 1 h. Membranes were incubated with the respective primary antibody (Table 22) diluted in 1% BSA in PBS-T (0.05 % Tween[®]20) overnight at 4°C. Before incubating for 1.5 h with a secondary antibody (Table 23), membranes were washed three times with PBS-T for 10 min. The membrane was then washed three times with PBS and the transferred proteins were visualized and analyzed with the 'Odyssey[®] infrared imaging system' (Table 3). Target proteins were normalized to the housekeeper β-actin.

2.2.4 Histology

Tissue processing and hematoxylin and eosin staining

Mice were sacrificed by Isoflurane and the gut was isolated and dissected. 0.5 cm sections of jejunum (centre of the small intestine) and distal ileum (final end of the small intestine) were sampled. After dissection, tissues were fixed in 4% formaldehyde solution in PBS (Table 9) overnight. Afterwards, tissues were

MATERIALS AND METHODS

transferred to embedding cassettes, dehydrated under vacuum in a tissue processor (Table 31) and embedded in paraffin wax (Table 3).

Table 31: Allocation of the tissue processor

Step	Solution	Time
1	70% EtOH	1 h
2	70% EtOH	1 h
3	80% EtOH	1 h
4	96% EtOH	1 h
5	96% EtOH	1 h
6	100% EtOH	1 h
7	100% EtOH	1 h
8	100% EtOH	1 h
9	Xylene	1 h
10	Xylene	1 h
11	Paraffin	1 h
12	Paraffin	1 h

Tissue sections of 6 μm were trimmed with a rotary microtome (Table 3), transferred to a floating bath, mounted on microscope slides (Table 7) and dried overnight at 37°C. The mounted tissue sections were rehydrated, stained and dehydrated in 16 steps using a multistainer (Table 32).

Table 32: Allocation of the multistainer

Step	Solution	Time
1	Xylene	3 min
2	Xylene	3 min
3	100% EtOH	2 min
4	96% EtOH	2 min
5	70% EtOH	1 min
6	Water	1 min
7	Hemalum	4 min
8	Water	2 min
9	Eosin	2 min
10	70% EtOH	1 min
11	96% EtOH	1 min
12	100% EtOH	1 min
13	100% EtOH	1.5 min
14	Xylene/EtOH	1.5 min
15	Xylene	2 min
16	Xylene	2 min

Determination of villus length

The determination of villus lengths was performed blinded. The length of a villus was defined as the distance between the tip of the villus and the centre of a virtual line marking the base of the villus. Per intestinal segment 10 villi were analyzed using a digital microscope (Table 3).

2.2.5 Immunohistochemistry

Preparation of primary colonic cell cultures

Primary colonic cell cultures were isolated and cultivated as described in 2.2.9, washed four times with 2 ml of '138 Buffer' (Table 17) and fixed with 4% formaldehyde solution in PBS (Table 9) for 12 min at room temperature. Afterwards, the cells were permeabilized with 0.5% saponin in PBS for 15 min.

Preparation of tissue

Tissues were fixed, dehydrated, embedded and trimmed as described in 2.2.4. Then the slides were placed in a rack and the tissues were deparaffinized and rehydrated at room temperature according to Table 33. For antigen retrieval, 1 l of citrate buffer (Table 16) was preheated and then slides were boiled for 20 min in a microwave at 1150 W (Table 3).

Table 33: Scheme for rehydration

Reagent	Concentration	Time
Xylol	100 %	2 x 5 min
Ethanol	100 %	2 x 5 min
Ethanol	100 %	1 x 2 min
Ethanol	96 %	2 x 2 min
Ethanol	80 %	2 x 2 min
Water		1 x 3 min

Immunofluorescence staining

Specimens were blocked in 1 % BSA in PBS for 30 min at room temperature and incubated with a combination of the primary antibody (Table 22) and 4',6-diamidino-2-phenylindole (DAPI, 1:250) diluted in PBS-T (0.05 % Tween-20) in a wet chamber over night at 4°C. After three washing steps in PBS for 3 min each, specimens were incubated with the secondary antibody diluted in PBS-T in the dark for 1 h at room temperature. Afterwards, slides were washed in PBS another three times, then mounted using fluorescent mounting medium and finally sealed with a cover slip. Specimens were examined using a confocal laser-scanning microscope (Table 3).

2.2.6 LC-MS/MS measurements

Extraction for bile acid analysis

Cecal content, feces and liver of mice fed a CD or a HFD were sampled and snap frozen. For extraction of bile acids from cecal contents and feces, samples were lyophilized for 8 h (Table 3) and ground. 20 mg of the samples were extracted twice with 800 μ l methanol. Samples were vortexed, shaken on a thermal shaker (Table 3) at 1000 rpm for 10 min at room temperature and centrifuged at 10000 x g for 30 min at room temperature. Afterwards, the supernatants of both extraction steps were pooled; the solvent was evaporated (Table 3) and samples were resolved in 1 ml of methanol. The extracts were diluted 1:50 in methanol. 50 μ l of the sample, 10 μ l bile acid internal standard mix (Table 20) and 50 μ l LCMS water were combined in a vial.

For extraction of bile acids from liver, 40 mg of powdered liver were mixed with 800 μ l methanol and shaken on a thermal shaker (Table 3) at 600 rpm for 10 min at room temperature. Samples were vortexed, spun down at 10000 x g for 5 min and supernatants were collected. The extraction step was repeated, supernatants were pooled and the methanol was evaporated (Table 3). Lipid extracts were resuspended in 800 μ l of methanol by shaking on a thermal shaker (Table 3) for 10 min at 40°C. 50 μ l of the sample, 10 μ l bile acid internal standard mix (Table 20) and 50 μ l LCMS water were combined in a HPLC vial. In order to prepare the standard curve in 7.5 μ l, 15 μ l, 75 μ l or 150 μ l of bile acid standard mix (Table 19), 10 μ l of deuterated internal standard mix (Table 20) and 500 μ l methanol were dried in vials. Finally, 50 μ l methanol and 50 μ l LCMS water were added.

LC-MS/MS measurement for bile acid analysis

10 μ l of bile acid extracts were injected in the LC system (Table 3) [132, 133]. A gradient (Table 34) of water (eluent A) and acetonitrile (eluent B) both containing 0.005% formic acid and 5 mM ammonium acetate was applied at a flow rate of 600 μ l/min to separate the bile acids by a reversed-phase separation (Table 3) at 40°C. The mass spectrometer (Table 3) operated in negative ion mode and the mass spectra of the analytes were recorded by scheduled multiple reaction monitoring. Analytes were quantified using the 'Analyst' Software (Table 4).

Table 34: Gradient for LC separation of bile acids

Total time [min]	Eluent A [%]	Eluent B [%]
0 -1	70	30
9-11	31	69
12-19	0	100
20-25	70	30

Extraction for C4 analysis

For 7 α -hydroxy-4-cholesten-3-one (C4) analysis the liver extract were further processed by adding 80 μ l of 100 ng/ml deuterated C4 standard solution, evaporated and resolved in 200 μ l hexane by shaking in a thermal shaker (Table 3) at 800 rpm for 10 min at 25°C. Afterwards, the samples were transferred to a new tube, centrifuged at 13000 x g for 10 min at 20°C and the supernatant transferred to a vial.

LC-MS/MS measurement for C4 analysis

10 μ l of C4 extracts were injected in the LC system (Table 3) [133]. A gradient (Table 35) of eluent A (water containing 0.005% formic acid and 5 mM ammonium acetate) and eluent B (70% acetonitrile and 30% isopropanol containing 0.005% formic acid and 2.5 mM ammonium acetate) was applied at a flow rate of 1000 μ l/min to separate the C4 by a reversed-phase separation (Table 3) at 40°C. The mass spectrometer (Table 3) operated in negative ion mode. Analytes were quantified using the 'Analyst' software (Table 4).

Table 35: Gradient for LC separation of C4

Total time [min]	Eluent A [%]	Eluent B [%]
0 -1	70	30
6-11	0	100
12-16	70	30

2.2.7 High-throughput 16S ribosomal RNA gene sequencing (carried out by Dr. Thomas Clavel, TUM)

Frozen fecal samples were processed, sequenced and analyzed by Dr. Thomas Clavel (Junior Research Group Intestinal Microbiome, ZIEL Institute for Food and Health, Technische Universität München, Freising-Weihenstephan, Germany) and Ilias Lagkourdos (Chair of Nutrition and Immunology, Technische Universität München, Freising-Weihenstephan, Germany), as described previously [134].

2.2.8 Plasma analysis

Plasma hormones and cytokines

6-weeks old C57BL/6N mice were fed a CD or HFD for 4 weeks. Prior to the experiment, animals were fasted for 2 h (8 a.m. to 10 a.m.) and then sacrificed by CO₂. The blood was collected from the heart by a 1 ml syringe with a 20 G cannula. Blood glucose levels were measured using a glucometer (Table 3). The collected blood was transferred to a blood collection tube coated with potassium-EGTA (Table 7). Additionally, 10 µl 'DPP IV Inhibitor' (Table 21) was added immediately after collection. The blood was placed on ice for 15 min and centrifuged at 1200 x g for 20 min at 4°C. Aliquots of the plasma were snap frozen in liquid nitrogen and stored at -80°C until further processing. Plasma hormone concentrations of GIP, GLP-1, GLP-2, insulin and IL-6 were analyzed by commercial kits according to manufacturer's instruction (Table 21).

Cholesterol and triglycerides

For lipid extraction, 40 mg of ground liver or 20-40 mg lyophilized and ground cecal content were mixed with 800 µl of chloroform. The homogenates were vortexed and shaken in a thermal shaker (Table 3) for 10 min at 1000 rpm at room temperature. Subsequently, 400 µl of methanol were added. The samples were vortexed, shaken in a thermal shaker (Table 3) at 1000 rpm for 10 min at room temperature and centrifuged for 5 min at 10000 x g. The lower phase was collected and evaporated. Finally, samples were resolved in 40 µl of ethanol. Cholesterol or triglyceride concentrations were analyzed in 3 µl of plasma or 3 µl of liver extract by commercial kits according to manufacturer's instruction (Table 21).

Endotoxin

Endotoxin levels in hepatic portal vein plasma were analyzed by the 'Limulus amoebocyte lysate chromogenic endpoint assay' (Table 21). Therefore, mice were sacrificed by an overdose of Isoflurane. Blood was removed from the *vena portae hepatis* by a 24 G cannula attached to a syringe flushed with sterile 200 mM EGTA solution. The blood was transferred to an endotoxin-free microcentrifuge tube (Table 7), kept on ice and within 10 min the sample was centrifuged for 10 min, 3000 x g at 4°C. Plasma (supernatant) was removed and stored at -80°C until further analysis. Plasma samples were diluted 1:10 in endotoxin-free water and 'PYROSPERSE™

Dispersing Agent' (Table 5) was added to each sample. Afterwards, the assay was performed according to manufacturer's instructions.

2.2.9 Primary colonic cell cultures

Isolation and cultivation of murine colonic crypts

Mice in the age of 10 weeks were sacrificed by cerebral dislocation; the colon was dissected, flushed and placed in a tissue culture dish filled with ice-cold PBS (Table 6). Afterwards, the tissue was chopped into 1 mm pieces with a scalpel, transferred to a 15 ml tube and washed three times with PBS (Table 6). The washing was followed by four digestion steps. In all steps 10 ml of 0.4 mg/ml collagenase solution in DMEM (Table 6) were added and the digestion took place in a water bath at 37°C. At the end of each digestion step, the tube was shaken for 30 sec and the tissue pieces were allowed to settle for 45 sec. After the first (10 min) and second (15 min) digestion period the supernatant was discarded, whereas the supernatants of the third (15 min) and fourth (15 min) period were collected. During the last two incubation steps the tube was given a short, vigorous shake every 5 min. Supernatants were centrifuged at 100 x g for 2 min. The pellet was resuspended in 10 ml 'culture medium' (DMEM, 10% FCS, 2 mM L-glutamine, 1 % penicillin/streptomycin) and centrifuged for 2 min at 100 x g. The suspension of digestion steps 3 and 4 were then combined, centrifuged for 2 min at 100 x g and resuspended in 3 ml of 'culture medium'. Enriched crypts were seeded on Matrigel[®]-coated (1:50) tissue culture test plates. For hormone secretion experiments or RNA isolation, crypts were dispensed on 12 wells of a 24-well plate (Table 7), each containing 500 µl 'culture medium'. For immunohistochemical analysis the crypt suspension was spread over 6 Matrigel[®]-coated cover slips (15 mm x 15 mm) placed in a 6-well plate. For calcium live cell imaging the crypt suspension was spread over 3 Matrigel[®]-coated round cover slips (ø 42 mm). Cover slips were placed in tissue culture dish (ø 53 mm) filled with 2 ml 'culture medium' each. The crypts were incubated for 24 h at 37°C and 5% CO₂.

Hormone secretion assay

After 24 h of cultivation, primary colonic cell cultures were washed three times with '138 Buffer' (Table 17) containing 0.1 % BSA. Then the cultures were stimulated with 200 µl of the respective effector solution and incubated at 37°C for 2 h. For baseline

secretion, cultures were stimulated with '138 Buffer' containing 0.1 % BSA. The following effectors were applied: 30 μ M of the primary bile acids cholic acid (CA) or chenodeoxycholic acid (CDCA), 30 μ M of the secondary bile acids deoxycholic acid (DCA) or lithocholic acid (LCA) and 1 mM of the short-chain fatty acid acetate or propionate. A mixture of 10 mM glucose, 10 μ M forskolin and 10 μ M 3-isobutyl-1-methylxanthine (IBMX) was used as positive control for obtaining maximal stimulation. Afterwards, supernatants were collected and centrifuged at 425 x g for 5 min at 4°C, transferred to new tubes, snap-frozen in liquid nitrogen and stored at -80°C until analysis of secreted hormones. The remaining cultures on the plate were immediately exposed to 500 μ l of 'Lysis buffer' (Table 18). After 20 min cultures were scraped of the culture plate and the cell suspensions were centrifuged and handled as mentioned above. Active GLP-1 was detected in supernatants and cell extracts by enzyme-linked immunosorbent assay (ELISA) (Table 21). For ELISA analysis extracts were diluted 1:8 in 'Assay buffer' (supplied by the manufacturer) and the assay was carried out according to manufactory's instructions. The amount of secreted GLP-1 was normalized to the amount of the entire GLP-1 (cell lysate + secreted) in each well.

Calcium live cell imaging

For measurement of intracellular calcium concentration the fluorescent calcium indicator fura-2 was applied. The excitation wavelength of fura-2 changes upon binding to calcium ions. To assess if DCA induces intracellular calcium signaling primary colonic cell cultures were isolated and cultivated as described before. Cultures grown for 24 h on round glass cover slips coated with Matrigel[®] (1:50) were washed three times with '138 Buffer' (Table 17) containing 10 mM glucose and inserted in the perfusion chamber (Table 3). Cells were loaded with 1 ml glucose-containing '138 Buffer' with 7 μ M fura-2AM, 0.01 % v/w pluronic F127, 375 μ M eserine (esterase inhibitor) and incubated in the dark for 15 min at 37°C, followed by 15 min at room temperature. After loading, the chamber was placed in the microscope stage of an inverted contrasting microscope (Table 3) which was surrounded by an incubator warming the air to 37°C during the experiment. Moreover, the chamber was connected to the perfusion system and the perfusion rate was set to 1 ml/min. Fura-2 was excited at 340 nm and 380 nm and the emission was measured at 510 nm as well. Afterwards, the 340 nm to 380 nm signal ratio was calculated by the 'Leica Application Suite' (Table 4) software.

In the beginning of the calcium live cell imaging, the system was flushed with glucose-containing '138 Buffer' until the 340/380 nm ratio was stable. Afterwards, 4 ml of 30 μ M, 50 μ M or 1 mM DCA solution was added. The change of the 340/380 nm ratio was washed out by 4 ml of glucose-containing '138 Buffer'. Finally, the system was flushed with 1 ml of 2 μ M ionomycin solution as positive control. The difference between maximal 340/380 nm ratio after stimulation with DCA and the 340/380 nm ratio at baseline was defined as Δ relative 340/380 nm ratio.

2.2.10 *Statistical analysis*

Statistical analysis was performed using GraphPad Prism 6. First data were tested for normal distribution. To evaluate diet and/or facility effects, unpaired two-tailed t-test, one-way or two-way ANOVA followed by appropriate *post hoc* test were applied. Differences were considered as significant if p-values were <0.05 (*), <0.01 (**), <0.001 (***) or 0.0001 (****). Data are represented as median or mean + SEM.

3 Results

3.1 Gut barrier integrity

In 2007, it was reported for the first time, that a high-fat diet (HFD) has the ability to impair gut barrier function [3]. The present study reports a more comprehensive analysis of whether gut barrier integrity is affected by fat content and fat source, by mouse strain and feeding period as well as by housing conditions.

3.1.1 Impact of different high-fat diets on gut barrier integrity in mice

3.1.1.1 Plant-based high-fat diets

Mouse models with different susceptibility to diet-induced obesity

Diet-induced obesity (DIO) in mouse models is usually induced by feeding diets rich in fatty acids leading to an appropriate expansion of adipose tissue. To investigate the influence of body fattening on colonic gut barrier integrity three mouse strains with different propensity to DIO were studied. AKR/J mice are prone to DIO, whereas SWR/J mice are resistant to DIO. C57BL/6J mice show an intermediate phenotype. These three mouse strains were exposed to a plant-based control diet (pCD) or a plant-based HFD with 48 kJ% from fat (pHFD48) in a specific pathogen-free (SPF) facility for 4 weeks. Concerning body mass, AKR/J mice gained about 10 g during the pHFD48 feeding intervention and C57BL/6J mice about 4 g. As expected SWR/J mice were resistant to body mass increase. The gain in body mass in AKR/J and C57BL/6J mice fed a pHFD48 could be attributed to a distinct expansion of fat mass compared to the corresponding control animals. Moreover, pHFD feeding impaired the oral glucose tolerance in AKR/J and C57BL/6J but not in SWR/J mice (Data Caroline Kless, [135]).

Electrophysiological measurements of tissue resistance as well as marker permeability in Ussing revealed no changes in none of the strains when fed the pHFD48. AKR/J, C57BL/6J and SWR/J showed strain-specific differences in colonic barrier characteristics. In proximal colonic tissue of DIO-prone AKR/J mice a lower transepithelial resistance ($36.2 \pm 2.0 \Omega \text{ cm}^2$) was observed compared to C57BL/6J mice ($43.8 \pm 2.2 \Omega \text{ cm}^2$, $p < 0.05$) and SWR/J mice ($43.3 \pm 1.6 \Omega \text{ cm}^2$, $p < 0.05$). In distal colon of AKR/J mice transepithelial resistance was reduced compared to the two

other strains as well ($p < 0.01$). Moreover, reduced transepithelial resistance in the AKR/J mice was accompanied by an elevated permeability ($1.14 \pm 0.07 \cdot 10^{-6} \text{ cm/s}$) compared to C57BL/6J mice ($0.54 \pm 0.06 \cdot 10^{-6} \text{ cm/s}$, $p < 0.0001$) and SWR/J ($0.50 \pm 0.06 \cdot 10^{-6} \text{ cm/s}$, $p < 0.0001$) mice in the distal colonic tissue (Figure 5). As in none of the strains the colonic gut barrier integrity was affected by HFD intervention the intermediate phenotype C57BL/6J was chosen for further analyses.

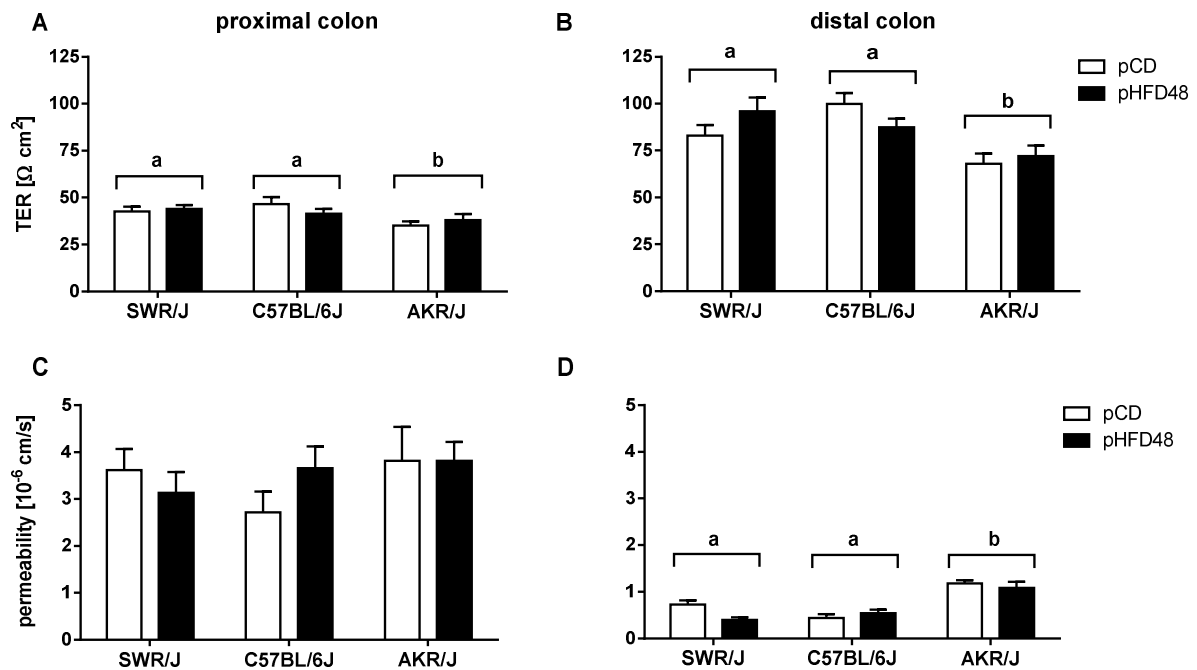


Figure 5: Transepithelial resistance and permeability of colonic tissue from mouse strains with different susceptibilities to diet-induced obesity. SWR/J, C57BL/6J and AKR/J mice were fed a control diet (pCD, 13 kJ% fat) or a plant-based high-fat diet (pHFD48, 48 kJ% fat) in a specific pathogen-free animal facility for 4 weeks. Transepithelial resistance (TER) of (A) proximal and (B) distal colon and permeability of fluorescein through the (C) proximal and (D) distal colonic tissue were determined in Ussing chambers. Data are represented as means + SEM. Statistical analysis was performed using two-way ANOVA with Tukey's post-hoc test. Data with different letters were significantly different at least $p < 0.05$. $n = 5-10$ mice per group.

RESULTS

Feeding period and fat content

To study whether DIO causes changes in barrier function in a time-dependent manner C57BL/6J mice were fed a pHFD48 or the corresponding pCD in a SPF animal facility for 1, 4, 8 or 12 weeks. Afterwards, the colonic barrier function was assessed *ex vivo* in Ussing chambers. Neither transepithelial resistance nor the permeability of fluorescein was found altered in proximal and distal colon among the pHFD and pCD groups over time (Figure 6).

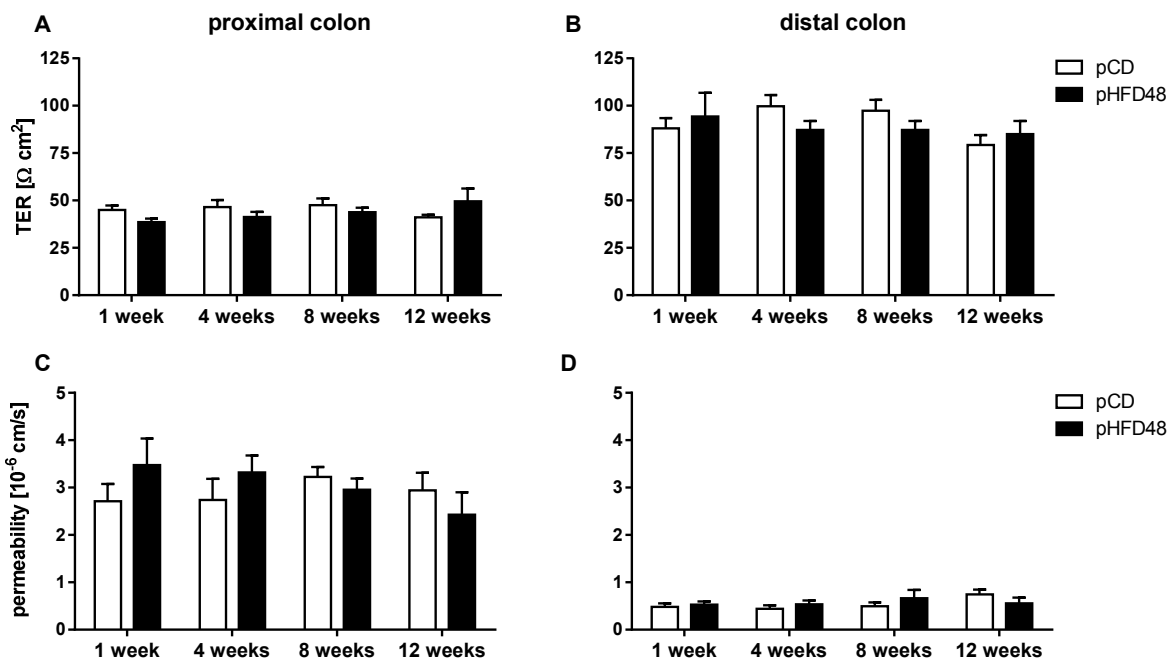


Figure 6: Transepithelial resistance and permeability of murine colonic tissues upon different high-fat feeding periods. C57BL/6J mice were fed either a control diet (pCD, 13 kJ% fat) or a plant-based high-fat diet (pHFD48, 48 kJ% fat) in a specific pathogen-free animal facility for 1, 4, 8 or 12 weeks. Transepithelial resistance (TER) of (A) proximal and (B) distal colon and permeability of fluorescein through the (C) proximal and (D) distal colonic tissue were determined in Ussing chambers. Data are represented as means + SEM. Statistical analysis was performed using two-way ANOVA with Tukey's post-hoc test. n = 4-7 mice per group.

In addition to colonic tissue, the upper part of the intestine was analyzed for functional impairment. C57BL/6J mice were fed either a pHFD48 or pCD for 24 weeks. It turned out that even after long-term HFD intervention the barrier markers transepithelial resistance and permeability of fluorescein in the small and large intestine remained unaltered between groups (Figure 7). Comparing the transepithelial resistance of different intestinal regions regardless of dietary intervention: the distal colon showed higher values compared to the jejunum

(distal colon $69.8 \pm 5.4 \Omega \text{ cm}^2$ vs. jejunum $42.1 \pm 4.5 \Omega \text{ cm}^2$, $p < 0.0001$), distal ileum (distal colon $69.8 \pm 5.4 \Omega \text{ cm}^2$ vs. distal ileum $29.63 \pm 1.2 \Omega \text{ cm}^2$, $p < 0.0001$) and proximal colon (distal colon $69.8 \pm 5.4 \Omega \text{ cm}^2$ vs. proximal colon $43.1 \pm 1.3 \Omega \text{ cm}^2$, $p < 0.0001$). Highest permeability was detected in jejunum ($6.28 \pm 0.01 \cdot 10^{-6} \text{ cm/s}$) and the lowest in the distal part of the large intestine ($0.64 \pm 0.04 \cdot 10^{-6} \text{ cm/s}$).

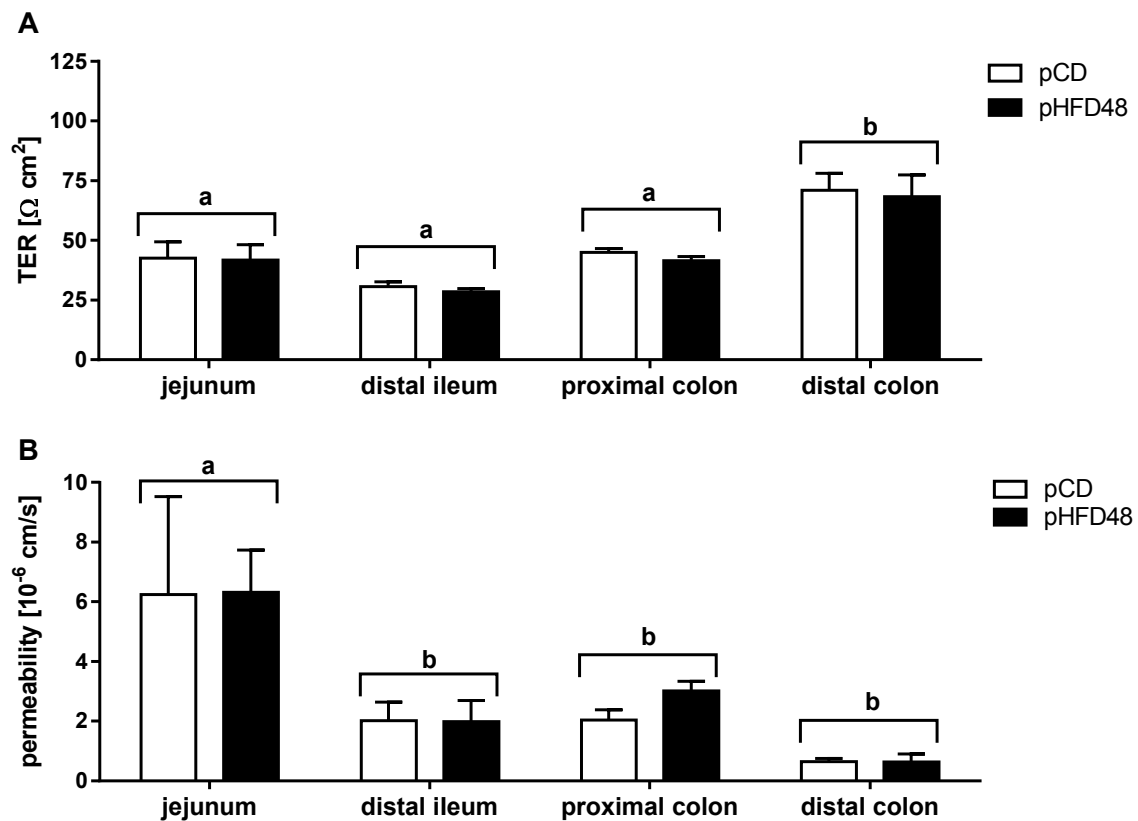


Figure 7: Transepithelial resistance and permeability of murine small and large intestine subsequent to long-term high-fat diet intervention. C57BL/6J mice housed in a specific pathogen-free animal facility were exposed either to a control diet (pCD, 13 kJ% fat) or a plant-based high-fat diet (pHFD48, 48 kJ% fat) for 24 weeks. Intestinal barrier function was assessed by measuring (A) transepithelial resistance (TER) and (B) permeability of fluorescein in small and large intestine. Data are represented as means + SEM. Statistical analysis was performed using two-way ANOVA with Tukey's post-hoc test. Data with different letters were significantly different at least $p < 0.05$. $n = 3-6$ mice per group.

Most of the published studies reporting impaired gut barrier integrity due to high-fat feeding used diets with at least 60 kJ% derived from fat [2, 3, 136]. We thus applied a plant-based high-fat diet with 61 kJ% fat (pHFD61). C57BL/6J mice were fed pHFD61 for either 4 or 12 weeks. However, the barrier indicators transepithelial

RESULTS

resistance and permeability of fluorescein remained unaltered between pCD and pHFD61 groups in the small and large intestine (Table 36).

Table 36: Transepithelial resistance and permeability of murine small and large intestine subsequent to increased fat proportion in the high-fat diet to 61 kJ% fat.

Gut section	Feeding period	Transepithelial resistance [$\Omega \text{ cm}^2$]		Permeability [10^{-6} cm/s]	
		pCD	pHFD61	pCD	pHFD61
Jejunum	4 weeks	35.8±2.8	29.7±2.9	6.7±1.2	7.8±3.0
	12 weeks	27.6±1.3	35.8±2.9	10.6±1.8	9.2±3.6
Distal colon	4 weeks	60.8±4.8	62.4±2.6	1.2±0.4	1.8±0.5
	12 weeks	69.2±5.1	61.1±6.5	1.9±1.2	0.7±0.2

Taken together, independent of duration and fat proportion of the plant-based HFD intervention no barrier dysfunction neither in small nor in large intestine could be observed *ex vivo* in C57BL/6J mice housed in the SPF facility.

3.1.1.2 Animal-based high-fat diets

Lard-based high-fat diets with varying fat proportions

Since plant-based HFDs did not affect gut barrier, we next studied the effects of animal-based HFDs with varying fat contents. At the age of 12 weeks mice were exposed to a plant-based control diet (pCD, 13 kJ% fat), a lard-based control diet (ICD, 13 kJ% fat) or lard-based high-fat diet with increasing fat content starting from 48 kJ% fat (IHFD48) raised to 75 kJ% fat (IHFD75) and 78 kJ% fat as a carbohydrate-free variant (IHFD78^{cf}) for 4 weeks in a SPF animal facility. At the end of the feeding period, mice of the IHFD48 and IHFD75 groups gained significantly more weight than the mice in the ICD group. In contrast, mice in the HFD78^{cf} group responded with the smallest increase in body mass. However, mice receiving HFD based on animal fat developed impaired glucose tolerance within 4 weeks (Data Caroline Kless, [135]). On the contrary, the lard-based HFDs evoked no alterations of the electrical resistance in small and large intestinal tissues assessed in Ussing chambers. Moreover, permeability of fluorescein also remained unaltered, except that an increased jejunal permeability was observed for the HFD78^{cf} group (Figure 8). Endotoxin level were measured in portal vein plasma, but no changes were induced by the lard-based diets (Data Valentina Schüppel, [135]). In summary, neither a

plant- nor an animal-based HFD caused a deterioration of the intestinal barrier of mice housed in an SPF facility.

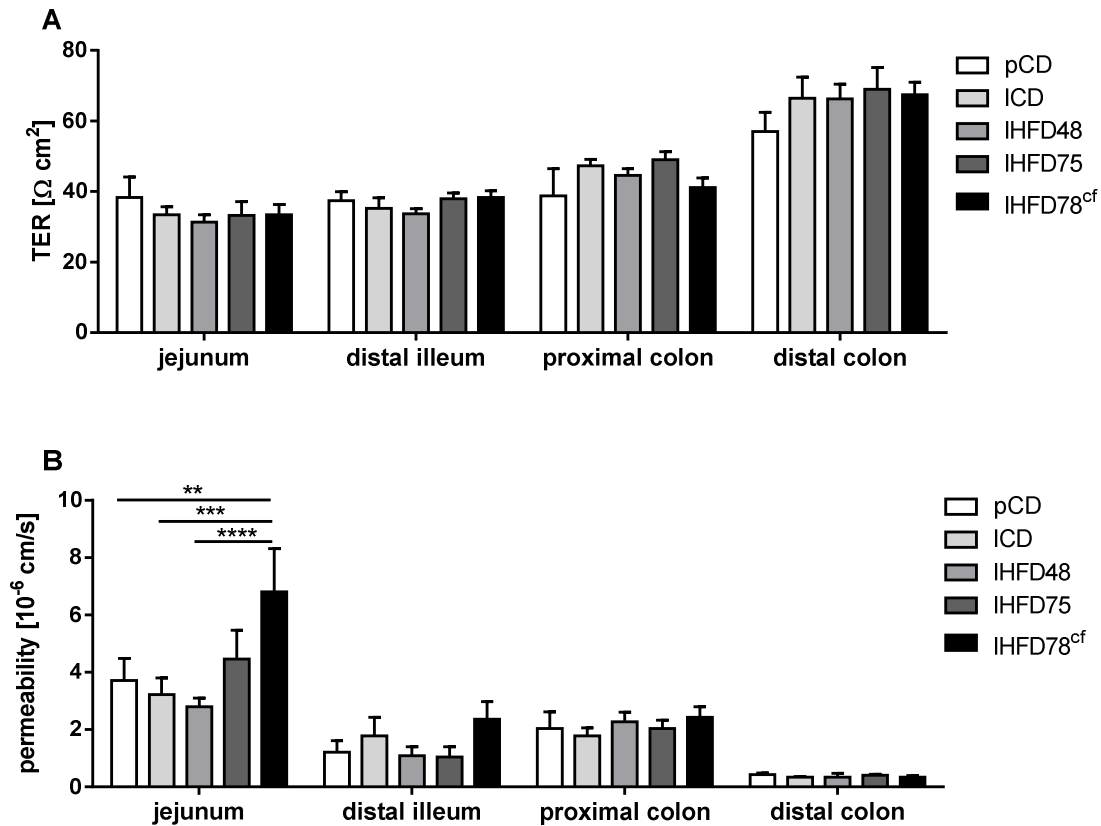


Figure 8: Transepithelial resistance and permeability of murine small and large intestine subsequent to a feeding trail with increasing fat proportion in the diet. C57BL/6J mice were fed a plant-based control diet (pCD, 13 kJ% fat), a lard-based control diet (ICD, 13 kJ% fat) or a lard-based high-fat diet with increasing fat content starting from 48 kJ% fat (IHFD48) to 75 kJ% fat (IHFD75) to 78 kJ% fat which was carbohydrate-free (IHFD78^{cf}) for 4 weeks. The intestinal barrier function was assessed by measuring the (A) transepithelial resistance (TER) and (B) permeability of fluorescein in the jejunum, distal ileum and colon. Data are represented as means + SEM. Statistical analysis was performed using two-way ANOVA with Tukey's post-hoc test. ** $p < 0.01$, *** $p < 0.001$, **** $p < 0.0001$. $n = 4-6$ mice per group.

RESULTS

Beef tallow-based high-fat diet in different animal facilities

In addition to palm oil and lard also a beef-tallow based HFD was employed and it was studied how it could affect intestinal barrier integrity. 10-weeks old C57BL/6N mice were exposed to a control (CD) or a beef tallow-based high-fat diet (HFD, 60 kJ% fat) either in a SPF or a conventional (CV) facility for 12 weeks. Gut barrier function was assessed by transepithelial resistance and of fluorescein isothiocyanate–dextran (FITC-dextran, average MW 3,000-5,000 g/mol) permeability in tissue samples, whereas translocation of bacterial components was assessed *in vivo*. Barrier function of DIO mice housed in the SPF facility remained unchanged after 12 weeks of feeding (Figure 9).

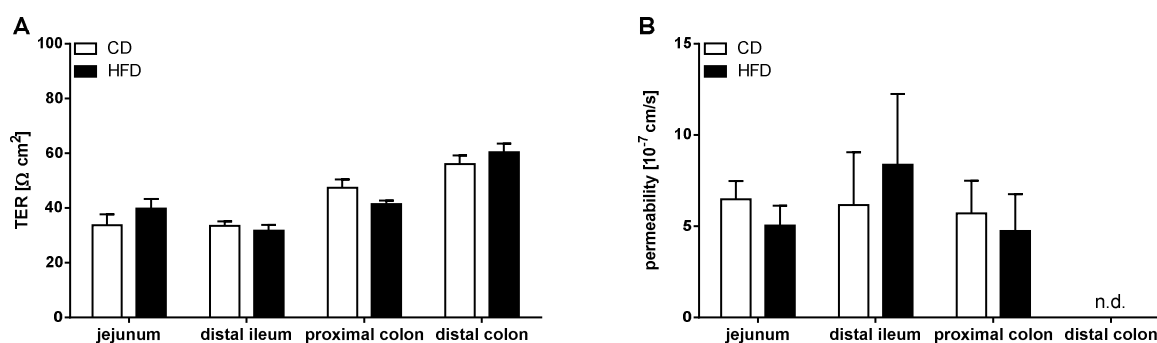


Figure 9: Transepithelial resistance and permeability of murine small and large intestine subsequent to housing in a specific pathogen-free animal facility. C57BL/6N mice were fed a control diet (CD, 11 kJ% fat) or a beef tallow-based high-fat diet (HFD, 60 kJ% fat) for 12 weeks. (A) Transepithelial resistance (TER) and (B) permeability of FITC-dextran (average MW 3,000-5,000 g/mol) were determined in Ussing chambers. Data are represented as means + SEM. Statistical analysis was performed using two-way ANOVA with Sidak's post-hoc test. n = 4-12 mice per group.

In contrast to findings from animals housed in the SPF facility, tissues of HFD mice housed in the CV facility had a significantly decreased transepithelial resistance in the jejunum (CD $55.2 \pm 4.2 \Omega \text{ cm}^2$ vs. HFD $38.4 \pm 4.2 \Omega \text{ cm}^2$, $p < 0.01$) and in proximal colon (CD $53.8 \pm 3.1 \Omega \text{ cm}^2$ vs. HFD $40.5 \pm 1.6 \Omega \text{ cm}^2$, $p < 0.05$) compared to the respective control animal. The permeability of FITC-dextran through the gut wall of the jejunum, proximal and distal colon, tended to be elevated in mice fed a HFD but did not reach significance (Figure 10).

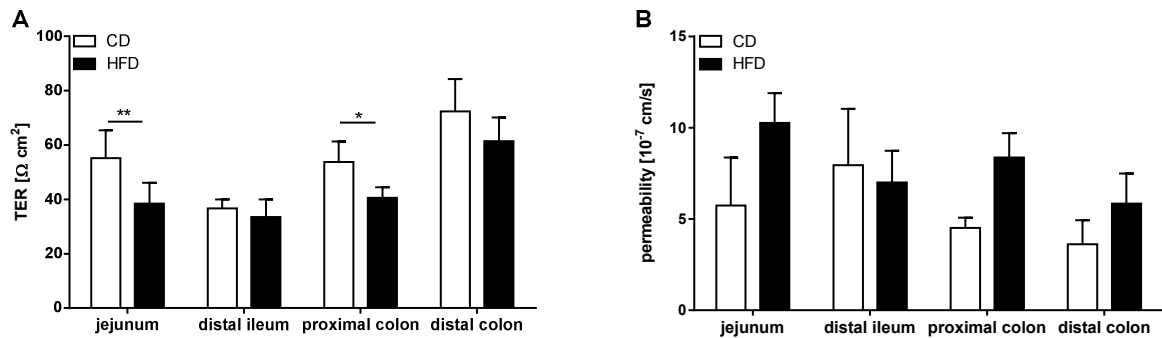


Figure 10: Transepithelial resistance and permeability of murine small and large intestine subsequent to housing in a conventional animal facility. C57BL/6N mice were fed a control diet (CD, 11 kJ% fat) or a beef tallow-based high-fat diet (HFD, 60 kJ% fat) for 12 weeks. (A) Transepithelial resistance (TER) and (B) permeability of FITC-dextran (average MW 3,000-5,000 g/mol) were determined in Ussing chambers. Data are represented as means + SEM. Statistical analysis was performed using two-way ANOVA with Sidak's post-hoc test. * $p < 0.05$, ** $p < 0.01$. $n = 4-6$ mice per group.

Analysis of plasma endotoxin levels of mice fed a CD or HFD in the SPF facility failed to detect any differences, whereas DIO mice housed in the CV facility had threefold increased endotoxin concentration compared to the respective CD group (Figure 11). Taken together these findings, a HFD based on beef tallow caused discrete gut barrier dysfunction in CV- but not SPF-housed C57BL/6N mice.

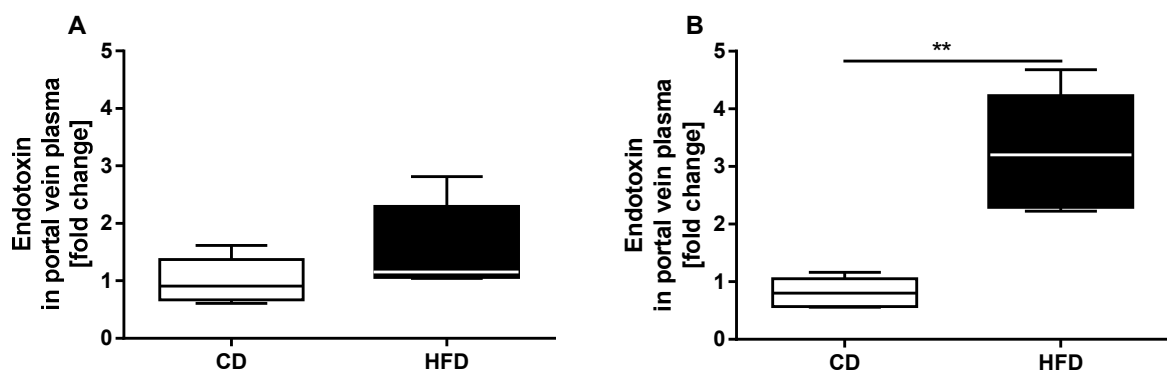


Figure 11: Changes of endotoxin in portal vein plasma due to diet and animal housing. Fold change of endotoxin in control diet (CD, 11 kJ% fat) or beef tallow-based high-fat diet (HFD, 60 kJ% fat) fed mice. The feeding trials were carried out either in a (A) specific pathogen-free or (B) conventional animal facility. Data are represented as median. Statistical analysis was performed using unpaired t-test with Welch's correction. ** $p < 0.01$. $n = 5$ mice per group.

3.1.2 Impairments in mice fed the beef tallow-based high-fat diet

In addition to assessing intestinal integrity in animals fed the beef tallow-based HFD in the conventional animal facility, inflammation markers in liver and adipose tissue, intestinal morphology, tight junction protein expression and distribution, cecal microbial diversity and composition, and the pattern of fecal bile acids were determined.

3.1.2.1 Inflammation markers in adipose tissue and liver

DIO is often associated with low-grade inflammation [2, 137]. To investigate the inflammatory tone after 12 weeks of dietary treatment in the two animal facilities, transcript levels of different pro-inflammatory cytokines/chemokines were measured. Expression levels of tumor necrosis factor (*Tnf*) and Interleukin-1 beta (*Il-1 β*) were analyzed in liver and adipose tissue. Additionally, serum amyloid A (*Saa*) in liver and monocyte chemoattractant protein-1 (*Mcp-1*) in adipose tissue were selected as markers. In liver, there were no changes in transcript levels of *Saa* and the pro-inflammatory cytokines irrespective of diet and housing conditions (Figure 12). In adipose tissue mRNA levels of *Tnf* ($p < 0.05$) and *Mcp-1* ($p < 0.0001$) were significantly increased in CV DIO mice compared to the respective controls. In contrast, mice fed a HFD but housed in the SPF facility had no changes in inflammatory markers in comparison to the corresponding controls. All transcript levels of the CD groups in both facilities were comparable. Interestingly, DIO mice displayed a higher *Mcp-1* expression ($p < 0.0001$) in adipose tissue in CV compared to SPF conditions (Figure 12).

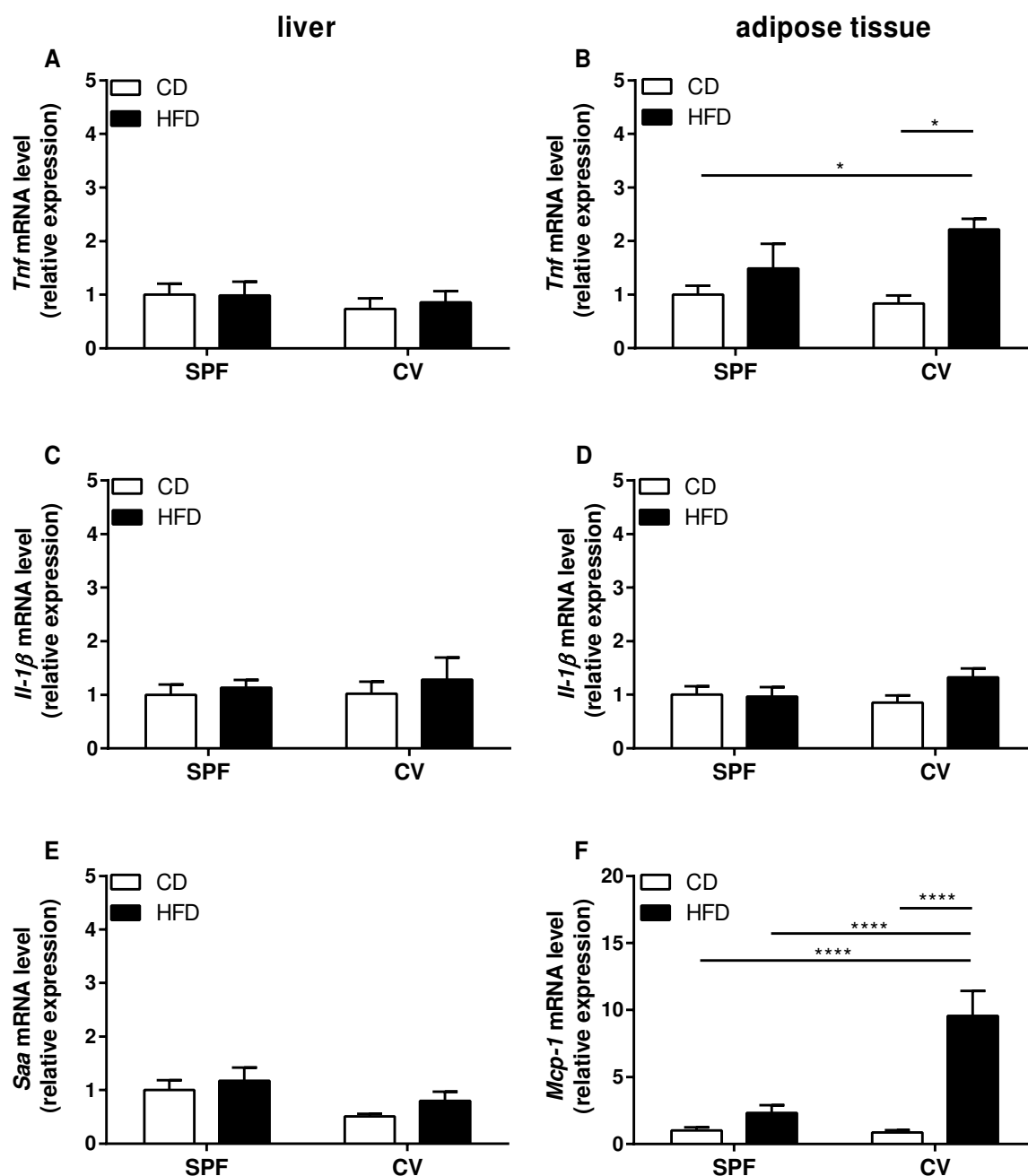


Figure 12: Transcription levels of inflammatory marker genes in liver and adipose tissue in response to a high-fat diet under different housing conditions. C57BL/6N mice were housed in a specific pathogen-free (SPF) or conventional (CV) animal facility and fed a control (CD, 11 kJ% fat) or beef tallow-based high-fat diet (HFD, 60 kJ% fat) for 12 weeks. In both, liver and adipose tissue transcript levels of (A and B) tumor necrosis factor (*Tnf*) and (C and D) interleukin-1 β (*Il-1 β*) were analyzed. Additionally, (E) serum amyloid A (*Saa*) in the liver and the (F) monocyte chemotactic protein 1 (*Mcp-1*) were determined in adipose tissue. Transcript levels of the inflammatory markers were normalized to *Gapdh* and *Hprt*. Data are represented as means + SEM. Statistical analysis was performed using two-way ANOVA with Tukey's post-hoc test. * $p < 0.05$, **** $p < 0.0001$. $n = 4-6$ mice per group.

RESULTS

3.1.2.2 Body mass and intestinal morphology

In both facilities, CV and SPF, after 12 weeks of diet treatment body mass of mice was significantly higher in HFD group compared to the CD group (SPF: CD 27.1±0.7 g vs. HFD 40.9±1.8 g, $p<0.0001$; CV: CD 29.0±0.9 g vs. HFD 38.0±1.0 g, $p<0.001$). The CD and HFD groups did not display significant differences between facilities. The length of the small and large intestine was not different between diet arms or facilities (Table 37).

Table 37: Body mass and intestinal length

	Facility	Diet	
		CD	HFD
Body mass [g]	SPF	27.1±0.7 ^a	40.9±1.8 ^b
	CV	29.0±0.9 ^a	38.0±1.0 ^b
Length			
Small intestine [cm]	SPF	33.3±0.5	33.8±0.4
	CV	32.7±0.7	32.8±0.3
Large intestine [cm]	SPF	7.3±0.3	7.7±0.3
	CV	6.9±0.2	7.0±0.2

Nutritional factors are known to cause adaptive changes in the architecture of the intestine [138, 139]. Hence the influence of a HFD on villus lengths in jejunum and ileum was assessed, but no differences between HFD and CD groups in both facilities were found (Table 38).

Table 38: Height of villi in small intestine

Gut section	Facility	Villus length [µm]	
		CD	HFD
Jejunum	SPF	420±16	424±13
	CV	471±16	433±16
Ileum	SPF	277±28	244±21
	CV	234±22	201±21

GLP-2 is a potent stimulator of intestinal growth, whereas IL-6 is involved in the inhibition of intestinal epithelial cell death [138, 140]. Both markers remained unaltered between mice fed a CD vs. HFD, housed in the CV facility (Figure 13).

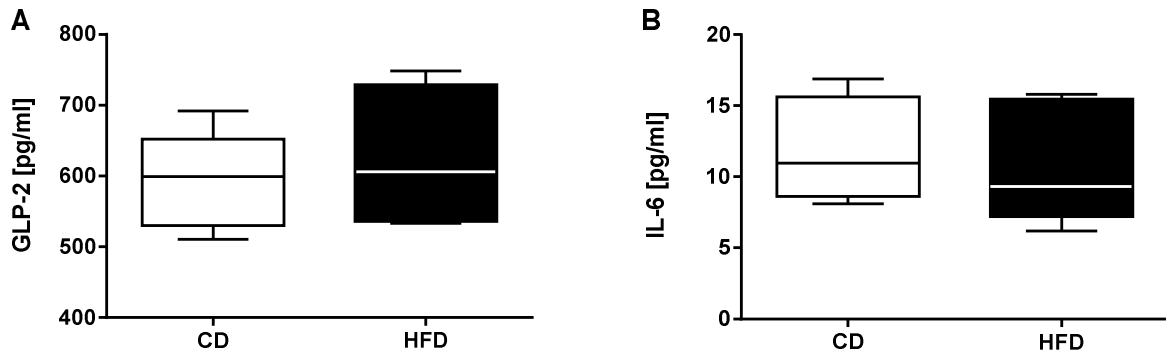


Figure 13: Plasma levels of GLP-2 and IL-6 in response to high-fat diet. C57BL/6N mice were housed in a conventional animal facility and fed a control (CD, 11 kJ% fat) or beef tallow-based high-fat diet (HFD, 60 kJ% fat) for 12 weeks. The plasma level of (A) glucagon-like peptide-2 (GLP-2) and (B) interleuin-6 (IL-6) were analyzed. Data are represented as median. Statistical analysis was performed using unpaired t-test. n = 4-5 mice per group.

RESULTS

3.1.2.3 Tight junction and scaffold proteins

Loss of barrier function is associated with a decrease of transepithelial resistance and an increase of permeability and this is accompanied by an alteration of tight junction proteins [3]. Therefore the expression of the tight junction proteins occludin, junctional adhesion molecule A (JAM-A), claudin-2, claudin-3 and claudin-5 as well as the tight junction associated protein zonula occludens-1 (ZO-1) were quantified in jejunal and colonic tissues of C57BL/5N mice fed a CD or a HFD in two different animal facilities. Regardless of the facility, there were no alterations in the expression levels occludin and JAM-A (Figure 14) or any of the claudins (Figure 15) or the scaffold protein ZO-1 (Figure 16) between mice fed a CD or HFD.

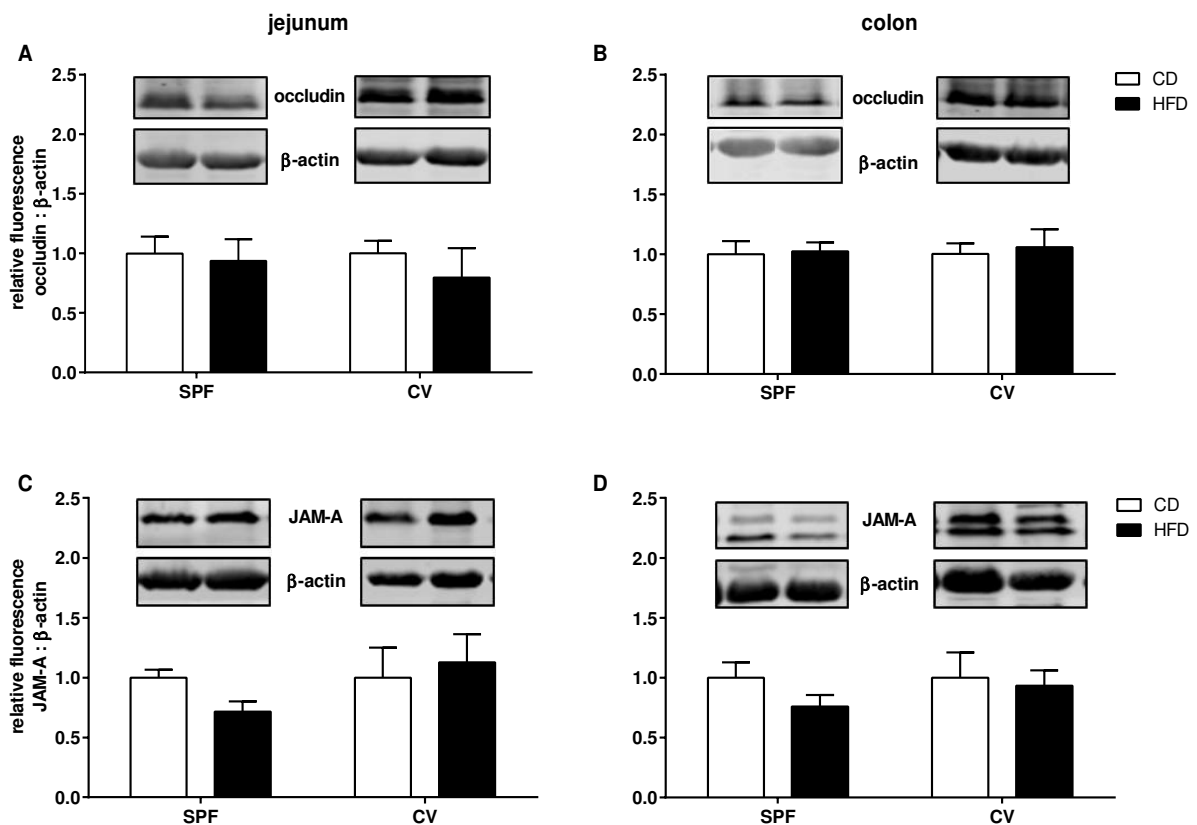


Figure 14: Jejunal and colonic protein expression levels of occludin and JAM-A in response to high-fat diet under different housing conditions. C57BL/6N mice were housed in a specific pathogen-free (SPF) or conventional animal (CV) facility and fed a control (CD, 11 kJ% fat) or beef tallow-based high-fat diet (HFD, 60 kJ% fat) for 12 weeks. There were no changes between the CD and HFD groups neither for occludin in the (A) jejunum and in the (B) colon nor for junctional adhesion molecule A (JAM-A) in the (C) jejunum and in the (D) colon. The proteins were isolated from the membrane and normalized to β -actin. Data are represented as means + SEM. Statistical analysis was performed with unpaired two-tailed t-test. n = 4-6 mice per group.

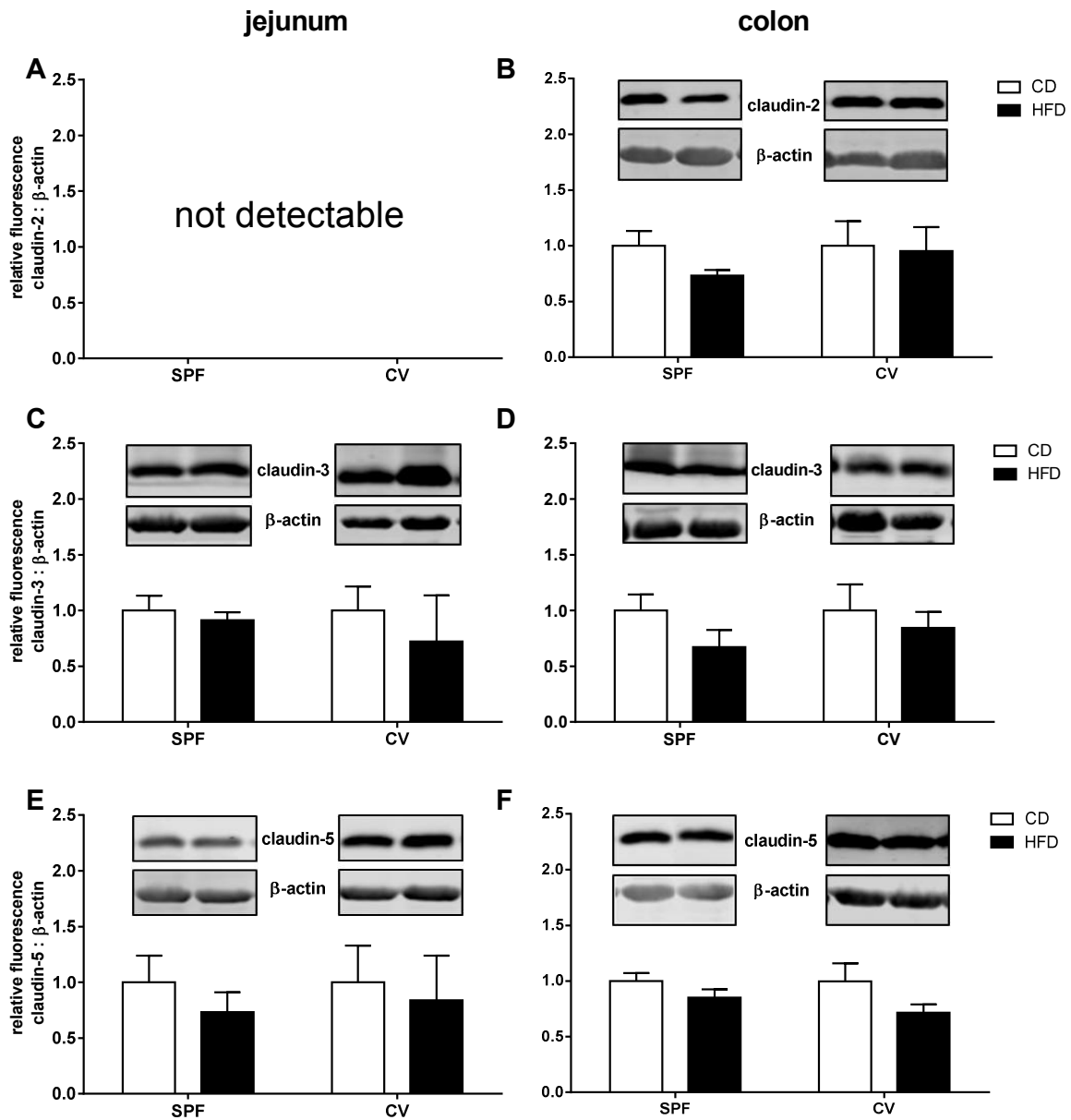


Figure 15: Jejunal and colonic protein expression levels of claudin-2, -3 and -5 in response to high-fat diet under different housing conditions. C57BL/6N mice were housed in a specific pathogen-free (SPF) or conventional (CV) animal facility and fed a control (CD, 11 kJ% fat) or beef tallow-based high-fat diet (HFD, 60 kJ% fat) for 12 weeks. There were no changes between the CD and HFD groups neither in the (A,C and E) jejunum nor in the (B,D and F) colon. All target proteins were normalized to β -actin. Data are represented as means + SEM. Statistical analysis was performed with unpaired two-tailed t-test. n = 4-6 mice per group.

RESULTS

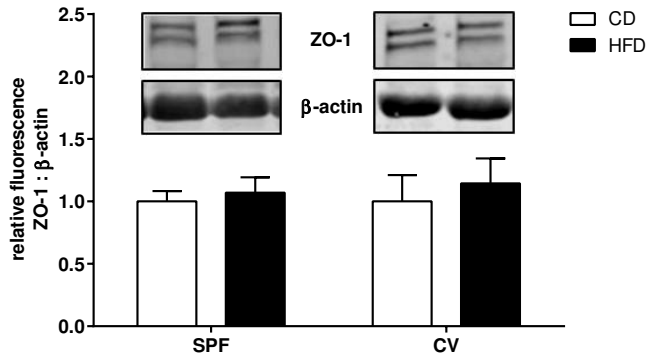


Figure 16: Colonic expression levels of ZO-1 in response to high-fat diet under different housing conditions. C57BL/6N mice were housed in a specific pathogen-free or conventional animal facility and fed a control (CD, 11 kJ% fat) or beef tallow-based high-fat diet (HFD, 60 kJ% fat) for 12 weeks. ZO-1 expression was normalized to β -actin. Data are represented as means + SEM. Statistical analysis was performed with unpaired two-tailed t-test. n = 4-6 mice per group.

Although by western blotting no obvious alterations in the protein expression of tight junction proteins after 12 weeks of diet treatment were detected, the localization and distribution of claudin-3 and claudin-5 was inspected next. In sections of jejunum and colon, HFD did not cause any obvious change in distribution of the tight junction proteins claudin-3 and claudin-5 (Figure 17).

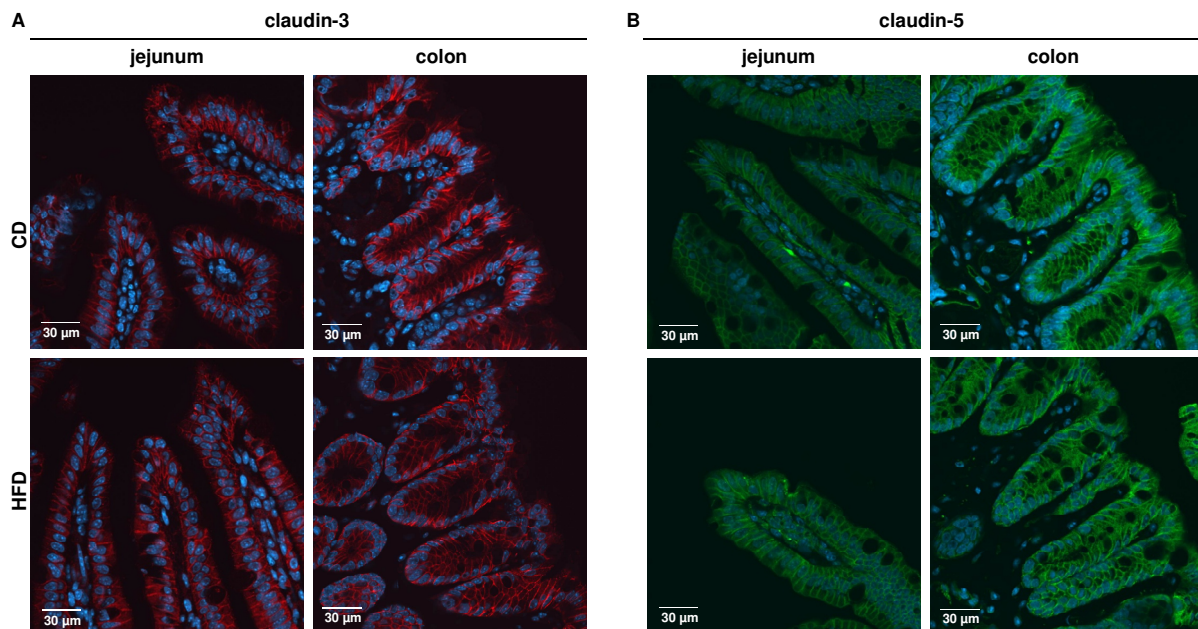


Figure 17: Immunolocalization of the tight junction proteins claudin-3 (red) and claudin-5 (green) in murine jejunum and colon in response to high-fat diet. Nuclei were stained with DAPI (blue). The sections were obtained from C57BL/6N mice housed in a conventional animal facility and fed a control (CD, 11 kJ% fat) or beef tallow-based high-fat diet (HFD, 60 kJ% fat) for 12 weeks. Microscopic fluorescence images of (A) claudin-3 and (B) claudin-5.

3.1.2.4 Gut microbiota

It is known that diet [81-83] and/or housing conditions of mice [141] can modify the intestinal microbiota signature. Since phenotypic differences in gut barrier integrity between mice housed in the two facilities were observed, the intestinal colonization of the mice was determined by high-throughput 16S rRNA gene sequencing. In the fecal samples a total of 91 operating taxonomic units (OTUs) with a relative abundance above 0.5% in at least one sample were determined. The microbial diversity between the samples (*beta*-diversity) indicated clear differences of the molecular species among the animals fed HFD and CD, irrespective of the facility. Whereas the phylogenetic make-up of CD mice of both facilities overlapped, the *beta*-diversity in the molecular species of DIO mice allowed an assignment to the housing condition (Figure 18A).

Concerning taxonomic composition at phylum level the relative sequence abundance of *Bacteroidetes* was decreased in the HFD groups compared to the control groups regardless of housing conditions. This decrease was mainly due to a sharp decline in *Porphyromonadaceae* and was accompanied by an increased sequence proportion in *Firmicutes*, reflected by a higher relative sequence abundance of the two main families of this phylum: *Lachnospiraceae* and *Ruminococcaceae* (Figure 18B). Regarding the different animal facilities, HFD mice in the CV facility had a higher number of molecular species and a lower relative abundance of *Bacteroidaceae* compared to HFD mice in the SPF facility.

Moreover, 19 OTUs were significantly altered by diet and/or housing conditions (Figure 18C). HFD was associated with the presence of the bile acid-dehydroxylating *Clostridium scindens*, regardless of the animal facility. Furthermore, the occurrence of 7 OTUs such as *Flavonifractor*, *Robinsoniella* and *Parabacteroides* species was related to CV mice fed a HFD.

RESULTS

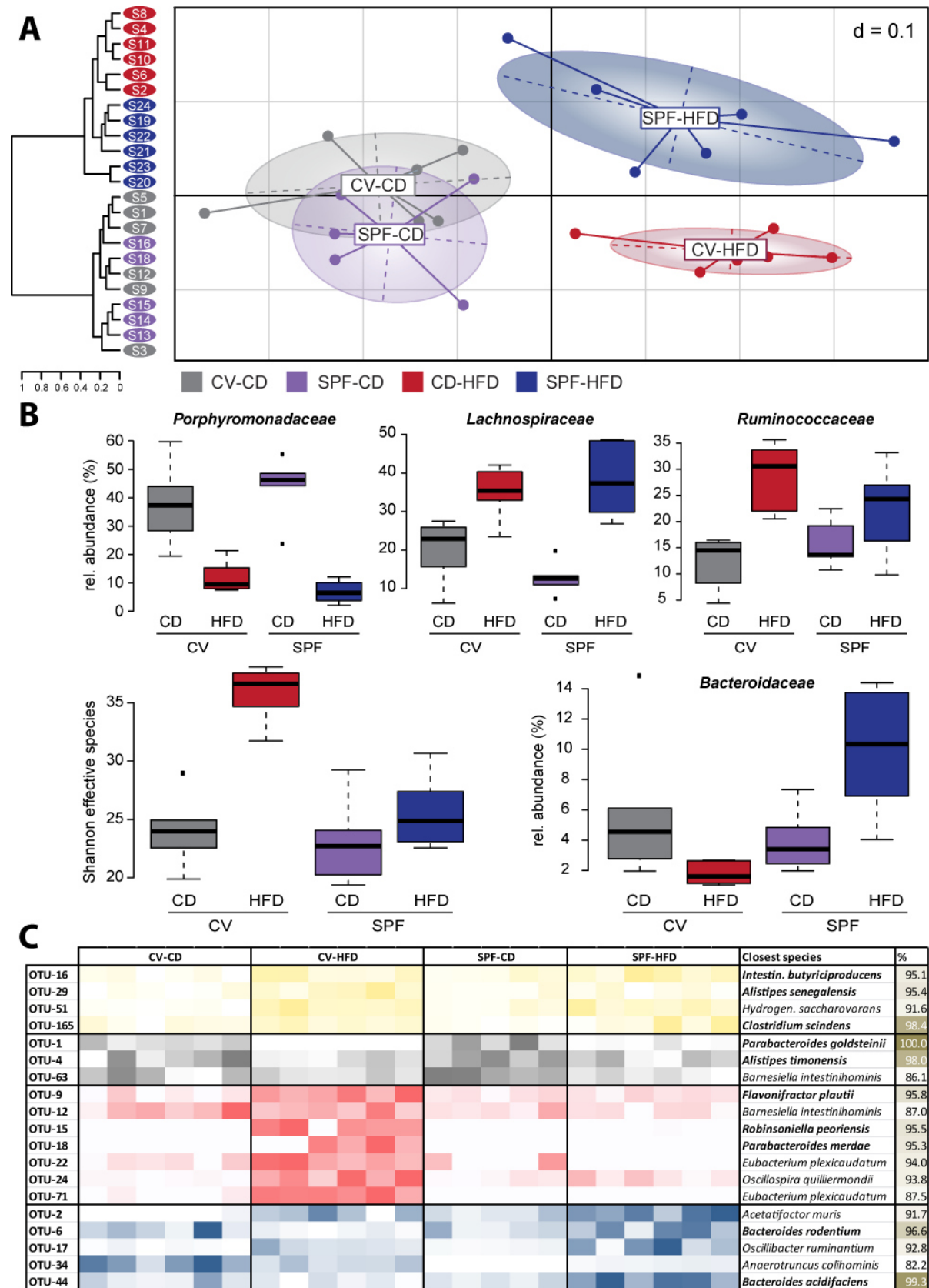


Figure 18: Fecal gut microbiota composition due to diet and housing. C57BL/6N mice were either housed in a specific pathogen-free (SPF) or conventional (CV) animal facility and were fed a control (CD, 11 kJ% fat) or beef tallow-based high-fat diet (HFD) for 12 weeks. (A) Multidimensional scaling showing diversity between samples (beta-diversity). (B) Box plots showing alpha-diversity and relative abundance of taxonomic groups. (C) Heatmap of OTU abundances those were significantly different between groups.

3.1.2.5 Bile acids in cecal content

As bile acids are required for dietary fat absorption the bile acid pool size is increased by HFD and more bile acids are excreted in response to a diet rich in dietary fat [112, 113]. The primary bile acids cholic acid (CA), chenodeoxycholic acid (CDCA), α -muricholic acid (α MCA) and β -muricholic acid (β MCA) as well as the secondary bile acids deoxycholic acid (DCA), lithocholic acid (LCA) and ω -muricholic acid (ω MCA) were analyzed in cecal samples by HPLC-MS/MS to assess whether housing conditions, diet and associated changes in microbial colonization alter also cecal bile acid patterns. When considering the diet, in both facilities the primary bile acid β MCA (SPF: CD 4621 \pm 919 nmol/g content vs. HFD 7889 \pm 930 nmol/g content, $p < 0.001$; CV: CD 2237 \pm 622 nmol/g content vs. HFD 4876 \pm 1008 nmol/g content, $p < 0.01$) and the secondary bile acid DCA (SPF: CD 5722 \pm 1340 nmol/g content vs. HFD 8729 \pm 895 nmol/g content, $p < 0.001$; CV: CD 3342 \pm 652 nmol/g content vs. HFD 10954 \pm 498 nmol/g content, $p < 0.0001$) were significantly increased in DIO mice compared to the corresponding controls (Figure 19). In addition, under CV conditions ω MCA was significantly elevated in the HFD group ($p < 0.01$). Moreover, the difference between cecal DCA concentration of DIO mice and respective controls was significantly increased in the CV facility compared to the SPF facility (SPF 3007 \pm 898 nmol/g content vs. HFD Δ 7612 \pm 498 nmol/g content, $p < 0.0001$).

RESULTS

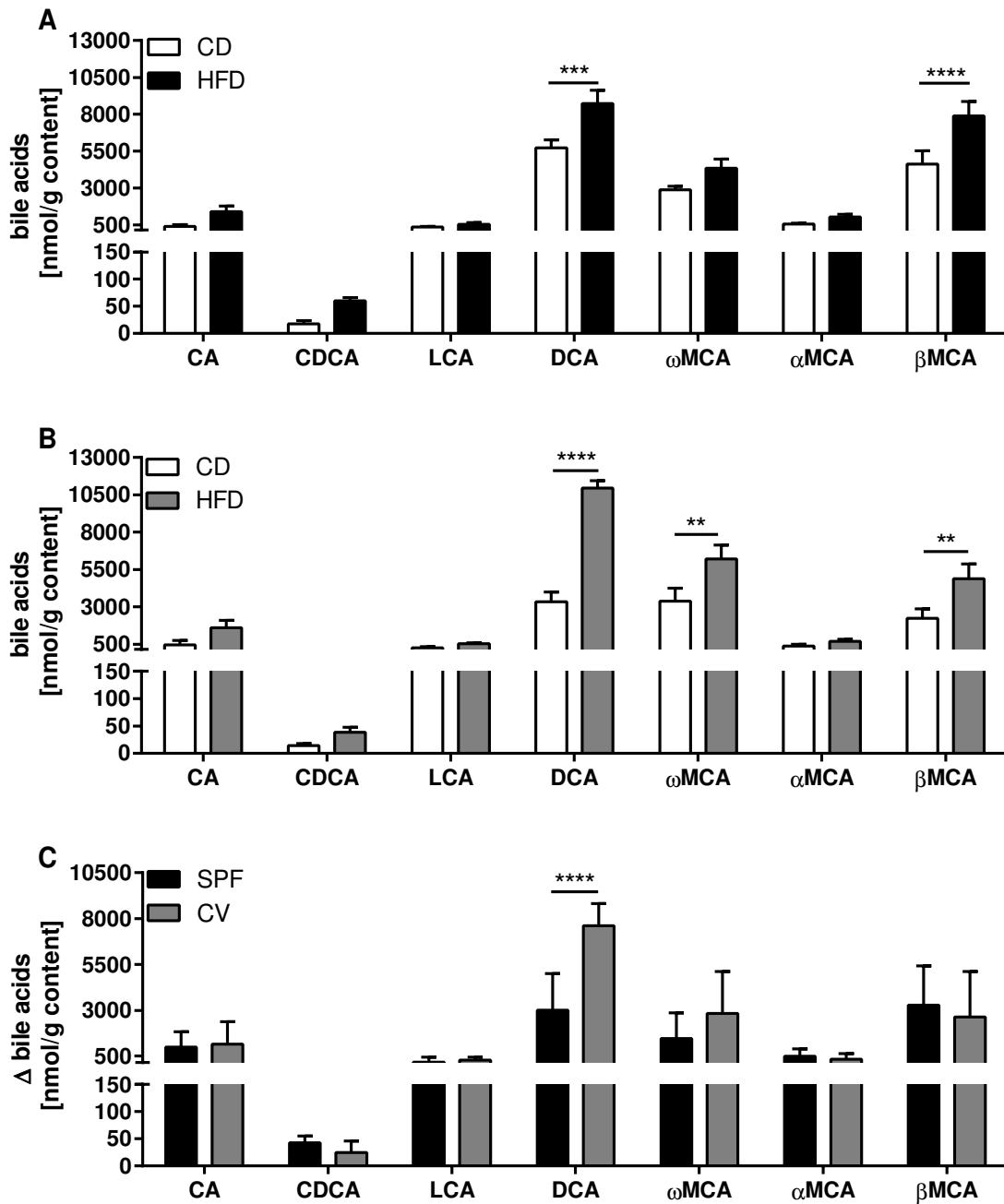


Figure 19: Bile acids concentrations in cecal samples in response to diet and facility. C57BL/6N mice were housed in a specific pathogen-free (SPF) or conventional animal (CV) facility and fed a control (CD) or beef tallow-based high-fat diet (HFD) for 12 weeks. The bile acids primary bile acids cholic acid (CA) chenodeoxycholic acid (CDCA), α -muricholic acid (α MCA) and β -muricholic acid (β MCA) as well as the secondary bile acid deoxycholic acid (DCA), ω -muricholic acid (ω MCA) and lithocholic acid (LCA) were analyzed in the cecal content of mice housed in a (A) SPF or (B) CV facility. (C) The difference of the cecal bile acid concentration between CD and HFD groups for each housing conditions was calculated. Data are represented as means + SEM. Statistical analysis was performed using two-way ANOVA with Sidak's post-hoc test. ** $p < 0.01$, *** $p < 0.001$, **** $p < 0.0001$. $n = 5-6$ mice per group.

Since a DCA-induced barrier dysfunction was reported before [142], cecal DCA concentration was correlated to the relative sequence abundance of molecular

species. The cecal concentrations of DCA correlated significantly with the relative sequence abundance of 6 molecular species within the order Clostridiales most closely related to *Acetatifactor muris*, *Eubacterium plexicaudatum*, and *Roseburia* spp., albeit with sequence similarity <95% (Figure 20).

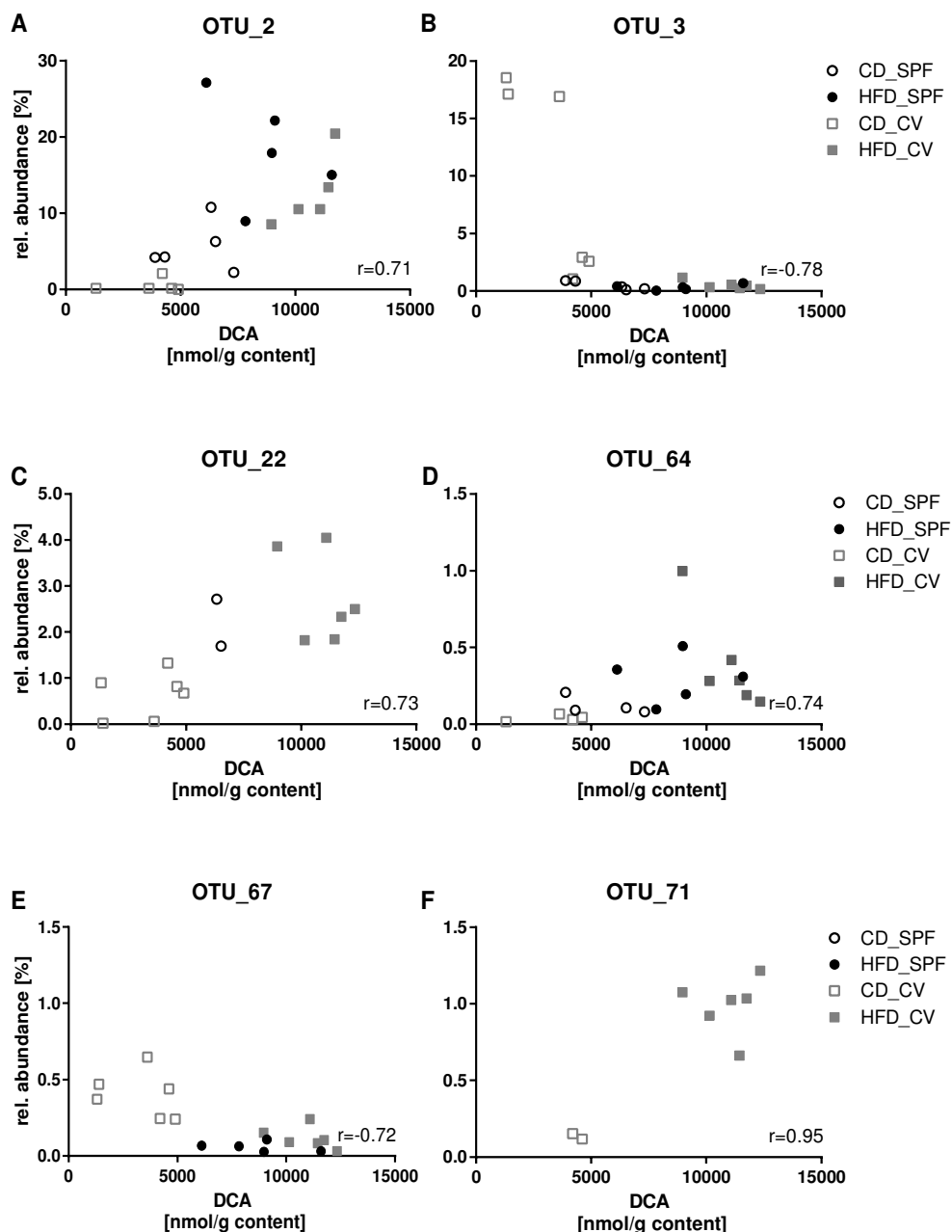


Figure 20: Cecal DCA is linked to microbiota composition. Pearson correlation plots between cecal DCA concentrations and the relative sequence abundance of molecular species (at least $p < 0.01$). OTUs are: (A) 2, *Acetatifactor muris* (91.6% similarity); (B) 3, *A. muris* (94.2%); (C) 22, *Eubacterium plexicaudatum* (93.5%); (D) 64, *Roseburia intestinalis* (94.5%); (E) 67, *Roseburia cecicola* (96.2%); (F) 71, *E. plexicaudatum* (88%).

3.2 Intestinal sensing and hormone secretion

Nutrients or microbial products of metabolism (e.g. bile acids and short-chain fatty acids) can be sensed in the intestine by specialized endocrine cells equipped with a variety of sensors [143]. Activation of the sensing system is coupled to secretion of gastrointestinal hormones such as glucose-dependent insulinotropic peptide (GIP), glucagon-like peptide-1 (GLP-1) and glucagon-like peptide-2 (GLP-2) into circulation [36]. To visualize incretin hormone secreting cells, murine ileal tissue sections were stained for GIP and GLP-1. The incretin hormone GIP is secreted by K cells which dominate the proximal small intestine, whereas GLP-1 is secreted from L cells which are more prominent in the distal small intestine and colon (Figure 21).

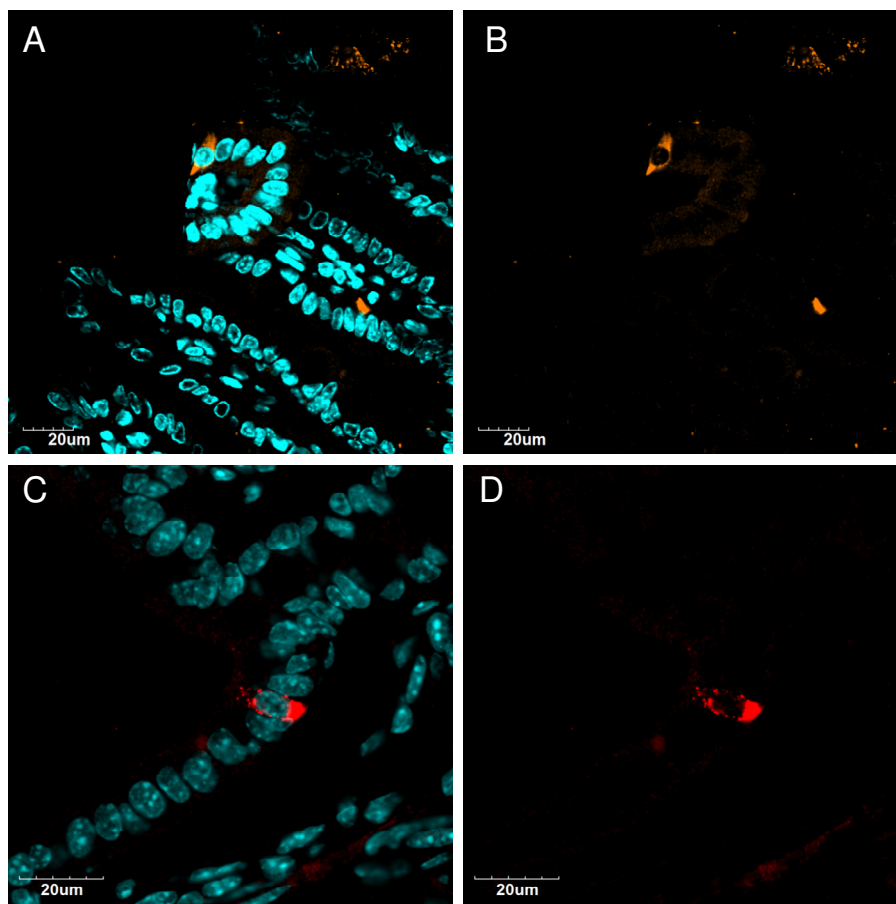


Figure 21: Ileal tissue stained for GIP (orange) and GLP-1 (red). Nuclei were stained with DAPI (turquoise). Microscopic fluorescence images of (A and B) K cells stained for GIP and (C and D) L cells stained for GLP-1 in murine ileum.

3.2.1 Effect of high-fat diet feeding on hormone secretion in vivo

For a short-term feeding experiment male C57BL/6N mice were housed in a CV facility and fed a CD (11 kJ% fat) or HFD (60 kJ% fat) for 4 weeks. After dietary intervention the body mass of mice fed a HFD was increased compared to the respective controls (CD 22.87 ± 0.27 g vs. HFD 29.87 ± 1.14 g, $p < 0.0001$). Moreover, fasting blood glucose levels were elevated as well in HFD fed mice (CD 157.8 ± 13.2 mg/dl vs. HFD 212.3 ± 12.3 mg/dl, $p < 0.01$, Figure 22)

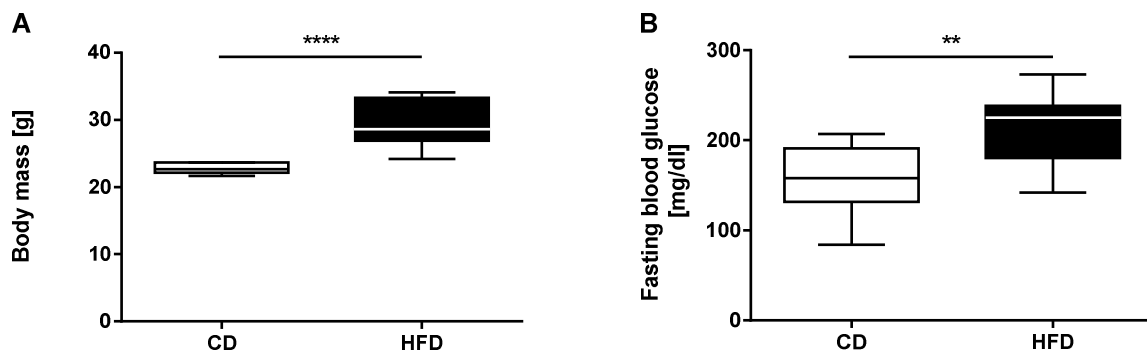


Figure 22: Body mass and fasting blood glucose after short-term high-fat diet treatment of mice. Male C57BL/6N mice were housed in a conventional animal facility and fed a control (CD, 11 kJ% fat) or high-fat diet (HFD, 60 kJ% fat). (A) Body mass and (B) fasting blood glucose after 4 weeks HFD treatment. Values are expressed as median. Statistical analysis was performed using unpaired two-tailed t-test. ** $p < 0.01$, **** $p < 0.0001$. $n = 7-10$ mice per group.

Plasma levels of hormones involved in blood glucose homeostasis were altered by HFD in mice treated for 4 weeks with the different diets. Insulin levels were 2.4-fold increased in the HFD group (CD 716.6 ± 41.0 pg/ml vs. HFD 1690 ± 228.5 pg/ml, $p < 0.01$). The levels of the incretin hormones GIP (CD 61.9 ± 4.9 pg/ml vs. HFD 141.9 ± 12.9 pg/ml, $p < 0.001$) and GLP-1 (CD 1.01 ± 0.08 pM vs. HFD 1.56 ± 0.20 pM, $p < 0.001$) were also significantly raised, whereas GLP-2 remained unaltered (Figure 23).

RESULTS

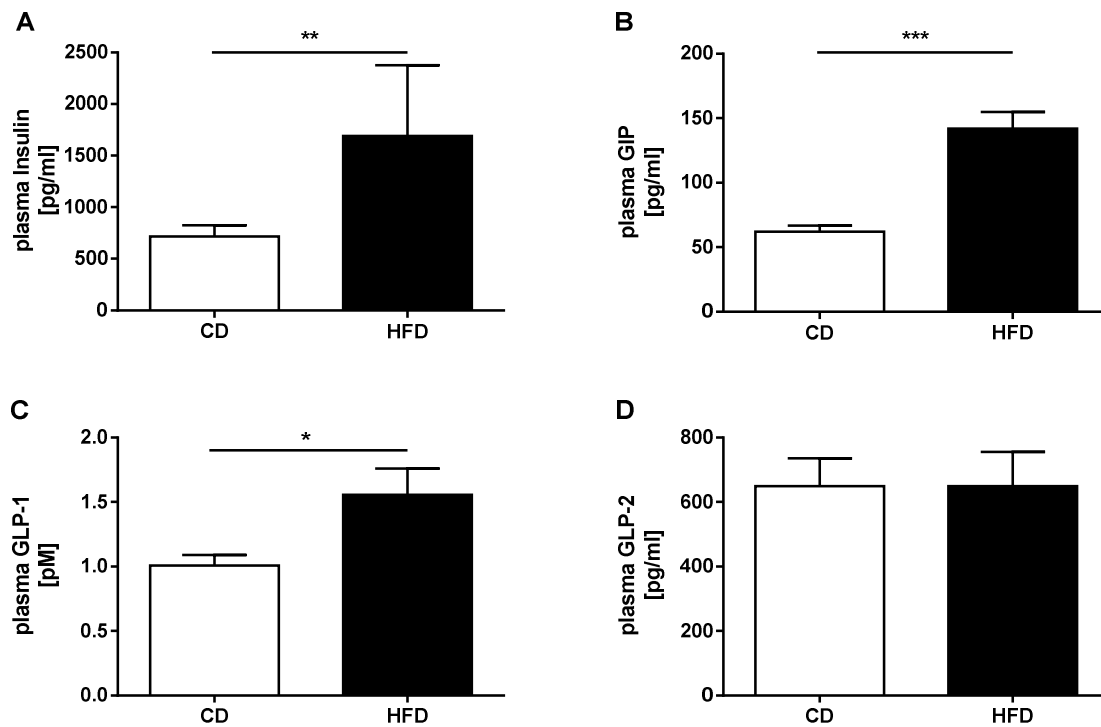


Figure 23: Plasma insulin, incretin hormones and GLP-2 levels after short-term high-fat diet intervention. Male C57BL/6N mice were housed in a conventional facility and fed a control (CD, 11 kJ% fat) or high-fat diet (HFD, 60 kJ% fat). Plasma (A) Insulin (B) GIP, (C) GLP-1 and (D) GLP-2 after 4 weeks of HFD intervention (HFD, 60 kJ% fat). Values are expressed means + SEM. Statistical analysis was performed using unpaired two-tailed t-test. * $p < 0.05$, ** $p < 0.01$, *** $p < 0.001$. $n = 5-10$ mice per group.

Additionally, transcript levels of the genes encoding the incretin hormones or of dipeptidyl peptidase-4 (DPP4) were determined in the corresponding main secretion sites after short-term HFD treatment. In the duodenum, transcript levels of *Gip* were significantly increased ($p < 0.05$) in the HFD group, whereas the transcript levels of *Dpp4* were significantly decreased ($p < 0.05$). In the colon, transcript levels of *Dpp4* and the *Gcg* gene encoding amongst others for GLP-1/2 remained inconspicuous (Table 39).

Table 39: Effects of short-term high-fat diet treatment on transcript levels of the hormones GIP and GLP-1/2 in the intestine. Transcript levels of duodenal *Gip* and colonic *Gcg* encoding for GLP-1/2 were determined after 4 weeks of high-fat diet intervention (HFD, 60 kJ% fat). Additionally, the mRNA level of the incretin hormone inactivating enzyme dipeptidyl peptidase-4 (*Dpp4*) was analyzed. Transcript levels were normalized to *Gapdh* and the control diet (CD) group was set to 1. Data are represented as means + SEM. Statistical analysis was performed using unpaired two-tailed t-test. Data with different superscript letters were significantly different at $p < 0.05$. n = 6 mice per group.

Gut section	Gene	Diet	
		CD	HFD
Duodenum	<i>Gip</i>	1.00±0.07 ^a	1.25±0.08 ^b
	<i>Dpp4</i>	1.00±0.11 ^a	0.68±0.06 ^b
Colon	<i>Gcg</i>	1.00±0.13	0.91±0.06
	<i>Dpp4</i>	1.00±0.11	1.30±0.16

3.2.2 Effect of high-fat diet treatment on bile acid metabolism

Cholesterol homeostasis is maintained by the liver by removing cholesterol from blood and by de novo synthesis. Cholesterol is either excreted directly into the bile or bile acids are synthesized from cholesterol in liver and transiently stored in the gallbladder. After food intake, bile acids are released into the duodenum by contraction of the gall bladder mediated by CCK and are either reabsorbed in the ileum and transported back to the liver *via* portal vein (enterohepatic circulation) or segregate with the feces [101]. In the short-term feeding experiment in C57BL/6N, mice were housed in the CV facility. The HFD contained 290 mg/kg cholesterol, whereas the CD was cholesterol-free.

Bile acids synthesis

After 4 weeks of diet intervention, cholesterol concentration in plasma accounted to HFD 3.33±0.24 mmol/l in the HFD group as compared to 1.61±0.15 mmol/l in the CD group ($p < 0.001$) and in the liver to 7.46±0.49 $\mu\text{mol/g}$ tissue in HFD animals compared to 5.43±0.66 $\mu\text{mol/g}$ tissue in CD animals ($p < 0.05$) (Figure 24). In contrast, triglyceride (TG) concentration in the plasma remained unaffected. However, TG concentration in the liver was 25.62±0.93 $\mu\text{mol/g}$ tissue in HFD animals compared to only 13.58±1.40 $\mu\text{mol/g}$ tissue ($p < 0.0001$) in mice of the CD group.

RESULTS

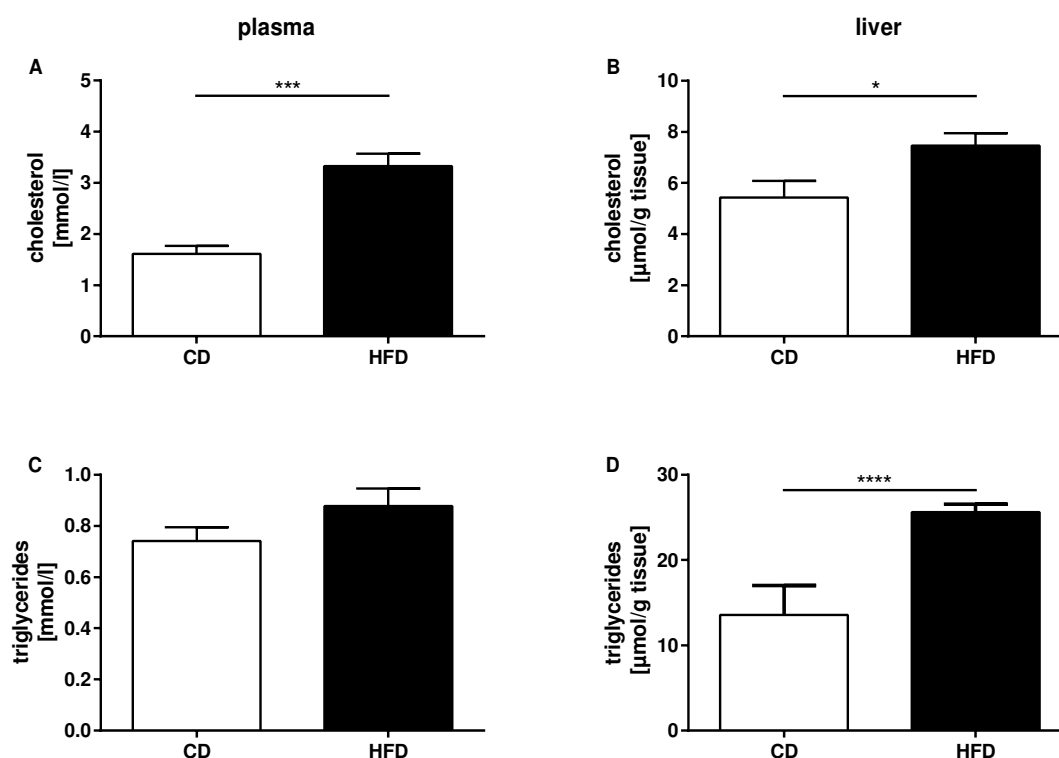


Figure 24: Cholesterol and triglyceride concentrations in plasma and liver tissue after short-term high-fat diet treatment. C57BL/6N mice were housed in a conventional facility and fed a control (CD, 11 kJ% fat) or high-fat diet (HFD, 60 kJ% fat) for 4 weeks. Cholesterol and triglyceride concentrations in (A and C) plasma and (B and D) liver. Values are expressed means + SEM. Statistical analysis was performed using unpaired two-tailed t-test. * $p < 0.05$, *** $p < 0.001$, **** $p < 0.0001$. $n = 5-6$ mice per group.

Moreover, mRNA levels of the key enzymes in the classic and the alternative bile acid biosynthesis pathways were determined in liver tissue. Cholesterol 7 α -hydroxylase (*Cyp7a1*), the key enzyme of the classic biosynthesis pathway, was increased in tissues of the HFD group but did not reach significance. Sterol 27-hydroxylase (*Cyp27a1*) the key enzyme of the alternative biosynthesis pathway was significantly increased ($p < 0.05$) by the HFD treatment (Table 40).

Table 40: Transcript levels of the two key enzymes of bile acid synthesis in the liver. The mRNA level of cholesterol 7 α -hydroxylase (*Cyp7a1*) and sterol 27-hydroxylase (*Cyp27a1*) were determined after 4 weeks of high-fat diet intervention (HFD, 60 kJ% fat). Transcript levels were normalized to *Gapdh* and the control diet (CD) group was set to 1. Data are represented as means + SEM. Statistical analysis was performed using unpaired two-tailed t-test. Data with different superscript letters are significantly different at $p < 0.05$. $n = 5-6$ mice per group.

Gene	Protein	Diet	
		CD	HFD
<i>Cyp7a1</i>	CYP7A1	1.00 ± 0.30	2.22 ± 0.73
<i>Cyp27a1</i>	CYP27A1	1.00 ± 0.09 ^a	1.45 ± 0.15 ^b

The hepatic bile acid precursor 7 α -hydroxy-4-cholesten-3-one (C4) and the primary bile acids CA and CDCA as well as the secondary bile acids DCA, ω MCA, LCA and UDCA were quantified in the liver, the cecal contents and the feces. C4 and total hepatic bile acids remained unaltered in animals of the HFD group, whereas levels of total bile acids in cecal contents ($p < 0.05$) and feces ($p < 0.01$) were elevated (Figure 25) with significantly increased concentrations of the secondary bile acids DCA and ω MCA (Figure 26).

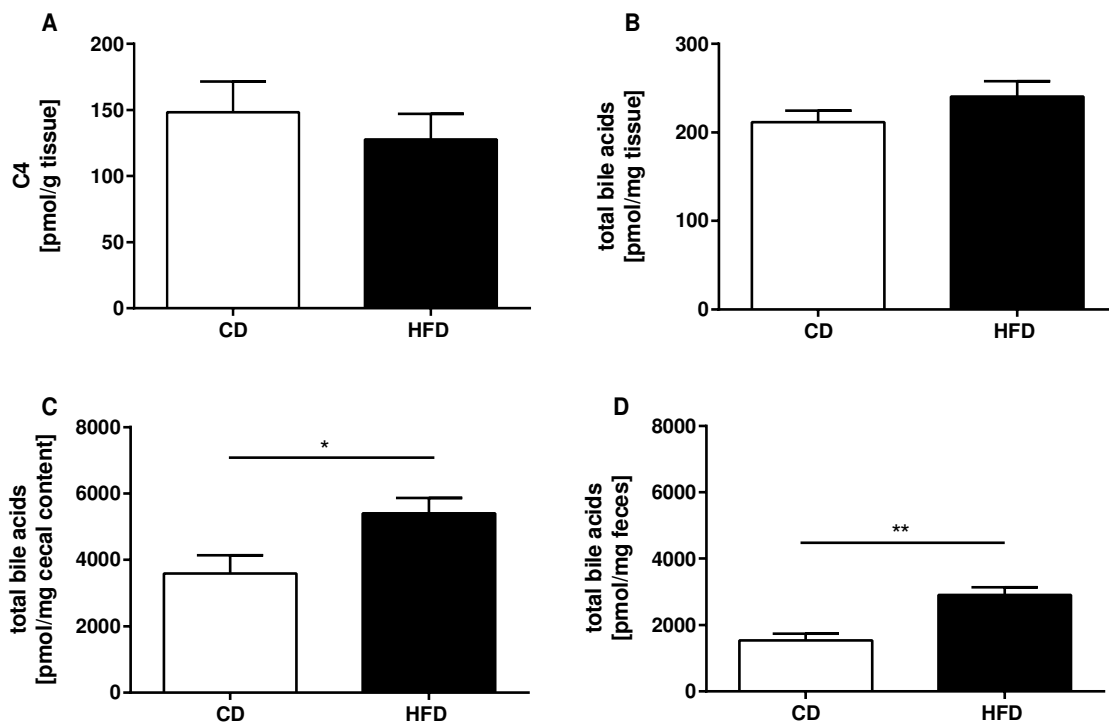


Figure 25: 7 α -hydroxy-4-cholesten-3-one (C4) and total bile acid concentrations in samples of mice fed a high-fat or control diet. C57BL/6N mice were fed a control (CD, 11 kJ% fat) or high-fat diet (HFD) for 4 weeks. (A) Hepatic C4 concentrations, (B) hepatic, (C) cecal and (D) fecal total bile acid concentrations were analyzed. Values are expressed means + SEM. Statistical analysis was performed using unpaired two-tailed t-test. * $p < 0.05$, ** $p < 0.01$. $n = 6$ mice per group.

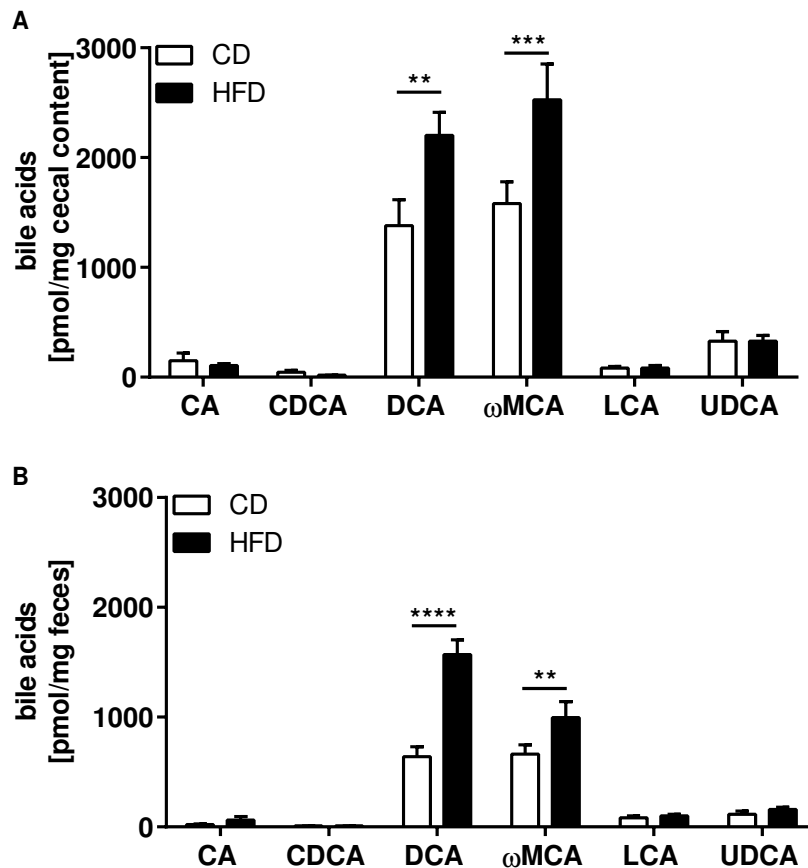


Figure 26: Bile acids concentrations in the cecal contents and feces in samples of mice fed a high-fat or control diet. C57BL/6N mice were housed in conventional animal facility and fed a control (CD, 11 kJ% fat) or high-fat diet (HFD) for 4 weeks. The bile acids primary bile acids cholic acid (CA) and chenodeoxycholic acid (CDCA) as well as the secondary bile acid deoxycholic acid (DCA), ω-muricholic acid (ωMCA), lithocholic acid (LCA) and ursodeoxycholic acid (UDCA) were analyzed in the (A) cecal content and (B) feces. Data are represented as means + SEM. Statistical analysis was performed using two-way ANOVA with Sidak's post-hoc test. ** $p < 0.01$, *** $p < 0.001$, **** $p < 0.0001$. $n = 6$ mice per group.

Enterohepatic circulation

Transcript levels of transporters and receptors involved in the enterohepatic circulation of bile acids were determined in liver, ileum or colon (Table 41), but no significant changes in the animals on HFD were found. In the liver the mRNA levels of bile salt export pump (BSEP, *Abcb11*), the sodium-taurocholate cotransporting polypeptide (NTCP, *Slc10a1*), the two basolateral receptors fibroblast growth factor receptor 4 (FGFR4, *Fgfr4*) and β Klotho (*β Klotho*), the nuclear receptors liver X receptor α (LXRα, *Nr1h2*), liver X receptor β (LXRβ, *Nr1h3*), farnesoid X receptor (FXR, *Nr1h4*) and small heterodimer partner (SHP, *Shp*) were determined. In the ileum the transcript levels of ileal transporters and receptors such as ileal bile acid

transporter (IBAT, *Slc10a2*), ileal bile acid binding protein (IBABP, *Fabp6*), the basolateral transporters organic solute transporter α (OST α , *Slc51a*) and organic solute transporter β (OST β , *Slc51b*), the nuclear receptors farnesoid X receptor (FXR, *Nr1h4*) and small heterodimer partner (SHP, *Shp*) and the fibroblast growth factor 15 (FGF15, *Fgf15*) were investigated. Additionally, the G protein-coupled bile acid receptor 1 (TGR5, *Gpbar1*) mRNA was considered.

Table 41: Transcript levels of receptors and transporters of the enterohepatic circulation. The mRNA levels were determined after 4 weeks of high-fat diet intervention (HFD, 60 kJ% fat) in liver, ileum or colon. Transcript levels were normalized to *Gapdh* and the control diet (CD, 11 kJ% fat) group was set to 1. Data are represented as means \pm SEM. Statistical analysis was performed using unpaired two-tailed t-test. n = 5-6 mice per group.

Organ	Function	Gene	Protein	Diet	
				CD	HFD
Liver	Canalicular transporter	<i>Abcb11</i>	BSEP	1.00 \pm 0.13	1.01 \pm 0.15
	Basolateral transporter	<i>Slc10a1</i>	NTCP	1.00 \pm 0.14	0.95 \pm 0.07
	Basolateral receptors	<i>Fgfr4</i>	FGFR4	1.00 \pm 0.11	0.98 \pm 0.09
		β <i>Klotho</i>	β <i>Klotho</i>	1.00 \pm 0.15	0.87 \pm 0.10
	Nuclear receptors	<i>Nr1h2</i>	LXR β	1.00 \pm 0.14	0.88 \pm 0.08
		<i>Nr1h3</i>	LXR α	1.00 \pm 0.18	0.93 \pm 0.15
		<i>Nr1h4</i>	FXR	1.00 \pm 0.16	1.31 \pm 0.20
		<i>Shp</i>	SHP	1.00 \pm 0.22	1.24 \pm 0.23
Ileum	Apical transporter	<i>Slc10a2</i>	ASBT, IBAT	1.00 \pm 0.15	1.05 \pm 0.16
	Internal binding protein	<i>Fabp6</i>	IBABP	1.00 \pm 0.09	1.01 \pm 0.15
	Basolateral transporters	<i>Slc51a</i>	OST α	1.00 \pm 0.10	0.89 \pm 0.13
		<i>Slc51b</i>	OST β	1.00 \pm 0.54	0.93 \pm 0.10
	Nuclear receptors	<i>Nr1h4</i>	FXR	1.00 \pm 0.10	0.87 \pm 0.05
		<i>Shp</i>	SHP	1.00 \pm 0.25	1.28 \pm 0.12
	Fibroblast growth factor	<i>Fgf15</i>	FGF15	1.00 \pm 0.15	0.69 \pm 0.13
	Bile acid receptor	<i>Gpbar1</i>	TGR5	1.00 \pm 0.05	1.02 \pm 0.10
Colon	Bile acid receptor	<i>Gpbar1</i>	TGR5	1.00 \pm 0.05	0.93 \pm 0.07

RESULTS

3.2.3 Microbial products of metabolism can induce GLP-1 secretion in vitro

Bile acids can be sensed *via* TGR5 and short-chain fatty acids *via* the free fatty acid receptor 2/3 (FFAR2/3) and both pathways have the ability to evoke a GLP-1 secretion from primary intestinal cells in cultures [45, 48, 49]. In the present work primary cell cultures were prepared from colonic crypts of C57BL/6N mice. In the colonic tissue and in the primary colonic cell cultures L cells containing GLP-1 were identified (Figure 27).

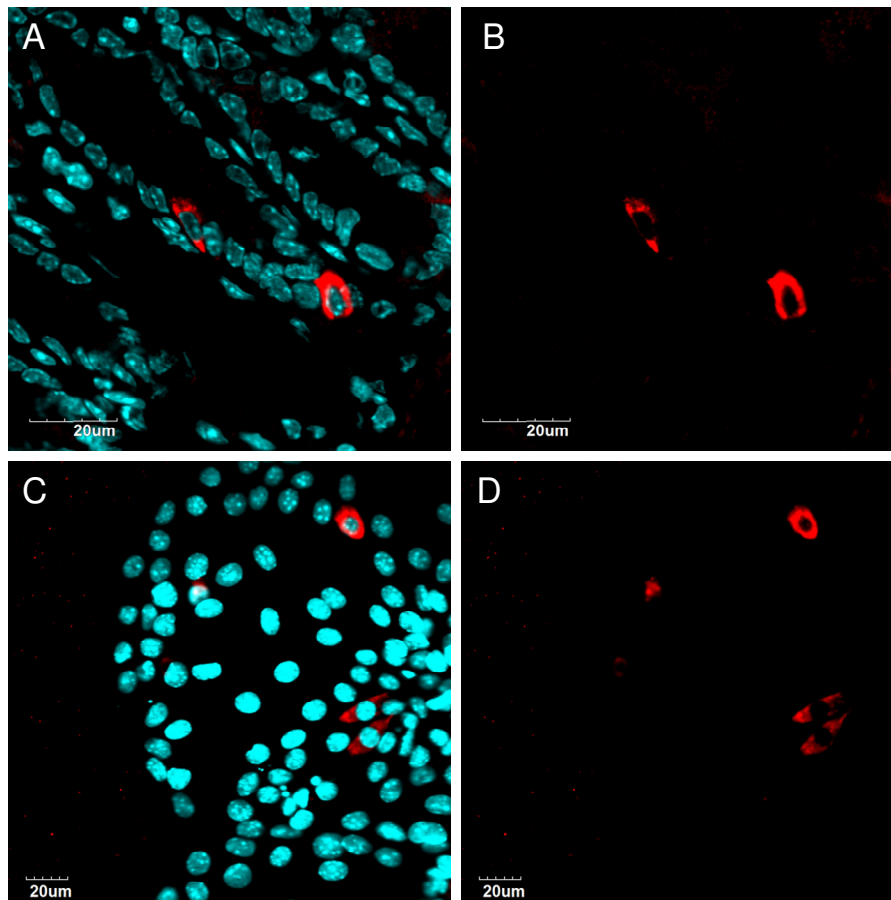


Figure 27: Colonic tissue and primary colonic cell culture stained for GLP-1 (red). Nuclei were stained with DAPI (turquoise). Microscopic fluorescence images of (A and B) colonic tissue and (C and D) primary colonic cell cultures.

3.2.3.1 Bile acid-mediated GLP-1 secretion

Mimicking effects of HFD by increasing DCA concentrations

Primary colonic cell cultures were exposed to increasing concentrations of the secondary bile acid DCA. GLP-1 secretion upon stimulation by 30 μM DCA ($p < 0.0001$) or 50 μM DCA ($p < 0.001$) was increased compared to baseline secretion, whereas 10 μM did not rise the secretion. An increase of the concentration from 30 μM DCA to 50 μM DCA did not further increase the GLP-1 level (Figure 28).

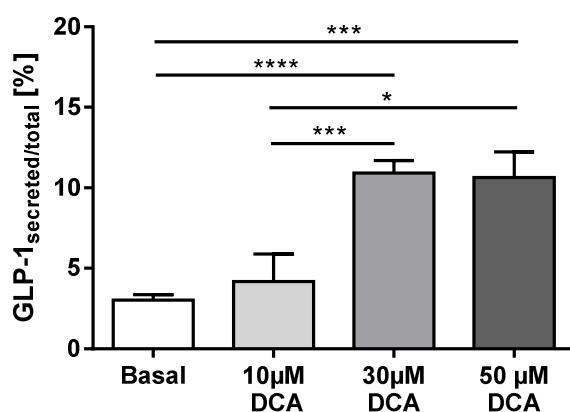


Figure 28: Deoxycholic acid-induced GLP-1 secretion in primary colonic crypt cultures. GLP-1 secretion was assessed upon treatment with buffer, 10 μM , 30 μM and 50 μM deoxycholic acid (DCA). Data are represented as means + SEM. Statistical analysis was performed using one-way ANOVA with Tukey's post-hoc test. * $p < 0.05$, **** $p < 0.0001$. $n = 3-18$ wells per group.

To assess whether enhanced GLP-1 secretion is associated with an increase in intracellular calcium response, primary colonic cell cultures were loaded with the fluorescent calcium indicator fura-2. After an equilibration phase, the primary cultures were perfused with DCA and the relative ratio of 340/380 nm - reflecting intracellular calcium levels - increased. This change in the relative ratio was reversible by washing DCA out with buffer. Only cell cultures responding at the end of the measurement to ionophore ionomycin were included in the analysis. The relative fluorescence ratio of 340/380 nm increased in a concentration-dependent manner after exposure to DCA as shown in Figure 29.

RESULTS

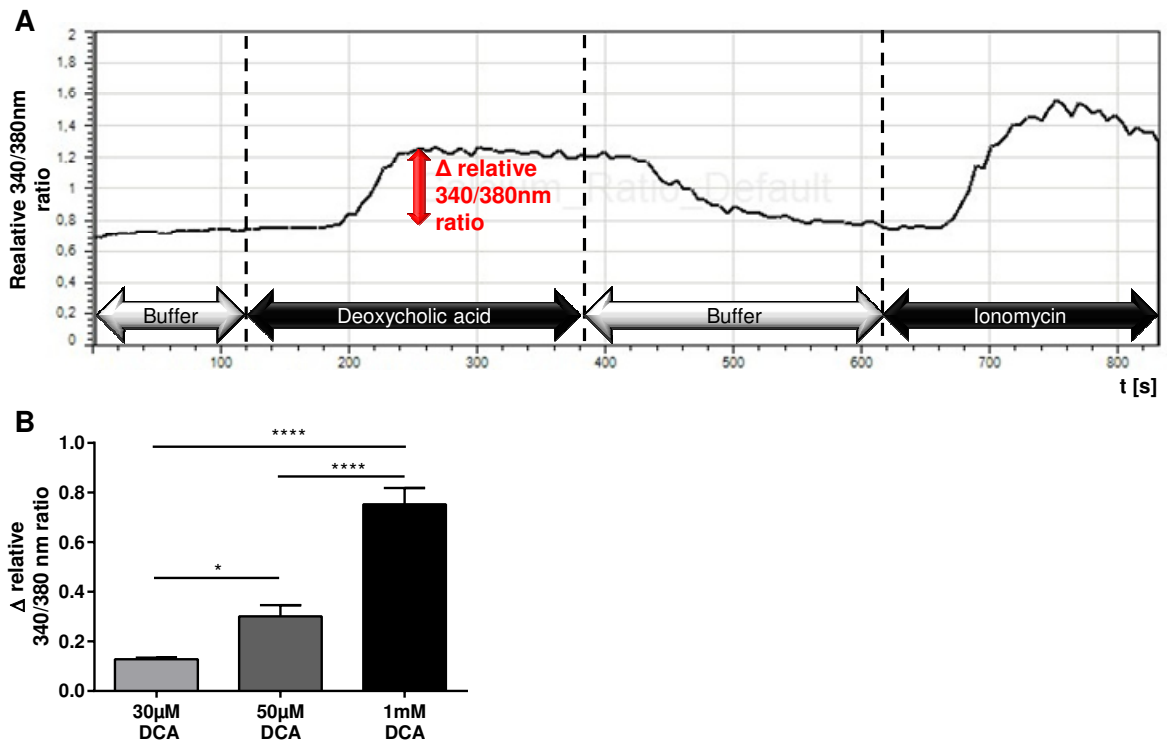


Figure 29: Deoxycholic acid-induced calcium changes in primary colonic cell cultures. Changes in the 340/380 nm ratio in with fura-2 stained primary colonic cell cultures upon stimulation with deoxycholic acid (DCA). (B) Calcium response from primary colonic cell culture due to increasing concentrations of DCA. Data are represented as means + SEM. Statistical analysis was performed using one-way ANOVA with Tukey's post-hoc test. * $p < 0.05$, **** $p < 0.0001$. $n = 5-6$ slides per group.

Effect of bile acids on GLP-1 secretion in primary colonic cell cultures prepared from mice fed the HFD

Diet-dependent alterations in GLP-1 secretion from primary colonic cell cultures exposed to the bile acids CA, CDCA, DCA and LCA were studied in cultures prepared from mice fed a HFD or CD for 4 weeks. There was a significant influence of the diet ($p < 0.01$) and bile acids ($p < 0.0001$) on GLP-1 secretion from primary cultures, but no interaction between diet and bile acids was found (Figure 30). Interestingly, GLP-1 secretion upon DCA stimulation was significantly higher in the primary colonic cell cultures prepared from HFD mice than the respective controls (CD 10.54 ± 0.95 % vs. HFD 17.26 ± 2.18 %, $p < 0.01$). However, basal and maximal GLP-1 secretion (as positive control) did not reveal significant alterations in GLP-1 secretion between primary colonic cell cultures obtained from CD or HFD fed animals.

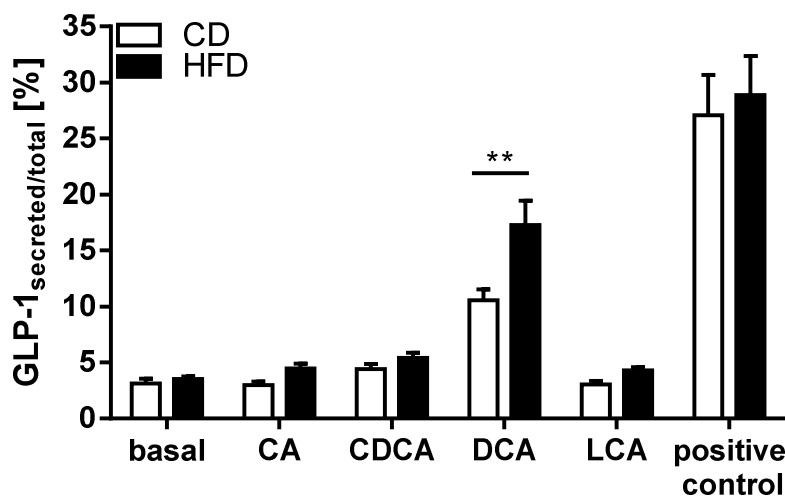


Figure 30: GLP-1 secretion from primary colonic cell cultures from mice fed a CD or HFD in response to different bile acids. C57BL/6N mice were fed a control (CD, 11 kJ% fat) or high-fat diet (HFD, 60 kJ% fat) for 4 weeks. GLP-1 secretion was induced by the bile acids primary bile acids cholic acid (CA) and chenodeoxycholic acid (CDCA) as well as by the secondary bile acids deoxycholic acid (DCA) and lithocholic acid (LCA). A combination of glucose, forskolin and IBMX was used as positive control. Data are represented as means + SEM. Statistical analysis was performed using two-way ANOVA with Sidak's post-hoc test. ** $p < 0.01$. $n = 7-13$ mice per group.

Despite changes in GLP-1 secretion upon DCA exposure, there were no changes in the *Gcg* encoding GLP-1 and *Gpbar1* encoding TGR5 mRNA levels between primary colonic cell cultures made up from HFD or CD animals (Figure 31).

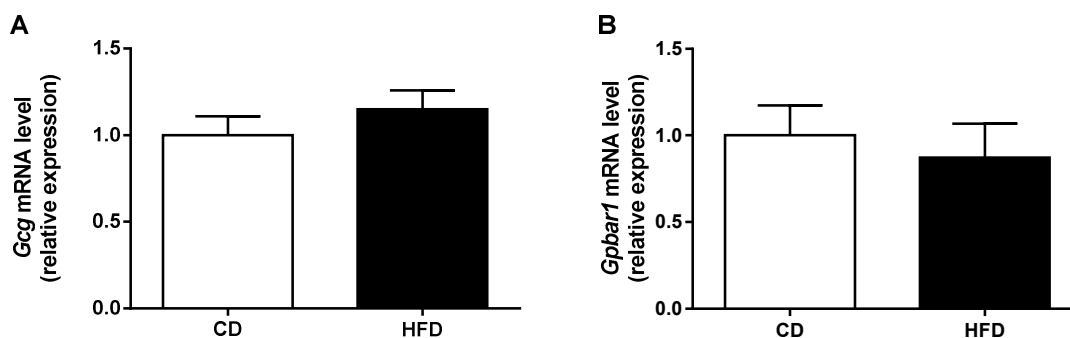


Figure 31: *Gcg* and *Gpbar1* gene expression levels in primary colonic cell cultures prepared from animals fed a HFD or CD for 4 weeks. C57BL/6N mice were fed a control (CD, 11 kJ% fat) or high-fat diet (HFD, 60 kJ% fat) for 4 weeks. (A) *Gcg* gene encoding GLP-1 and (B) *Gpbar1* encoding TGR5 mRNA levels of primary colonic cell cultures after dietary intervention. Data are represented as means + SEM. Statistical analysis was performed using unpaired two-tailed *t*-test. $n = 5-6$ mice per group.

RESULTS

3.2.3.2 Short-chain fatty acids-mediated GLP-1 secretion

Furthermore, short-chain fatty acids-induced GLP-1 secretion was also analyzed in primary colonic cultures originating from mice fed either a CD or HFD diet for 4 weeks. Cultures were either stimulated with 1 mM acetate or 1 mM propionate (Figure 32). Propionate evoke a significantly higher GLP-1 secretion from cultures generated from mice fed a HFD than from the respective controls ($p < 0.01$).

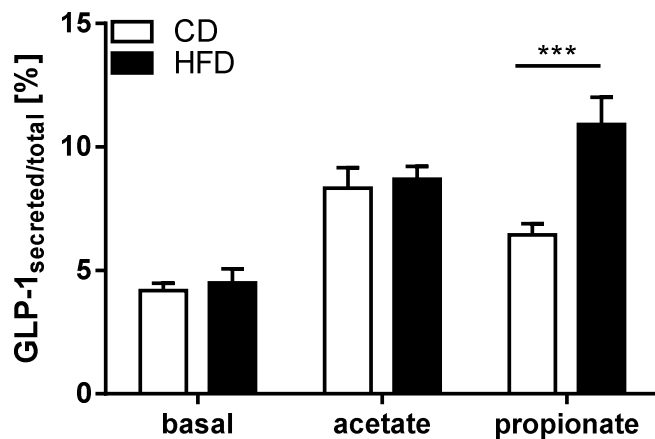


Figure 32: Short-chain fatty-induced GLP-1 secretion from primary colonic cell cultures prepared from mice fed a CD or HFD for 4 weeks. C57BL/6N mice were fed a control (CD, 11 kJ% fat) or high-fat diet (HFD, 60 kJ% fat) for 4 weeks. GLP-1 secretion was induced by the short-chain fatty acids 1 mM acetate and 1 mM propionate. Data are represented as means + SEM. Statistical analysis was performed using two-way ANOVA with Sidak's post-hoc test. *** $p < 0.001$. $n = 8-10$ mice per group.

4 Discussion

4.1 Gut barrier integrity depends on housing conditions

4.1.1 Determinants of gut barrier impairment

Obesity and diets high in saturated fat are considered to impair structural and functional integrity of the gut. Although the prime observation was made in mice fed a diet free of any carbohydrates [2], the concept has been propagated within a range of studies [3, 117-119, 144-146]. In animal studies, diet-induced obesity (DIO) is usually provoked by feeding high-fat diets (HFDs) with at least 45% up to 80% of the overall energy derived from fat. The basic fat component was either animal-derived represented by lard or beef tallow, or plant-derived with corn, palm or soy oil as source [2, 3, 117, 118, 136, 144-147]. In the present study, gut barrier function was mainly assessed in Ussing chambers by measurements of transepithelial resistance and permeability *ex vivo*.

Strain-dependent differences in susceptibility to DIO are known in mice [148]: AKR/J mice are prone to DIO, whereas SWR/J mice are resistant and C57BL/6J mice show an intermediate phenotype. These strains were exposed to a plant-based HFD (48 kJ% fat) to study the effects on colonic barrier function, but neither of the three strains revealed any significant change in barrier tightness, although electrical resistance and permeability parameter were strain-dependent, as previously described [149]. As C57BL/6J mice exhibited an intermediate DIO phenotype, this model was selected to survey further risk factors for gut barrier impairment.

First, the onset of colonic barrier dysfunction was investigated by prolonging the duration of HFD intervention from 1 week up to 24 weeks. In contrast to other studies in rodents [150, 151], the intestinal permeability remained unaffected. In the next series of experiments the percentage of the energy coming from fat was increased from 48 kJ% to 61 kJ%. Although the oral glucose tolerance showed impairments as previously reported [2, 135], small and large intestinal barrier function - judged by electrical resistance and tracer permeability - remained unaffected. This finding is striking, since data concerning the impact of the dietary fat proportion on intestinal permeability were indistinct. Cani *et al.* reported an aggravation of the intestinal

permeability by increasing the fat content from 40 kJ% to 72 kJ% from fat [2], whereas Benoit *et al.* demonstrated the opposite [152]. Therefore it was questionable, whether these controversial findings were dependent on the fat quality rather than on the quantity. Beside a different fatty acid composition, animal-based diets contain cholesterol, which was recently proposed to promote acute intestinal inflammation [153]. Consequently, we next changed the basic fat component from palm oil to lard. The used lard-based diet was the same in essence carbohydrate-free HFD that caused gut barrier dysfunction in the study by *Cani et al.* [2]. Although an extensive assessment of the intestinal barrier integrity including plasma LPS levels, urinary excretion of polyethylene glycol, transepithelial resistance and tight junction protein and mRNA expression was performed in animals fed the HFD, no indication of any significant changes in intestinal barrier tightness was discovered [135]. Next to the impact of mouse strains as well as fat quantity and quality on gut barrier integrity, we were also interested in the influence of animal housing. In a final experiment, genetically identical mice were exposed to the same HFD which contained beef tallow as fat source. Animals were kept in two different animal facilities with different hygienic status. And here the HFD deteriorated the intestinal barrier of mice housed in a conventional (CV) facility, whereas the same HFD was without any effect when mice were housed in a specific pathogen-free (SPF) facility.

In summary, under SPF housing conditions susceptibility to DIO, duration of HFD treatment, percentage of energy coming from fat in the HFD and the source of the basic fat component of the HFD were not the determining factors for gut barrier impairment. Finally, the hygienic status of the animal facilities and in turn the microbial colonization of the gut may be important as a determinant for maintenance or deterioration of gut barrier function in DIO mice.

4.1.2 Intestinal microbial colonization and intestinal barrier function

According to the paradigm that obesity causes a disturbance in intestinal barrier function, an increased intestinal permeation of LPS into the systemic circulation resulting in a metabolic endotoxemia is discussed [2]. Since this initial report by *Cani et al.* [2], a series of other studies have demonstrated such a metabolic endotoxemia in DIO mice as well [2, 3, 117-119, 144-146]. In the present study, HFD caused a metabolic endotoxemia in mice only when animals were housed in the CV

facility. Endotoxin analysis in the plasma indicates increased gastrointestinal permeability but it does not allow defining the region. We thus additionally analyzed transepithelial resistance and permeability of the small and large intestine in Ussing chambers. In conformity with the absence of metabolic endotoxemia, the region-dependent barrier evaluation remained inconspicuous for animals housed in the SPF facility. In contrast, the jejunal and proximal colonic barrier function was deteriorated in DIO mice housed in the CV facility. Only few electrophysiological studies have assessed intestinal barrier integrity in DIO rodents so far [136, 147, 150, 154]. Lam *et al.* reported a decrease in transepithelial resistance considering only the proximal colon [147], whereas Stenman *et al.* revealed a barrier dysfunction also in the jejunum and colon [136]. The present work however, is the first electrophysiological study considering the influence of the hygienic status of animal facilities on gut barrier tightness.

Beside a metabolic endotoxemia, obesity is associated with low-grade inflammation. Therefore, we studied gene expression of inflammatory markers in liver and adipose tissue. In the liver, no changes by DIO were found at all. However, levels of the pro-inflammatory cytokines/chemokines *Tnf* and *Mcp-1* were elevated in the adipose tissue of DIO mice when kept in the CV facility. The unchanged inflammatory tone under SPF conditions was in accordance with the absent metabolic endotoxemia. Since LPS is considered to promote adipose tissue inflammation *via* the TLR4/CD14 pathway accompanied by infiltration of macrophages into adipose tissue [2, 118, 155], the higher levels of LPS found in obese CV mice may have secondarily caused the changes in adipose tissue.

As an adaptation to HFD is assumed to mediate morphological changes in the intestine, villus length of the electrophysiological investigated sections of the small intestine were assessed. In contrast to other studies [138, 139], no elongated villi in small intestine of DIO mice were observed - regardless of the animal facility. Villus length seems in fact to depend on diet fat quality. Sagher *et al.* demonstrated a reduction in villus length by feeding rats a diet high in saturated fatty acids, whereas diets high in mono- or polyunsaturated fatty acids increased villi length [156]. In accordance with the unaltered villus length we also observed no differences in GLP-2 and IL-6 levels, which contribute to cell homeostasis in the intestine [138, 140, 157].

Despite the absence of macroscopic changes in gut morphology, protein expression levels of several tight junction proteins were determined in the jejunum and colon by western blotting. Most of the studies investigating the influence of HFD on tight junctions considered the tight junction protein occludin and the scaffold protein ZO-1 as markers [117, 135, 158-161]. In the study by Cani and colleagues, ZO-1 but not occludin expression was decreased [3]. In the present study, occludin and ZO-1 protein expression levels remained unaffected by DIO and this is in line with most of the other studies [117, 135, 159, 161]. Mice lacking the tight junction protein JAM-A were reported to have an increased intestinal permeability [18]. We thus assessed JAM-A protein levels but no changes were found, whereas in rats HFD caused a decreased JAM-A expression in the small intestine but not in the large intestine [151]. Finally, three members of the claudin family, claudin-2, -3 and -5 were profiled. Barrier tightening claudins are known to be down-regulated and redistributed in inflammatory bowel disease such as Crohn`s disease associated with increased permeability [24]. In our DIO mice claudin-3 and claudin-5 levels remained unaltered, though. The pore-forming tight junction protein claudin-2 was found up-regulated in patients suffering from Crohn`s disease [24, 25], whereas HFD did not change intestinal claudin-2 expression [118, 158, 161]. Although our analysis did not provide evidence for any change in tight junction protein expression, proteins in the junctional complexes undergo phosphorylation such as of the myosin light chain and can rearrange quickly [160, 162]. TNF for example is known to induce phosphorylation of myosin light chain by activating myosin light chain kinase leading to the endocytosis of occludin and to tight junction disruption [163]. Since these processes were not studied here, we cannot exclude that they contributed to the increased permeability found in animal of the HFD group kept in the CV facility.

Feeding a HFD is also known to enlarge the bile acid pool size in mice and to increase fecal bile acid excretion as shown previously [112, 113]. The most hydrophobic bile acids such as deoxycholic acid (DCA) and lithocholic acid (LCA) were claimed to disrupt the epithelium and thus we analyzed bile acid concentrations in our cecal samples using LC-MS/MS technology [142]. In accordance with other studies in rodents, the cecal concentration of the secondary bile acid DCA was significantly increased in mice fed the HFD independent of the facility [136, 164]. However, the differences between cecal DCA concentration of the HFD and of the CD group were significantly higher in the CV facility compared to the SPF facility.

DCA or LCA were shown to decrease transepithelial resistance and increase monolayer permeability in a dose-dependent manner in Caco-2 cells in concentrations between 50 μ M to 250 μ M [165]. Moreover, upwards from 10% of rat bile juice added to Caco-2 cell monolayer transepithelial resistance was reduced and permeability increased. A combination of rat bile juice and a fat emulsion yielded additive effects on the permeability but not on the transepithelial resistance [151]. Stenman *et al.* reported a DCA-induced barrier dysfunction in murine small and large intestine after exposure of tissues to 1-3 mM DCA in Ussing chambers [142]. Münch *et al.* also reported that a concentration of 1 mM DCA decreased barrier function in human colonic biopsies [166]. Supplementary, the transmucosal passage of killed *Escherichia coli* ascended in the presence of minimum 100 μ M DCA. However, the order of magnitude of 1 mM DCA corresponded to physiological concentrations in the feces of mice under HFD conditions [142]. Stenman *et al.* defined the HFD-induced alterations in the fecal bile acid profile of mice as the main cause for intestinal barrier dysfunction but not obesity *per se* [136, 167]. How bile acids can impair the gut barrier function apart from causing cell lysis and membrane solubilization remains to be determined. It is speculated that bile acids could inhibit the fusion of two adjacent junctions [168] or cause changes in the phosphorylation status of tight junction proteins inducing a redistribution of proteins in the junctional complex [169]. The higher absolute increase of cecal DCA concentrations in the cecum of mice housed in the CV animal facility may thus be causative for the observed changes in gut barrier integrity. However, since barrier function was not decreased in the SPF facility despite increased DCA levels an additional determinant needed to be considered – the intestinal microbial colonization. A significant role of the microbiome for the maintenance of an intact gut epithelium is also suggested by studies with probiotics [146], prebiotics [158] and antibiotics [3, 144].

Studies have shown that the intestinal microbiota is shaped by diet and hygienic status of the animal facility [81-84, 141] but whether this also alters gut barrier integrity is not known in essence. The increase of the *Firmicutes/Bacteroidetes* ratio in response to HFD found in the present studies is in accordance with other studies [82, 84] and was found similarly in both animal facilities. In contrast, the increased *alpha*-diversity found in feces samples of CV DIO mice with a deteriorated gut barrier was unexpected, since HFD is usually linked to a decrease in bacterial diversity [81, 84]. The diversity index (Shannon index) used to quantify species diversity appears

to reflect better the true diversity within a ecosystem, since not only the presence or absence of taxa but also the evenness is considered. Individual bacterial species such as *Akkermansia muciniphila* were recently proposed to be associated with the control of gut barrier function during DIO [170]. In the present study, *Akkermansia muciniphila* turned not out to be a candidate regulated by diet and/or housing conditions. Interestingly, we found the relative sequence abundance of *Clostridium scindens* increased in response to HFD regardless of the facility and this bacterial species is involved in the formation of secondary bile acids by 7 α -dehydroxylation [171]. Moreover, cecal DCA concentrations correlated quite well with the relative abundance of bacterial species from the order *Clostridiales*. For example *Acetatifactor muris*, which is known from the intestine of obese mice, may play a significant role on gut barrier homeostasis [172]. Therefore, the involvement of bacteria from the order *Clostridiales* should be studied further.

Recently, the mucus layer that covers as a viscous barrier the entire gut surface has received considerable attention and it has been demonstrated that mucus secretion and bacterial penetration through the mucus is altered in disease [173]. Muc2 is the most abundant gel-forming mucin expressed in the intestine. Mucins are highly glycosylated and in animals treated with HFD oligosaccharide chains of colonic mucins were found to be altered [174]. It is thus perceivable that a HFD and/or obesity can affect mucus quantity, mucus quality and its functional characteristics. It has also been reported that a reduction in the thickness of the mucus layer is accompanied by metabolic endotoxemia or *vice versa* [170] but findings are ambiguous [152]. Jakobsson *et al.* demonstrated different penetration of the inner colonic mucus layer by bacteria in genetically identical mice but housed in different rooms of the same animal facility. As the mucus phenotypes were reproduced by colonization of germ-free mice with the respective microbiota, it was substantiated that different microorganisms affect the colonic mucus barrier differently [141].

In conclusion, the phenotypic changes found in gut barrier integrity between mice fed a HFD but housed under different hygienic conditions were associated with alterations in the intestinal microbial colonization, the luminal levels of secondary bile acids, the portal LPS levels and the inflammatory tone in adipose tissue. Thus, the present study demonstrates that the intestinal barrier integrity in mice fed a HFD depends on the hygienic environment and is independent of obesity.

4.2 GLP-1 secretion can be affected by microbial products

4.2.1 Bile acid homeostasis is slightly altered by feeding a high-fat diet

There is only one major route to eliminate cholesterol from the body and that is by conversion of cholesterol into bile acids followed by biliary excretion and finally fecal loss. In diets based on animal fat (lard and beef tallow) the cholesterol amount is considerably higher than in control diets usually replacing fat by carbohydrates. Since luminal bile acids and in particular DCA were shown to have effects on the epithelium and alter its tightness, it was assessed whether the bile acid homeostasis is affected by HFD since the beef tallow-based diet provided 0.03% (wt/wt) cholesterol.

In the intestinal lumen dietary cholesterol or cholesterol from biliary secretion is absorbed by the sterol transporter Niemann-Pick C1-Like1, incorporated together with triglycerides into chylomicrons and released into the circulation *via* the lymphatic system [175]. In accordance with other studies our cholesterol-containing HFD caused a hypercholesterolemia [119, 176] but not a hypertriglyceridemia [135, 176]. Although in the present study hepatic cholesterol levels were elevated, the cholesterol-derived bile acid intermediate 7 α -hydroxy-4-cholesten-3-one (C4) and total hepatic bile acid pool remained unaltered. However, cecal and fecal bile acid concentrations were elevated in animals receiving the HFD.

In contrast to other studies [112, 113, 177], cholesterol 7 α -hydroxylase (*Cyp7a1*) mRNA expression was not markedly up-regulated, but *Cyp7a1* expression is known to have feedforward and feedback regulation by bile acids and their intermediates [178]. The liver X receptor α (LXR α) is the dominant protein of the feedforward regulation. Mice lacking LXR α cannot induce *Cyp7a1* expression in response to cholesterol feeding [112]. Oxysterols as intermediates of the bile acid synthesis are ligands of LXR α and can stimulate the transcription of *Cyp7a1* [179]. In the present study the mRNA level of sterol 27-hydroxylase (*Cyp27a1*) which converts cholesterol into the oxysterol 27-hydroxycholesterol, was elevated in the liver of animals receiving the cholesterol-containing HFD. Consequently, probably more oxysterols were formed from cholesterol and *Cyp7a1* expression in turn could be elevated. However, the farnesoid X receptor (FXR) is a key transcriptional factor in the feedback regulation of *Cyp7a1*. Bile acids bind to FXR, thereby the transcription of small heterodimer partner (SHP) is activated which in turn represses the *Cyp7a1*

transcription [178]. Mice lacking SHP exhibit an impaired negative feedback regulation [180]. As in the present study hepatic *Fxr* and *Shp* gene expression showed a tendency towards up-regulation in HFD animals, an inhibition of *Cyp7a1* expression *via* negative feedback regulation is likely. Besides slight regulatory effects on the *Cyp7a1* regulation, bile acid transporters, receptors and binding proteins within the enterohepatic circle were not affected in gene expression by the cholesterol-containing HFD intervention except a reduced ileal expression of the fibroblast growth factor 15 (*Fgf15*). This finding is also known from humans with impaired glucose tolerance or type 2 diabetes mellitus [181, 182]. In addition to its regulatory effects on bile acid synthesis, *Fgf15* (*Fgf19* is human the ortholog) controls also energy homeostasis. Administration of recombinant FGF19 to DIO mice was shown to increase the metabolic rate accompanied by a weight reduction and improved glucose homeostasis [183]. In our study the decreased *Fgf15* expression may have contributed to the development of DIO.

4.2.2 Incretin hormone secretion is altered in high-fat diet condition

DIO is generally associated with increased fasting plasma levels of blood glucose, insulin and the incretin hormones glucose-dependent insulintropic peptide (GIP) and glucagon-like peptide-1 (GLP-1) [184] and this was confirmed in the present study with the mice on HFD. Duodenal transcript and plasma levels of GIP were elevated. These observations are in accordance to other studies reporting elevated GIP secretion in diabetic patients and in healthy men after short-term overfeeding [185, 186] but the insulintropic activity of GIP is diminished [187]. GLP-1 plasma levels remain unchanged or even tend to be reduced in diabetes [188] but are increased in response to short-term overfeeding [189]. It must be pointed out that the majority of studies measures total GLP-1 concentrations and not only the biologically active forms GLP-1 (7-36) and GLP-1 (7-36 amide). In the present study, transcript levels of the GLP-1-encoding *Gcg* gene were unaltered, but fasting active GLP-1 levels were increased. These findings are in accordance with Nakajima *et al.* describing fasting and postprandial GLP-1 levels as increased during the development of obesity and glucose intolerance in rats [190]. The authors suggested that the enhanced GLP-1 secretion was due to an increased sensitivity to luminal stimuli to attenuate the development of impaired glucose tolerance and obesity.

Since incretin action is impaired in obese and diabetic conditions, the enhancement of hormone secretion from the gastrointestinal tract is considered as a therapeutic target. Current approaches to improve incretin action are the applications of exogenous GLP-1 receptor agonists mimicking GLP-1 or dipeptidyl peptidase 4 inhibitors reducing the GLP-1 degradation in the circulation [191].

4.2.3 GLP-1 secretion upon stimulation by bile acid- and short-chain fatty acid is enhanced in primary colonic cell cultures from animals fed a high-fat diet

Sensing of dietary constituents such as carbohydrates [38-40], lipids [42-44] and proteins [41] causes a release of GLP-1/2 from enteroendocrine L cells. In addition to nutrient-stimuli, for example bile acids or microbial products such as short-chain fatty acids are supposed to be involved in GLP-1 release [45-49].

Microbial fermentation products of dietary fibers so-called short-chain fatty acids are possible stimuli for GLP-1 secretion. The short-chain fatty acids acetate, propionate and butyrate are mainly formed in the large intestine. The short-chain fatty acids concentration in the lumen of the proximal colon amount to around 100 mM, whereas plasma concentrations are several orders of magnitude lower [192]. They activate the free fatty acids receptors 2 (FFAR2) and 3 (FFAR3) with a half maximal effective concentration (EC_{50}) of 0.3-1 mM and have been shown to cause PYY and GLP-1 release [193]. Whether these receptors are located in the apical or basolateral membrane of the L cells is still not defined but based on the EC_{50} value a basolateral localization is very likely [46]. Tolhurst *et al.* reported an enhanced GLP-1 secretion from primary colonic cell cultures upon stimulation by short-chain fatty acids. Moreover, FFAR2 and FFAR3 contribute to short-chain fatty acid-mediated GLP-1 secretion as in mice lacking FFAR2 or FFAR3 the secretory GLP-1 response was impaired *in vivo* and *in vitro* [45]. Additionally, intra-colonic application of propionate promoted GLP-1 release in wild type animals but not in mice lacking FFAR2 [47]. In the present study it was observed that propionate but not acetate was able to elicit a GLP-1 release that was significantly elevated in primary colonic cell cultures obtained from DIO mice exhibiting a hyperglycemia and hyperinsulinemia. Propionate is known to have a higher affinity for FFAR3 than acetate [194] and intestinal FFAR3 in DIO mice may be expressed at higher levels which could explain the findings. As luminal

short-chain fatty acids concentrations are relatively constant, it is plausible that there is a chronic stimulatory effect on the L cells *via* FFAR2 and FFAR3 contributing to the circulating fasting GLP-1 levels [45, 47]. This effect in combination with an up-regulation of FFAR2 or FFAR3 might explain the elevated circulating plasma GLP-1 level observed in DIO mice in the present study. Beside in intestinal L cells, FFAR2 and FFAR3 are expressed in pancreatic β cells. Recently, Tang *et al.* provided evidence that under HFD-induced diabetic condition acetate levels were elevated in the plasma and were able to inhibit glucose-stimulated insulin secretion *via* FFAR2 and FFAR3 [195]. Therefore, microbial fermentation products can affect incretin output and in turn insulin secretion from β cells but also the insulin secretion directly via the short-chain fatty acid receptors expressed in the β cells. And, both pathways may be altered in obese and/or diabetic mammals.

Bile acids are also potent stimulators of GLP-1/2 secretion. The primary bile acids such as CA and CDCA are transformed by the microbiota to the secondary bile acids e.g. DCA and LCA in the large intestine [101]. Bile acids are agonists of the G protein-coupled receptor TGR5 and are shown to elicit GLP-1/2 release. Reimann *et al.* demonstrated an enrichment of TGR5 in the enteroendocrine L cell population in the intestine [72]. The EC_{50} of bile acids for binding to TGR5 ranges from 0.5 μ M up to 10 μ M (LCA \geq DCA > CDCA > CA) [56, 57]. Bile acid-mediated GLP-1 output was reported from immortalized enteroendocrine cell lines such as STC-1, NCI-H716 or GLUTag and mixed primary intestinal cell cultures [48, 49, 196]. Additionally, intra-intestinal administration of DCA or a tauro-conjugate of CA was shown to increase plasma GLP-1 levels in healthy men [197, 198]. DCA is the most abundant secondary bile acid in humans or rodents and fecal DCA were found to be elevated after HFD feeding in the present study. Therefore, we focused on DCA and for the first time we demonstrated a concentration-dependent effect on GLP-1 release in primary colonic cell cultures similar to an effect on GLP-1 secretion from the STC-1 cell line [196] (Figure 33A). GLP-1 release from L cells activated by the G coupled-receptor TGR5 was reported to be a cAMP-dependent mechanism inducing intracellular calcium increase [59]. Initially receptor activation was demonstrated by cAMP formation [56, 57] and later by intracellular calcium increase in model cell lines [49]. In the present study, we showed for the first time the stimulus-secretion coupling in murine primary colonic cultures. It should be noted that

DCA evoked a higher GLP-1 secretion compared to LCA, although LCA has a higher receptor affinity to TGR5. This observation might be explained by a poor solubility of the monohydroxy bile acid LCA in water/buffer [199].

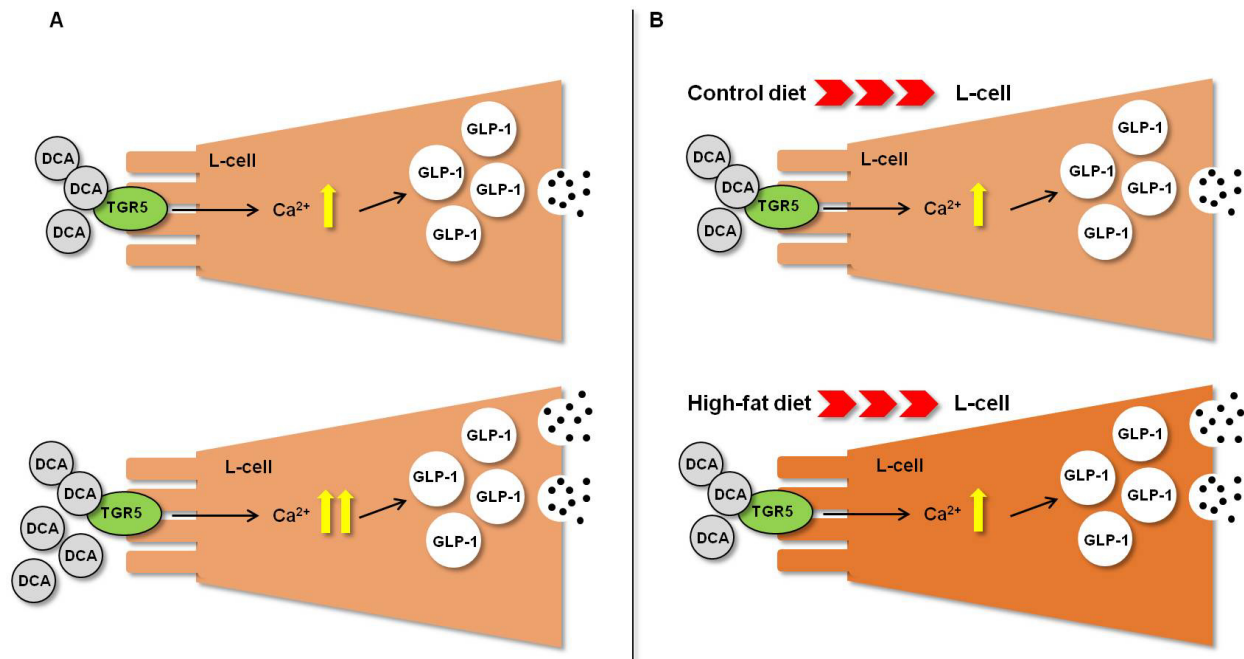


Figure 33: Dexoycholic acid (DCA) induced glucagon-like peptide 1 (GLP-1) secretion from primary colonic cell cultures. DCA triggers GLP-1 secretion in a concentration-dependent manner. (B) HFD intervention enhances responsiveness of DCA-induced GLP-1 secretion of primary colonic cell cultures.

Based on elevated fecal bile acid concentrations and enhanced GLP-1 secretion in DIO mice *in vivo*, bile acid-mediated GLP-1 secretion from primary colonic cell cultures prepared from DIO mice was investigated. In contrast to a recently published study, reporting an enhanced basal secretion from small intestinal cultures generated from mice fed a HFD for 2 weeks [200], the basal secretion in our primary colonic cell cultures from DIO mice was not elevated. Interestingly, DCA evoked elevated GLP-1 release from colonic primary cell cultures obtained from DIO mice compared to controls. Unaltered *Gcg* gene expression and basal secretion from primary colonic cell cultures gave reason to the assumption that the elevation might be arise from a higher sensitivity to sense DCA in DIO status (Figure 33B). Although TGR5 mRNA levels were not elevated in colonic crypt cultures derived from DIO mice, it could be not excluded that TGR5 participates in the enhanced responsiveness to DCA in cultures prepared from HFD fed mice. Of note, dietary compounds such as cholesterol and palmitic acid both included in the HFD were shown to be involved in

the regulation of G protein coupled receptors by affecting membrane composition and posttranslational modifications [201]. To further elucidate the mechanism of bile acid-triggered GLP-1 secretion primary cell cultures obtained from TGR5-deficient mice should be investigated.

There is growing evidence that the activation of TGR5 by bile acids is involved in regulation of satiety, glucose tolerance and energy metabolism and for that reason TGR5 is a promising target for diabetes therapy. For instance, in diabetic patients the rectal administration of taurocholate was shown to increase plasma GLP-1 and to lower plasma glucose significantly [202]. Bile acids sequestrants such as colestimide or colesevelam are also employed to alter GLP-1 response as these non-absorbable resins interrupt the enterohepatic circulation by binding bile acids. Consequently, the concentration of bile acids in the distal intestine is increased and GLP-1 secretion from L cells is enhanced [203]. Harach *et al.* demonstrated in TGR5-deficient mice that TGR5 is responsible for an elevated GLP-1 secretion when applying anionic exchange resins [204]. Whether the administration of bile acids sequestrants lead to increased GLP-1 secretion followed by an improvement of insulin resistance in diabetic patients is discussed controversially [205-208].

Bile acids may not only affect GLP-1 output but may contribute also to the maintenance of the intestinal epithelium *via* control of growth and repair mediated by GLP-2. Parker *et al.* for example reported a bile acid-mediated GLP-1 and GLP-2 release from GLUTag cells [49]. Moreover, mice lacking TGR5 exhibited a deteriorated intestinal barrier integrity and a TGR5 agonist ameliorated dextran sulphate sodium-induced colitis in mice [209, 210]. Total GLP-2 fasting plasma levels were not elevated in our DIO mice *in vivo*. It must be pointed out however that for the detection of murine GLP-2 there are only assays available detecting both biological active GLP-2 (1-33) and inactive GLP-2 (3-33) forms. Unfortunately, due to technical feasibility GLP-2 secretion was not sufficiently measurable from primary colonic cell cultures. The co-secretion of GLP-1 and GLP-2 from the same cell type suggests the possibility that DCA also affects GLP-2 secretion *via* TGR5 and this may contribute to maintenance of the gut barrier and epithelial integrity in DIO mice.

5 Conclusions

The present study is the first comprehensive assessment of gut barrier integrity in response to HFD in mice including the effects of diet on intestinal microbial colonization and GLP-1/2 secretion in response to bile acids and short-chain fatty acid (Figure 34).

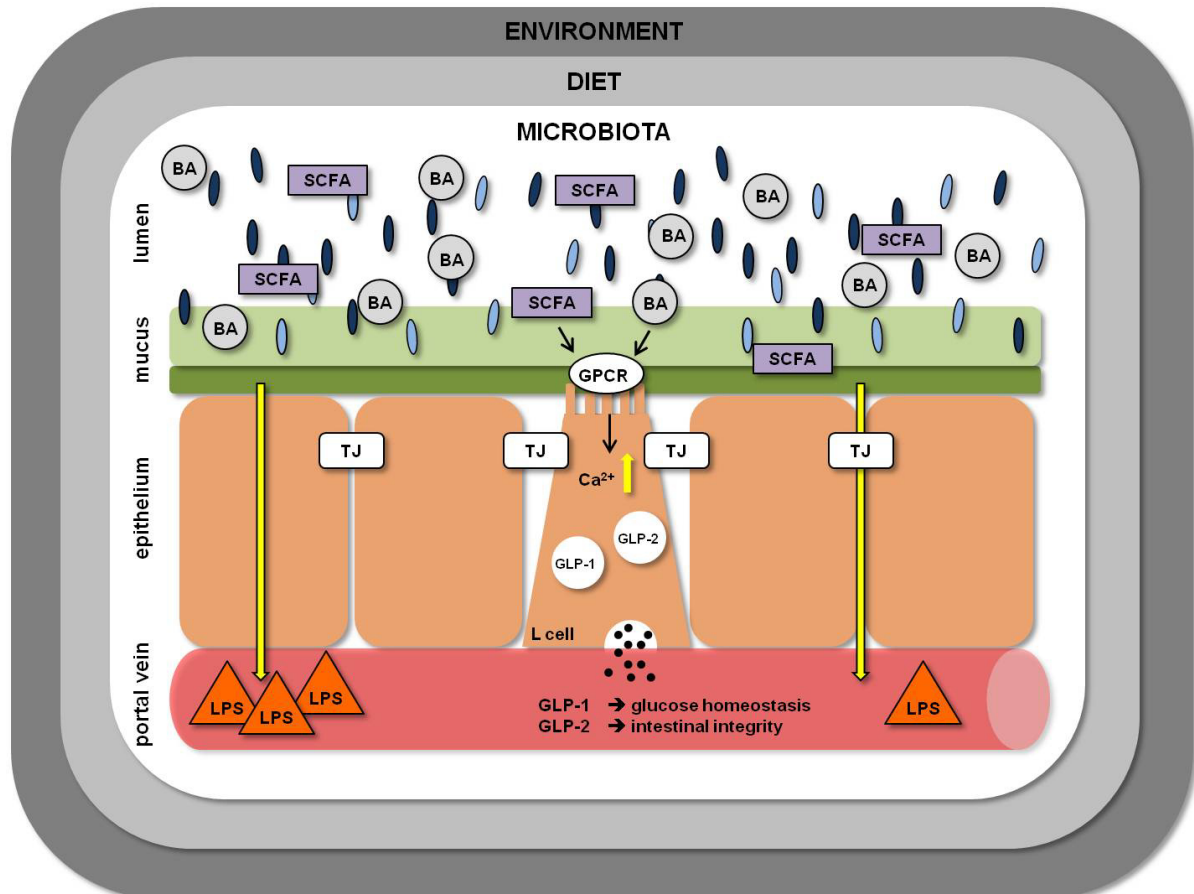


Figure 34: Gut barrier integrity and glucose homeostasis are interlinked via enteroendocrine secretion. Abbreviations: BA, bile acids; GLP-1, glucagon-like peptide-1; GLP-2, glucagon-like peptide-2; GPCR, G protein-coupled receptor; LPS, lipopolysaccharide; SCFA, short-chain fatty acid; TJ, tight junctions.

HFD was demonstrated to induce DIO in C57BL/6 mice within four weeks needed to attenuate glucose tolerance indicated by fasting hyperglycemia, fasting hyperinsulinemia and elevated incretin hormone secretion *in vivo*.

Our animal studies employing different mouse strains, a variety of diets and different feeding regimes and times revealed that none of these parameters altered intestinal barrier function. The only determinant on background of a high (animal) fat diet that was found to impair the gut barrier was the animal facility, more specifically a

CONCLUSIONS

conventional animal quarter. Comparing such a conventional facility to a SPF facility under the same experimental conditions (mouse strain, diet etc.) the intestinal microbial colonization was identified as a pivotal factor for maintaining epithelial integrity in obese animals fed a high-fat diet. A dietary factor that contributes to the intestinal homeostasis is cholesterol and the bile acids derived thereof.

Cecal and fecal bile acid concentrations and in particular the concentration of the secondary bile acid DCA were enhanced in mice receiving a diet based on animal fat. The higher load of the intestine and the microbiome with bile acids and in particular DCA may cause higher GLP-1 (possibly GLP-2) release *via* TGR5 as shown for DCA-mediated GLP-1 secretion investigated in primary colonic cell cultures. This response appears to be enhanced in obese animals as suggested by studies in primary colonic cell cultures prepared from DIO mice. Such an augmented responsiveness was also observed for GLP-1 release in response to short-chain fatty acids. Therefore, the bile acid receptor TGR5 and the short-chain fatty acid receptors FFAR2/FFAR3 become interesting targets for diabetes treatment.

Taken together, our studies do not provide strong evidence or support for the hypothesis that high-fat diets and/or obesity cause *a priori* an increased gut permeability followed by LPS translocation and an increased inflammatory tone. Even the identical diet as used in the study by *Cani et al.* [2] failed to produce significant changes in the gut functions assessed in our studies. However, the new findings in our experiments are that the fat component used in the diet is a crucial parameter for gut integrity. Animal fat sources provide a high cholesterol intake and a diet-dependent increase the secondary bile acid DCA. In turn the microbiome is affected and depending on the hygiene status of the animals and their facilities the intestinal epithelial integrity is altered.

6 Appendix

6.1 Figures and tables

List of figures

Figure 1: The intestinal barrier consists of three layers of defense.	5
Figure 2: Overview of primary and secondary bile acids.....	14
Figure 3: Enterohepatic circulation and metabolic regulation by bile acids.....	17
Figure 4: Experimental setup of an Ussing chamber.	31
Figure 5: Transepithelial resistance and permeability of colonic tissue from mouse strains with different susceptibilities to diet-induced obesity.	48
Figure 6: Transepithelial resistance and permeability of murine colonic tissues upon different high-fat feeding periods.	49
Figure 7: Transepithelial resistance and permeability of murine small and large intestine subsequent to long-term high-fat diet intervention.....	50
Figure 8: Transepithelial resistance and permeability of murine small and large intestine subsequent to a feeding trail with increasing fat proportion in the diet.....	52
Figure 9: Transepithelial resistance and permeability of murine small and large intestine subsequent to housing in a specific pathogen-free animal facility.	53
Figure 10: Transepithelial resistance and permeability of murine small and large intestine subsequent to housing in a conventional animal facility.	54
Figure 11: Changes of endotoxin in portal vein plasma due to diet and animal housing.	54
Figure 12: Transcription levels of inflammatory marker genes in liver and adipose tissue in response to a high-fat diet under different housing conditions.	56
Figure 13: Plasma levels of GLP-2 and IL-6 in response to high-fat diet.....	58
Figure 14: Jejunal and colonic protein expression levels of occludin and JAM-A in response to high-fat diet under different housing conditions.	59
Figure 15: Jejunal and colonic protein expression levels of claudin-2, -3 and -5 in response to high-fat diet under different housing conditions.	60
Figure 16: Colonic expression levels of ZO-1 in response to high-fat diet under different housing conditions.	61
Figure 17: Immunolocalization of the tight junction proteins claudin-3 (red) and claudin-5 (green) in murine jejunum and colon in response to high-fat diet.	61
Figure 18: Fecal gut microbiota composition due to diet and housing.....	63
Figure 19: Bile acids concentrations in cecal samples in response to diet and facility.....	65
Figure 20: Cecal DCA is linked to microbiota composition.	66

Figure 21: Ileal tissue stained for GIP (orange) and GLP-1 (red).67

Figure 22: Body mass and fasting blood glucose after short-term high-fat diet treatment of mice.....68

Figure 23: Plasma insulin, incretin hormones and GLP-2 levels after short-term high-fat diet intervention.....69

Figure 24: Cholesterol and triglyceride concentrations in plasma and liver tissue after short-term high-fat diet treatment.....71

Figure 25: 7 α -hydroxy-4-cholesten-3-one (C4) and total bile acid concentrations in samples of mice fed a high-fat or control diet.....72

Figure 26: Bile acids concentrations in the cecal contents and feces in samples of mice fed a high-fat or control diet.73

Figure 27: Colonic tissue and primary colonic cell culture stained for GLP-1 (red).....75

Figure 28: Deoxycholic acid-induced GLP-1 secretion in primary colonic crypt cultures.76

Figure 29: Deoxycholic acid-induced calcium changes in primary colonic cell cultures.77

Figure 30: GLP-1 secretion from primary colonic cell cultures from mice fed a CD or HFD in response to different bile acids.78

Figure 31: Gcg and Gpbar1 gene expression levels in primary colonic cell cultures prepared from animals fed a HFD or CD for 4 weeks.....78

Figure 32: Short-chain fatty-induced GLP-1 secretion from primary colonic cell cultures prepared from mice fed a CD or HFD for 4 weeks.79

Figure 33: Dexoycholic acid (DCA) induced glucagon-like petide 1 (GLP-1) secretion from primary colonic cell cultures.....90

Figure 34: Gut barrier integrity and glucose homoestasis are interlinked *via* enteroendocrine secretion.....92

List of tables

Table 1: Commonly used probes for assessment of intestinal barrier integrity.....	8
Table 2: Intestinal sensor proteins for nutrient and non-nutrient stimuli.	9
Table 3: Equipment	20
Table 4: Software applications.....	21
Table 5: Chemicals and reagents	21
Table 6: Commercial media and solutions for cell culture	22
Table 7: Consumables.....	23
Table 8: Krebs buffer (carbogen-gassed, pH 7.4).....	23
Table 9: 10xPhosphate buffered saline (pH 7.4).....	23
Table 10: Lysis buffer for western blotting (pH 7.4).....	23
Table 11: 4xLaemmli buffer (pH 6.8)	24
Table 12: 3xResolving gel buffer (pH 8.8).....	24
Table 13: 1xStacking gel buffer (pH 6.8)	24
Table 14: 1xRunning buffer	24
Table 15: Transfer buffer	24
Table 16: Citrate buffer (pH 6.0)	24
Table 17: 138 Buffer (pH 7.4)	24
Table 18: Lysis buffer for primary cell cultures.....	25
Table 19: Bile acid standard mix in MetOH: water (1:1).....	25
Table 20: Bile acids internal standard mix in methanol: water (1:1)	25
Table 21: Commercial kits and enzymes	26
Table 22: Primary antibodies	26
Table 23: Secondary antibodies	26
Table 24: Primer sequences.....	27
Table 25: Primer sequences and probes using the Universal Probe Library (UPL).....	27
Table 26: Parameters for the husbandry.....	28
Table 27: Composition of the diets	30
Table 28: Programme for one-step real-time RT-PCR	35
Table 29: qRT-PCR program for analysis of gene expression of inflammatory markers	36
Table 30: qRT-PCR program for analysis of gene expression in the enterohepatic circulation and gut hormones.....	37
Table 31: Allocation of the tissue processor	39
Table 32: Allocation of the multistainer	39
Table 33: Scheme for rehydration.....	40
Table 34: Gradient for LC separation of bile acids	42
Table 35: Gradient for LC separation of C4	42

Table 36: Transepithelial resistance and permeability	51
Table 37: Body mass and intestinal length	57
Table 38: Height of villi in small intestine	57
Table 39: Effects of short-term high-fat diet treatment on transcript levels of the hormones GIP and GLP-1/2 in the intestine.	70
Table 40: Transcript levels of the two key enzymes of bile acid synthesis in the liver.	71
Table 41: Transcript levels of receptors and transporters of the enterohepatic circulation. ...	74

6.2 List of abbreviations

$\alpha/\beta/\omega$ MCA	$\alpha/\beta/\omega$ muricholic acid
APS	ammonium persulfate
BA	bile acid
BSA	bovine serum albumin
BSEP	bile salt export pump
C4	7 α -hydroxy-4-cholesten-3-one
CA	cholic acid
cAMP	cyclic adenosine monophosphate
CCK	cholecystokinin
CD	control diet
CDCA	chenodeoxycholic acid
CV	conventional
CYP7A1	cholesterol 7 α -hydroxylase
CYP7B1	oxysterol 7 α -hydroxylase
CYP27A1	sterol 27-hydroxylase
DCA	deoxycholic acid
DAPI	4',6-diamidino-2-phenylindole
DIO	diet-induced obesity
DPP4	dipeptidyl peptidase 4
DTT	dithiothreitol
EC ₅₀	half maximal effective concentration
EDTA	ethylenediaminetetraacetic acid
EEC	enteroendocrine cells
EGTA	ethylene glycol-bis(2-aminoethylether)-N,N,N',N'-tetraacetic acid
ELISA	Enzyme linked immunosorbent assay
FELASA	Federation of European Laboratory Animal Science Associations
FFAR2/3	free fatty acid receptor 2/3
FXR	farnesoid receptor X
FGF15/19	fibroblast growth factor 15
FGFR4	fibroblast growth factor receptor 4
FITC-dextran	fluorescein isothiocyanate–dextran
GALT	gut-associated lymphoid tissue
GIP	glucose-dependent insulintropic peptide
GLP-1/2	glucagon-like peptide-1/2
GPCR	G protein coupled receptors
HCA	hyocholic acid

HDCA	hyodeoxycholic acid
HEPES	4-(2-hydroxyethyl)-1-piperazineethanesulfonic acid
HFD	high-fat diet
IBABP	ileal bile acid binding protein
IBAT	ileal bile acid transporter
IBMX	3-isobutyl-1-methylxanthine
ICH	immunohistochemistry
IL	interleukin
JAM	junctional adhesion molecule
LBP	LPS-binding protein
LCA	lithocholic acid
ICD	lard-based control diet
IHFD	lard-based high-fat diet
LPS	lipopolysaccharide
LXR	liver X receptor
MCP-1	monocyte chemotactic protein 1
MW	molecular weight
NOD	nucleotide binding oligomerization domain
NTCP	sodium-taurocholate cotransporting polypeptide
OATP	organic anion transporting polypeptide
OST α/β	organic solute transporter α/β
OTU	operating taxonomic unit
PBS	phosphate-buffered saline
pCD	plant-based control diet
PCR	polymerase chain reaction
PEPT1	proton-coupled peptide transporter 1
pHFD	plant-based high-fat diet
PMSF	phenylmethanesulfonyl fluoride
PYY	peptide YY
RNA	ribonucleic acid
rRNA	ribosomal ribonucleic acid
SDS	sodium dodecyl sulphate
SGLT1	sodium-dependent glucose transporter 1
SHP	small heterodimer partner
SIgA	secretory immunoglobulin A
SPF	specific pathogen-free
TAMPs	tight junction associated MARVEL proteins
TEMED	N,N,N',N'-Tetramethylethylenediamine
TER	transepithelial resistance
TG	triglyceride
TLR	toll-like receptor
TNF	tumour necrosis factor
Tris	tris(hydroxymethyl)aminomethane
UDCA	ursodeoxycholic acid
UPL	universal probe library
WB	western blot
ZO	zonula occludens

6.3 References

1. **Fact sheet N°311: Obesity and overweight**
2. Cani PD, Amar J, Iglesias MA, Poggi M, Knauf C, Bastelica D, Neyrinck AM, Fava F, Tuohy KM, Chabo C *et al*: **Metabolic endotoxemia initiates obesity and insulin resistance**. *Diabetes* 2007, **56**(7):1761-1772.
3. Cani PD, Bibiloni R, Knauf C, Waget A, Neyrinck AM, Delzenne NM, Burcelin R: **Changes in gut microbiota control metabolic endotoxemia-induced inflammation in high-fat diet-induced obesity and diabetes in mice**. *Diabetes* 2008, **57**(6):1470-1481.
4. Clevers H: **The intestinal crypt, a prototype stem cell compartment**. *Cell* 2013, **154**(2):274-284.
5. Groschwitz KR, Hogan SP: **Intestinal barrier function: molecular regulation and disease pathogenesis**. *The Journal of allergy and clinical immunology* 2009, **124**(1):3-20; quiz 21-22.
6. Vandenbroucke E, Mehta D, Minshall R, Malik AB: **Regulation of endothelial junctional permeability**. *Annals of the New York Academy of Sciences* 2008, **1123**:134-145.
7. Ulluwishewa D, Anderson RC, McNabb WC, Moughan PJ, Wells JM, Roy NC: **Regulation of tight junction permeability by intestinal bacteria and dietary components**. *The Journal of nutrition* 2011, **141**(5):769-776.
8. Johansson ME, Hansson GC: **Microbiology. Keeping bacteria at a distance**. *Science* 2011, **334**(6053):182-183.
9. Pelaseyed T, Bergstrom JH, Gustafsson JK, Ermund A, Birchenough GM, Schutte A, van der Post S, Svensson F, Rodriguez-Pineiro AM, Nystrom EE *et al*: **The mucus and mucins of the goblet cells and enterocytes provide the first defense line of the gastrointestinal tract and interact with the immune system**. *Immunological reviews* 2014, **260**(1):8-20.
10. Johansson ME, Ambort D, Pelaseyed T, Schutte A, Gustafsson JK, Ermund A, Subramani DB, Holmen-Larsson JM, Thomsson KA, Bergstrom JH *et al*: **Composition and functional role of the mucus layers in the intestine**. *Cellular and molecular life sciences : CMLS* 2011, **68**(22):3635-3641.
11. Atuma C, Strugala V, Allen A, Holm L: **The adherent gastrointestinal mucus gel layer: thickness and physical state in vivo**. *American journal of physiology Gastrointestinal and liver physiology* 2001, **280**(5):G922-929.
12. Johansson ME, Phillipson M, Petersson J, Velcich A, Holm L, Hansson GC: **The inner of the two Muc2 mucin-dependent mucus layers in colon is devoid of bacteria**. *Proceedings of the National Academy of Sciences of the United States of America* 2008, **105**(39):15064-15069.
13. Mandel LJ, Bacallao R, Zampighi G: **Uncoupling of the molecular 'fence' and paracellular 'gate' functions in epithelial tight junctions**. *Nature* 1993, **361**(6412):552-555.
14. Amasheh S, Fromm M, Gunzel D: **Claudins of intestine and nephron - a correlation of molecular tight junction structure and barrier function**. *Acta physiologica* 2011, **201**(1):133-140.
15. Raleigh DR, Marchiando AM, Zhang Y, Shen L, Sasaki H, Wang Y, Long M, Turner JR: **Tight junction-associated MARVEL proteins marveld3, tricellulin, and occludin have distinct but overlapping functions**. *Molecular biology of the cell* 2010, **21**(7):1200-1213.

16. Schulzke JD, Gunzel D, John LJ, Fromm M: **Perspectives on tight junction research.** *Annals of the New York Academy of Sciences* 2012, **1257**:1-19.
17. Luissint AC, Nusrat A, Parkos CA: **JAM-related proteins in mucosal homeostasis and inflammation.** *Seminars in immunopathology* 2014, **36**(2):211-226.
18. Laukoetter MG, Nava P, Lee WY, Severson EA, Capaldo CT, Babbin BA, Williams IR, Koval M, Peatman E, Campbell JA *et al*: **JAM-A regulates permeability and inflammation in the intestine in vivo.** *The Journal of experimental medicine* 2007, **204**(13):3067-3076.
19. Furuse M, Hirase T, Itoh M, Nagafuchi A, Yonemura S, Tsukita S, Tsukita S: **Occludin: a novel integral membrane protein localizing at tight junctions.** *The Journal of cell biology* 1993, **123**(6 Pt 2):1777-1788.
20. Ikenouchi J, Furuse M, Furuse K, Sasaki H, Tsukita S, Tsukita S: **Tricellulin constitutes a novel barrier at tricellular contacts of epithelial cells.** *The Journal of cell biology* 2005, **171**(6):939-945.
21. Steed E, Rodrigues NT, Balda MS, Matter K: **Identification of MarvelD3 as a tight junction-associated transmembrane protein of the occludin family.** *BMC cell biology* 2009, **10**:95.
22. Saitou M, Furuse M, Sasaki H, Schulzke JD, Fromm M, Takano H, Noda T, Tsukita S: **Complex phenotype of mice lacking occludin, a component of tight junction strands.** *Molecular biology of the cell* 2000, **11**(12):4131-4142.
23. Holmes JL, Van Itallie CM, Rasmussen JE, Anderson JM: **Claudin profiling in the mouse during postnatal intestinal development and along the gastrointestinal tract reveals complex expression patterns.** *Gene expression patterns : GEP* 2006, **6**(6):581-588.
24. Zeissig S, Burgel N, Gunzel D, Richter J, Mankertz J, Wahnschaffe U, Kroesen AJ, Zeitz M, Fromm M, Schulzke JD: **Changes in expression and distribution of claudin 2, 5 and 8 lead to discontinuous tight junctions and barrier dysfunction in active Crohn's disease.** *Gut* 2007, **56**(1):61-72.
25. Prasad S, Mingrino R, Kaukinen K, Hayes KL, Powell RM, MacDonald TT, Collins JE: **Inflammatory processes have differential effects on claudins 2, 3 and 4 in colonic epithelial cells.** *Laboratory investigation; a journal of technical methods and pathology* 2005, **85**(9):1139-1162.
26. Bauer H, Zweimueller-Mayer J, Steinbacher P, Lametschwandtner A, Bauer HC: **The dual role of zonula occludens (ZO) proteins.** *Journal of biomedicine & biotechnology* 2010, **2010**:402593.
27. Nusrat A, Turner JR, Madara JL: **Molecular physiology and pathophysiology of tight junctions. IV. Regulation of tight junctions by extracellular stimuli: nutrients, cytokines, and immune cells.** *American journal of physiology Gastrointestinal and liver physiology* 2000, **279**(5):G851-857.
28. Fagarasan S, Honjo T: **Intestinal IgA synthesis: regulation of front-line body defences.** *Nature reviews Immunology* 2003, **3**(1):63-72.
29. Creely SJ, McTernan PG, Kusminski CM, Fisher f M, Da Silva NF, Khanolkar M, Evans M, Harte AL, Kumar S: **Lipopolysaccharide activates an innate immune system response in human adipose tissue in obesity and type 2 diabetes.** *American journal of physiology Endocrinology and metabolism* 2007, **292**(3):E740-747.
30. Schertzer JD, Tamrakar AK, Magalhaes JG, Pereira S, Bilan PJ, Fullerton MD, Liu Z, Steinberg GR, Giacca A, Philpott DJ *et al*: **NOD1 activators link innate immunity to insulin resistance.** *Diabetes* 2011, **60**(9):2206-2215.

31. Murphy K, Travers, P., Walport, M.: **Innate Immunity**. In: *Janeway's Immunobiology*. 7th edn.; 2007: 39-108.
32. Mantis NJ, Rol N, Corthesy B: **Secretory IgA's complex roles in immunity and mucosal homeostasis in the gut**. *Mucosal immunology* 2011, **4**(6):603-611.
33. Bischoff SC, Barbara G, Buurman W, Ockhuizen T, Schulzke JD, Serino M, Tilg H, Watson A, Wells JM: **Intestinal permeability--a new target for disease prevention and therapy**. *BMC gastroenterology* 2014, **14**:189.
34. Bjarnason I, MacPherson A, Hollander D: **Intestinal permeability: an overview**. *Gastroenterology* 1995, **108**(5):1566-1581.
35. Salles Teixeira TF, Boroni Moreira AP, Silva Souza NC, Frias R, Gouveia Peluzio Mdo C: **Intestinal permeability measurements: general aspects and possible pitfalls**. *Nutricion hospitalaria* 2014, **29**(2):269-281.
36. Psichas A, Reimann F, Gribble FM: **Gut chemosensing mechanisms**. *The Journal of clinical investigation* 2015.
37. Nguyen CA, Akiba Y, Kaunitz JD: **Recent advances in gut nutrient chemosensing**. *Current medicinal chemistry* 2012, **19**(1):28-34.
38. Parker HE, Adriaenssens A, Rogers G, Richards P, Koepsell H, Reimann F, Gribble FM: **Predominant role of active versus facilitative glucose transport for glucagon-like peptide-1 secretion**. *Diabetologia* 2012, **55**(9):2445-2455.
39. Gorboulev V, Schurmann A, Vallon V, Kipp H, Jaschke A, Klessen D, Friedrich A, Scherneck S, Rieg T, Cunard R *et al*: **Na(+)-D-glucose cotransporter SGLT1 is pivotal for intestinal glucose absorption and glucose-dependent incretin secretion**. *Diabetes* 2012, **61**(1):187-196.
40. Roder PV, Geillinger KE, Zietek TS, Thorens B, Koepsell H, Daniel H: **The role of SGLT1 and GLUT2 in intestinal glucose transport and sensing**. *PloS one* 2014, **9**(2):e89977.
41. Diakogiannaki E, Pais R, Tolhurst G, Parker HE, Horscroft J, Rauscher B, Zietek T, Daniel H, Gribble FM, Reimann F: **Oligopeptides stimulate glucagon-like peptide-1 secretion in mice through proton-coupled uptake and the calcium-sensing receptor**. *Diabetologia* 2013, **56**(12):2688-2696.
42. Hirasawa A, Tsumaya K, Awaji T, Katsuma S, Adachi T, Yamada M, Sugimoto Y, Miyazaki S, Tsujimoto G: **Free fatty acids regulate gut incretin glucagon-like peptide-1 secretion through GPR120**. *Nature medicine* 2005, **11**(1):90-94.
43. Chu ZL, Carroll C, Alfonso J, Gutierrez V, He H, Lucman A, Pedraza M, Mondala H, Gao H, Bagnol D *et al*: **A role for intestinal endocrine cell-expressed G protein-coupled receptor 119 in glycemic control by enhancing glucagon-like Peptide-1 and glucose-dependent insulinotropic Peptide release**. *Endocrinology* 2008, **149**(5):2038-2047.
44. Edfalk S, Steneberg P, Edlund H: **Gpr40 is expressed in enteroendocrine cells and mediates free fatty acid stimulation of incretin secretion**. *Diabetes* 2008, **57**(9):2280-2287.
45. Tolhurst G, Heffron H, Lam YS, Parker HE, Habib AM, Diakogiannaki E, Cameron J, Grosse J, Reimann F, Gribble FM: **Short-chain fatty acids stimulate glucagon-like peptide-1 secretion via the G-protein-coupled receptor FFAR2**. *Diabetes* 2012, **61**(2):364-371.

46. Nohr MK, Pedersen MH, Gille A, Egerod KL, Engelstoft MS, Husted AS, Sichlau RM, Grunddal KV, Poulsen SS, Han S *et al*: **GPR41/FFAR3 and GPR43/FFAR2 as cosensors for short-chain fatty acids in enteroendocrine cells vs FFAR3 in enteric neurons and FFAR2 in enteric leukocytes.** *Endocrinology* 2013, **154**(10):3552-3564.
47. Psichas A, Sleeth ML, Murphy KG, Brooks L, Bewick GA, Hanyaloglu AC, Ghatei MA, Bloom SR, Frost G: **The short chain fatty acid propionate stimulates GLP-1 and PYY secretion via free fatty acid receptor 2 in rodents.** *International journal of obesity* 2014.
48. Thomas C, Gioiello A, Noriega L, Strehle A, Oury J, Rizzo G, Macchiarulo A, Yamamoto H, Matakı C, Pruzanski M *et al*: **TGR5-mediated bile acid sensing controls glucose homeostasis.** *Cell metabolism* 2009, **10**(3):167-177.
49. Parker HE, Wallis K, le Roux CW, Wong KY, Reimann F, Gribble FM: **Molecular mechanisms underlying bile acid-stimulated glucagon-like peptide-1 secretion.** *British journal of pharmacology* 2012, **165**(2):414-423.
50. Cote CD, Zadeh-Tahmasebi M, Rasmussen BA, Duca FA, Lam TK: **Hormonal signaling in the gut.** *The Journal of biological chemistry* 2014, **289**(17):11642-11649.
51. Habib AM, Richards P, Cairns LS, Rogers GJ, Bannon CA, Parker HE, Morley TC, Yeo GS, Reimann F, Gribble FM: **Overlap of endocrine hormone expression in the mouse intestine revealed by transcriptional profiling and flow cytometry.** *Endocrinology* 2012, **153**(7):3054-3065.
52. Egerod KL, Engelstoft MS, Grunddal KV, Nohr MK, Secher A, Sakata I, Pedersen J, Windelov JA, Fuchtbauer EM, Olsen J *et al*: **A major lineage of enteroendocrine cells coexpress CCK, secretin, GIP, GLP-1, PYY, and neurotensin but not somatostatin.** *Endocrinology* 2012, **153**(12):5782-5795.
53. Sykaras AG, Demenis C, Cheng L, Pisitkun T, McLaughlin JT, Fenton RA, Smith CP: **Duodenal CCK cells from male mice express multiple hormones including ghrelin.** *Endocrinology* 2014, **155**(9):3339-3351.
54. Baggio LL, Drucker DJ: **Biology of incretins: GLP-1 and GIP.** *Gastroenterology* 2007, **132**(6):2131-2157.
55. Elrick H, Stimmler L, Hlad CJ, Jr., Arai Y: **Plasma Insulin Response to Oral and Intravenous Glucose Administration.** *The Journal of clinical endocrinology and metabolism* 1964, **24**:1076-1082.
56. Maruyama T, Miyamoto Y, Nakamura T, Tamai Y, Okada H, Sugiyama E, Nakamura T, Itadani H, Tanaka K: **Identification of membrane-type receptor for bile acids (M-BAR).** *Biochemical and biophysical research communications* 2002, **298**(5):714-719.
57. Kawamata Y, Fujii R, Hosoya M, Harada M, Yoshida H, Miwa M, Fukusumi S, Habata Y, Itoh T, Shintani Y *et al*: **A G protein-coupled receptor responsive to bile acids.** *The Journal of biological chemistry* 2003, **278**(11):9435-9440.
58. Hov JR, Keitel V, Laerdahl JK, Spomer L, Ellinghaus E, ElSharawy A, Melum E, Boberg KM, Manke T, Balschun T *et al*: **Mutational characterization of the bile acid receptor TGR5 in primary sclerosing cholangitis.** *PLoS one* 2010, **5**(8):e12403.
59. Bala V, Rajagopal S, Kumar DP, Nalli AD, Mahavadi S, Sanyal AJ, Grider JR, Murthy KS: **Release of GLP-1 and PYY in response to the activation of G protein-coupled bile acid receptor TGR5 is mediated by Epac/PLC-epsilon pathway and modulated by endogenous H2S.** *Frontiers in physiology* 2014, **5**:420.

60. Duboc H, Tache Y, Hofmann AF: **The bile acid TGR5 membrane receptor: from basic research to clinical application.** *Digestive and liver disease : official journal of the Italian Society of Gastroenterology and the Italian Association for the Study of the Liver* 2014, **46**(4):302-312.
61. Maruyama T, Tanaka K, Suzuki J, Miyoshi H, Harada N, Nakamura T, Miyamoto Y, Kanatani A, Tamai Y: **Targeted disruption of G protein-coupled bile acid receptor 1 (Gpbar1/M-Bar) in mice.** *The Journal of endocrinology* 2006, **191**(1):197-205.
62. Poole DP, Godfrey C, Cattaruzza F, Cottrell GS, Kirkland JG, Pelayo JC, Bunnett NW, Corvera CU: **Expression and function of the bile acid receptor GpBAR1 (TGR5) in the murine enteric nervous system.** *Neurogastroenterology and motility : the official journal of the European Gastrointestinal Motility Society* 2010, **22**(7):814-825, e227-818.
63. Keitel V, Cupisti K, Ullmer C, Knoefel WT, Kubitz R, Haussinger D: **The membrane-bound bile acid receptor TGR5 is localized in the epithelium of human gallbladders.** *Hepatology* 2009, **50**(3):861-870.
64. Watanabe M, Houten SM, Matak C, Christoffolete MA, Kim BW, Sato H, Messaddeq N, Harney JW, Ezaki O, Kodama T *et al*: **Bile acids induce energy expenditure by promoting intracellular thyroid hormone activation.** *Nature* 2006, **439**(7075):484-489.
65. Watanabe M, Horai Y, Houten SM, Morimoto K, Sugizaki T, Arita E, Matak C, Sato H, Tanigawara Y, Schoonjans K *et al*: **Lowering bile acid pool size with a synthetic farnesoid X receptor (FXR) agonist induces obesity and diabetes through reduced energy expenditure.** *The Journal of biological chemistry* 2011, **286**(30):26913-26920.
66. Calmus Y, Guechot J, Podevin P, Bonnefis MT, Giboudeau J, Poupon R: **Differential effects of chenodeoxycholic and ursodeoxycholic acids on interleukin 1, interleukin 6 and tumor necrosis factor-alpha production by monocytes.** *Hepatology* 1992, **16**(3):719-723.
67. Pols TW, Nomura M, Harach T, Lo Sasso G, Oosterveer MH, Thomas C, Rizzo G, Gioiello A, Adorini L, Pellicciari R *et al*: **TGR5 activation inhibits atherosclerosis by reducing macrophage inflammation and lipid loading.** *Cell metabolism* 2011, **14**(6):747-757.
68. Kumar DP, Rajagopal S, Mahavadi S, Mirshahi F, Grider JR, Murthy KS, Sanyal AJ: **Activation of transmembrane bile acid receptor TGR5 stimulates insulin secretion in pancreatic beta cells.** *Biochemical and biophysical research communications* 2012, **427**(3):600-605.
69. Drucker DJ, Jin T, Asa SL, Young TA, Brubaker PL: **Activation of proglucagon gene transcription by protein kinase-A in a novel mouse enteroendocrine cell line.** *Molecular endocrinology* 1994, **8**(12):1646-1655.
70. Abello J, Ye F, Bosshard A, Bernard C, Cuber JC, Chayvialle JA: **Stimulation of glucagon-like peptide-1 secretion by muscarinic agonist in a murine intestinal endocrine cell line.** *Endocrinology* 1994, **134**(5):2011-2017.
71. Reimer RA, Darimont C, Gremlich S, Nicolas-Metral V, Ruegg UT, Mace K: **A human cellular model for studying the regulation of glucagon-like peptide-1 secretion.** *Endocrinology* 2001, **142**(10):4522-4528.
72. Reimann F, Habib AM, Tolhurst G, Parker HE, Rogers GJ, Gribble FM: **Glucose sensing in L cells: a primary cell study.** *Cell metabolism* 2008, **8**(6):532-539.

73. Sato T, Vries RG, Snippert HJ, van de Wetering M, Barker N, Stange DE, van Es JH, Abo A, Kujala P, Peters PJ *et al*: **Single Lgr5 stem cells build crypt-villus structures in vitro without a mesenchymal niche.** *Nature* 2009, **459**(7244):262-265.
74. Sato T, Clevers H: **Growing self-organizing mini-guts from a single intestinal stem cell: mechanism and applications.** *Science* 2013, **340**(6137):1190-1194.
75. Petersen N, Reimann F, Bartfeld S, Farin HF, Ringnalda FC, Vries RG, van den Brink S, Clevers H, Gribble FM, de Koning EJ: **Generation of L cells in mouse and human small intestine organoids.** *Diabetes* 2014, **63**(2):410-420.
76. Petersen N, Reimann F, van Es JH, van den Berg BM, Kroone C, Pais R, Jansen E, Clevers H, Gribble FM, de Koning EJ: **Targeting development of incretin-producing cells increases insulin secretion.** *The Journal of clinical investigation* 2015, **125**(1):379-385.
77. Sommer F, Backhed F: **The gut microbiota--masters of host development and physiology.** *Nature reviews Microbiology* 2013, **11**(4):227-238.
78. Sekirov I, Russell SL, Antunes LC, Finlay BB: **Gut microbiota in health and disease.** *Physiological reviews* 2010, **90**(3):859-904.
79. Ley RE, Turnbaugh PJ, Klein S, Gordon JI: **Microbial ecology: human gut microbes associated with obesity.** *Nature* 2006, **444**(7122):1022-1023.
80. Ley RE, Backhed F, Turnbaugh P, Lozupone CA, Knight RD, Gordon JI: **Obesity alters gut microbial ecology.** *Proceedings of the National Academy of Sciences of the United States of America* 2005, **102**(31):11070-11075.
81. Turnbaugh PJ, Backhed F, Fulton L, Gordon JI: **Diet-induced obesity is linked to marked but reversible alterations in the mouse distal gut microbiome.** *Cell host & microbe* 2008, **3**(4):213-223.
82. Murphy EF, Cotter PD, Healy S, Marques TM, O'Sullivan O, Fouhy F, Clarke SF, O'Toole PW, Quigley EM, Stanton C *et al*: **Composition and energy harvesting capacity of the gut microbiota: relationship to diet, obesity and time in mouse models.** *Gut* 2010, **59**(12):1635-1642.
83. Fleissner CK, Huebel N, Abd El-Bary MM, Loh G, Klaus S, Blaut M: **Absence of intestinal microbiota does not protect mice from diet-induced obesity.** *The British journal of nutrition* 2010, **104**(6):919-929.
84. Daniel H, Moghaddas Gholami A, Berry D, Desmarchelier C, Hahne H, Loh G, Mondot S, Lepage P, Rothballer M, Walker A *et al*: **High-fat diet alters gut microbiota physiology in mice.** *The ISME journal* 2014, **8**(2):295-308.
85. Turnbaugh PJ, Ley RE, Mahowald MA, Magrini V, Mardis ER, Gordon JI: **An obesity-associated gut microbiome with increased capacity for energy harvest.** *Nature* 2006, **444**(7122):1027-1031.
86. Backhed F, Manchester JK, Semenkovich CF, Gordon JI: **Mechanisms underlying the resistance to diet-induced obesity in germ-free mice.** *Proceedings of the National Academy of Sciences of the United States of America* 2007, **104**(3):979-984.
87. Sjogren K, Engdahl C, Henning P, Lerner UH, Tremaroli V, Lagerquist MK, Backhed F, Ohlsson C: **The gut microbiota regulates bone mass in mice.** *Journal of bone and mineral research : the official journal of the American Society for Bone and Mineral Research* 2012, **27**(6):1357-1367.

88. Backhed F, Ding H, Wang T, Hooper LV, Koh GY, Nagy A, Semenkovich CF, Gordon JI: **The gut microbiota as an environmental factor that regulates fat storage.** *Proceedings of the National Academy of Sciences of the United States of America* 2004, **101**(44):15718-15723.
89. Stappenbeck TS, Hooper LV, Gordon JI: **Developmental regulation of intestinal angiogenesis by indigenous microbes via Paneth cells.** *Proceedings of the National Academy of Sciences of the United States of America* 2002, **99**(24):15451-15455.
90. Larsson E, Tremaroli V, Lee YS, Koren O, Nookaew I, Fricker A, Nielsen J, Ley RE, Backhed F: **Analysis of gut microbial regulation of host gene expression along the length of the gut and regulation of gut microbial ecology through MyD88.** *Gut* 2012, **61**(8):1124-1131.
91. Tremaroli V, Backhed F: **Functional interactions between the gut microbiota and host metabolism.** *Nature* 2012, **489**(7415):242-249.
92. Moschetta A, Xu F, Hagey LR, van Berge-Henegouwen GP, van Erpecum KJ, Brouwers JF, Cohen JC, Bierman M, Hobbs HH, Steinbach JH *et al*: **A phylogenetic survey of biliary lipids in vertebrates.** *Journal of lipid research* 2005, **46**(10):2221-2232.
93. Russell DW: **The enzymes, regulation, and genetics of bile acid synthesis.** *Annual review of biochemistry* 2003, **72**:137-174.
94. Schwarz M, Russell DW, Dietschy JM, Turley SD: **Alternate pathways of bile acid synthesis in the cholesterol 7 α -hydroxylase knockout mouse are not upregulated by either cholesterol or cholestyramine feeding.** *Journal of lipid research* 2001, **42**(10):1594-1603.
95. Kuipers F, Bloks VW, Groen AK: **Beyond intestinal soap--bile acids in metabolic control.** *Nature reviews Endocrinology* 2014, **10**(8):488-498.
96. Hylemon PB, Zhou H, Pandak WM, Ren S, Gil G, Dent P: **Bile acids as regulatory molecules.** *Journal of lipid research* 2009, **50**(8):1509-1520.
97. Martin FP, Dumas ME, Wang Y, Legido-Quigley C, Yap IK, Tang H, Zirah S, Murphy GM, Cloarec O, Lindon JC *et al*: **A top-down systems biology view of microbiome-mammalian metabolic interactions in a mouse model.** *Molecular systems biology* 2007, **3**:112.
98. Dawson PA, Lan T, Rao A: **Bile acid transporters.** *Journal of lipid research* 2009, **50**(12):2340-2357.
99. Bortolini O, Medici A, Poli S: **Biotransformations on steroid nucleus of bile acids.** *Steroids* 1997, **62**(8-9):564-577.
100. Begley M, Gahan CG, Hill C: **The interaction between bacteria and bile.** *FEMS microbiology reviews* 2005, **29**(4):625-651.
101. Lefebvre P, Cariou B, Lien F, Kuipers F, Staels B: **Role of bile acids and bile acid receptors in metabolic regulation.** *Physiological reviews* 2009, **89**(1):147-191.
102. Hofmann AF, Eckmann L: **How bile acids confer gut mucosal protection against bacteria.** *Proceedings of the National Academy of Sciences of the United States of America* 2006, **103**(12):4333-4334.
103. Makishima M, Okamoto AY, Repa JJ, Tu H, Learned RM, Luk A, Hull MV, Lustig KD, Mangelsdorf DJ, Shan B: **Identification of a nuclear receptor for bile acids.** *Science* 1999, **284**(5418):1362-1365.
104. Parks DJ, Blanchard SG, Bledsoe RK, Chandra G, Consler TG, Kliwer SA, Stimmel JB, Willson TM, Zavacki AM, Moore DD *et al*: **Bile acids: natural ligands for an orphan nuclear receptor.** *Science* 1999, **284**(5418):1365-1368.

105. Wang H, Chen J, Hollister K, Sowers LC, Forman BM: **Endogenous bile acids are ligands for the nuclear receptor FXR/BAR.** *Molecular cell* 1999, **3**(5):543-553.
106. Ridlon JM, Kang DJ, Hylemon PB, Bajaj JS: **Bile acids and the gut microbiome.** *Current opinion in gastroenterology* 2014, **30**(3):332-338.
107. Zhang Y, Kast-Woelbern HR, Edwards PA: **Natural structural variants of the nuclear receptor farnesoid X receptor affect transcriptional activation.** *The Journal of biological chemistry* 2003, **278**(1):104-110.
108. Inagaki T, Choi M, Moschetta A, Peng L, Cummins CL, McDonald JG, Luo G, Jones SA, Goodwin B, Richardson JA *et al*: **Fibroblast growth factor 15 functions as an enterohepatic signal to regulate bile acid homeostasis.** *Cell metabolism* 2005, **2**(4):217-225.
109. Ma K, Saha PK, Chan L, Moore DD: **Farnesoid X receptor is essential for normal glucose homeostasis.** *The Journal of clinical investigation* 2006, **116**(4):1102-1109.
110. Reddy BS: **Diet and excretion of bile acids.** *Cancer research* 1981, **41**(9 Pt 2):3766-3768.
111. Cummings JH, Wiggins HS, Jenkins DJ, Houston H, Jivraj T, Drasar BS, Hill MJ: **Influence of diets high and low in animal fat on bowel habit, gastrointestinal transit time, fecal microflora, bile acid, and fat excretion.** *The Journal of clinical investigation* 1978, **61**(4):953-963.
112. Peet DJ, Turley SD, Ma W, Janowski BA, Lobaccaro JM, Hammer RE, Mangelsdorf DJ: **Cholesterol and bile acid metabolism are impaired in mice lacking the nuclear oxysterol receptor LXR alpha.** *Cell* 1998, **93**(5):693-704.
113. Tiemann M, Han Z, Soccio R, Bollineni J, Shefer S, Sehayek E, Breslow JL: **Cholesterol feeding of mice expressing cholesterol 7alpha-hydroxylase increases bile acid pool size despite decreased enzyme activity.** *Proceedings of the National Academy of Sciences of the United States of America* 2004, **101**(7):1846-1851.
114. Devkota S, Wang Y, Musch MW, Leone V, Fehlner-Peach H, Nadimpalli A, Antonopoulos DA, Jabri B, Chang EB: **Dietary-fat-induced taurocholic acid promotes pathobiont expansion and colitis in Il10^{-/-} mice.** *Nature* 2012, **487**(7405):104-108.
115. Laugerette F, Vors C, Peretti N, Michalski MC: **Complex links between dietary lipids, endogenous endotoxins and metabolic inflammation.** *Biochimie* 2011, **93**(1):39-45.
116. Gu Y, Yu S, Park JY, Harvatine K, Lambert JD: **Dietary cocoa reduces metabolic endotoxemia and adipose tissue inflammation in high-fat fed mice.** *The Journal of nutritional biochemistry* 2014, **25**(4):439-445.
117. Everard A, Geurts L, Van Roye M, Delzenne NM, Cani PD: **Tetrahydro iso-alpha acids from hops improve glucose homeostasis and reduce body weight gain and metabolic endotoxemia in high-fat diet-fed mice.** *PloS one* 2012, **7**(3):e33858.
118. Kim KA, Gu W, Lee IA, Joh EH, Kim DH: **High fat diet-induced gut microbiota exacerbates inflammation and obesity in mice via the TLR4 signaling pathway.** *PloS one* 2012, **7**(10):e47713.

119. Kaliannan K, Hamarneh SR, Economopoulos KP, Nasrin Alam S, Moaven O, Patel P, Malo NS, Ray M, Abtahi SM, Muhammad N *et al*: **Intestinal alkaline phosphatase prevents metabolic syndrome in mice.** *Proceedings of the National Academy of Sciences of the United States of America* 2013, **110**(17):7003-7008.
120. Haub S, Ritze Y, Ladel I, Saum K, Hubert A, Spruss A, Trautwein C, Bischoff SC: **Serotonin receptor type 3 antagonists improve obesity-associated fatty liver disease in mice.** *The Journal of pharmacology and experimental therapeutics* 2011, **339**(3):790-798.
121. Neal MD, Leaphart C, Levy R, Prince J, Billiar TR, Watkins S, Li J, Cetin S, Ford H, Schreiber A *et al*: **Enterocyte TLR4 mediates phagocytosis and translocation of bacteria across the intestinal barrier.** *Journal of immunology* 2006, **176**(5):3070-3079.
122. Tomita M, Ohkubo R, Hayashi M: **Lipopolysaccharide transport system across colonic epithelial cells in normal and infective rat.** *Drug metabolism and pharmacokinetics* 2004, **19**(1):33-40.
123. Ghoshal S, Witta J, Zhong J, de Villiers W, Eckhardt E: **Chylomicrons promote intestinal absorption of lipopolysaccharides.** *Journal of lipid research* 2009, **50**(1):90-97.
124. Erridge C, Attina T, Spickett CM, Webb DJ: **A high-fat meal induces low-grade endotoxemia: evidence of a novel mechanism of postprandial inflammation.** *The American journal of clinical nutrition* 2007, **86**(5):1286-1292.
125. Laugerette F, Vors C, Geloën A, Chauvin MA, Soulage C, Lambert-Porcheron S, Peretti N, Alligier M, Burcelin R, Laville M *et al*: **Emulsified lipids increase endotoxemia: possible role in early postprandial low-grade inflammation.** *The Journal of nutritional biochemistry* 2011, **22**(1):53-59.
126. Amar J, Burcelin R, Ruidavets JB, Cani PD, Fauvel J, Alessi MC, Chamontin B, Ferrieres J: **Energy intake is associated with endotoxemia in apparently healthy men.** *The American journal of clinical nutrition* 2008, **87**(5):1219-1223.
127. Ghanim H, Abuaysheh S, Sia CL, Korzeniewski K, Chaudhuri A, Fernandez-Real JM, Dandona P: **Increase in plasma endotoxin concentrations and the expression of Toll-like receptors and suppressor of cytokine signaling-3 in mononuclear cells after a high-fat, high-carbohydrate meal: implications for insulin resistance.** *Diabetes care* 2009, **32**(12):2281-2287.
128. Nicklas W, Baneux P, Boot R, Decelle T, Deeny AA, Fumanelli M, Illgen-Wilcke B, Felasa: **Recommendations for the health monitoring of rodent and rabbit colonies in breeding and experimental units.** *Laboratory animals* 2002, **36**(1):20-42.
129. Mahler M, Berard M, Feinstein R, Gallagher A, Illgen-Wilcke B, Pritchett-Corning K, Raspa M: **FELASA recommendations for the health monitoring of mouse, rat, hamster, guinea pig and rabbit colonies in breeding and experimental units.** *Laboratory animals* 2014, **48**(3):178-192.
130. Ussing HH, Zerahn K: **Active transport of sodium as the source of electric current in the short-circuited isolated frog skin.** *Acta physiologica Scandinavica* 1951, **23**(2-3):110-127.
131. Clarke LL: **A guide to Ussing chamber studies of mouse intestine.** *American journal of physiology Gastrointestinal and liver physiology* 2009, **296**(6):G1151-1166.

132. Glicksman C, Wright M, Bell D, Fridström A: **A Fast and Robust HPLC Separation of Bile Acids, and their Conjugates, with Ascentis® Express C18.** *Reporter* 2012, **49**:3-4.
133. Steiner C, von Eckardstein A, Rentsch KM: **Quantification of the 15 major human bile acids and their precursor 7 α -hydroxy-4-cholesten-3-one in serum by liquid chromatography-tandem mass spectrometry.** *Journal of chromatography B, Analytical technologies in the biomedical and life sciences* 2010, **878**(28):2870-2880.
134. Lagkouvardos I, Klaring K, Heinzmann SS, Platz S, Scholz B, Engel KH, Schmitt-Kopplin P, Haller D, Rohn S, Skurk T *et al*: **Gut metabolites and bacterial community networks during a pilot intervention study with flaxseeds in healthy adult men.** *Molecular nutrition & food research* 2015.
135. Kless C, Muller VM, Schuppel VL, Lichtenegger M, Rychlik M, Daniel H, Klingenspor M, Haller D: **Diet-induced obesity causes metabolic impairment independent of alterations in gut barrier integrity.** *Molecular nutrition & food research* 2015, **59**(5):968-978.
136. Stenman LK, Holma R, Korpela R: **High-fat-induced intestinal permeability dysfunction associated with altered fecal bile acids.** *World journal of gastroenterology : WJG* 2012, **18**(9):923-929.
137. Lee YS, Li P, Huh JY, Hwang IJ, Lu M, Kim JI, Ham M, Talukdar S, Chen A, Lu WJ *et al*: **Inflammation is necessary for long-term but not short-term high-fat diet-induced insulin resistance.** *Diabetes* 2011, **60**(10):2474-2483.
138. Kolodziejczak D, Spanier B, Pais R, Kraiczy J, Stelzl T, Gedrich K, Scherling C, Zietek T, Daniel H: **Mice lacking the intestinal peptide transporter display reduced energy intake and a subtle maldigestion/malabsorption that protects them from diet-induced obesity.** *American journal of physiology Gastrointestinal and liver physiology* 2013, **304**(10):G897-907.
139. de Wit NJ, Bosch-Vermeulen H, de Groot PJ, Hooiveld GJ, Bromhaar MM, Jansen J, Muller M, van der Meer R: **The role of the small intestine in the development of dietary fat-induced obesity and insulin resistance in C57BL/6J mice.** *BMC medical genomics* 2008, **1**:14.
140. Baldassano S, Amato A, Cappello F, Rappa F, Mule F: **Glucagon-like peptide-2 and mouse intestinal adaptation to a high-fat diet.** *The Journal of endocrinology* 2013, **217**(1):11-20.
141. Jakobsson HE, Rodriguez-Pineiro AM, Schutte A, Ermund A, Boysen P, Bemark M, Sommer F, Backhed F, Hansson GC, Johansson ME: **The composition of the gut microbiota shapes the colon mucus barrier.** *EMBO reports* 2014.
142. Stenman LK, Holma R, Eggert A, Korpela R: **A novel mechanism for gut barrier dysfunction by dietary fat: epithelial disruption by hydrophobic bile acids.** *American journal of physiology Gastrointestinal and liver physiology* 2013, **304**(3):G227-234.
143. Psichas A, Sleeth ML, Murphy KG, Brooks L, Bewick GA, Hanyaloglu AC, Ghatei MA, Bloom SR, Frost G: **The short chain fatty acid propionate stimulates GLP-1 and PYY secretion via free fatty acid receptor 2 in rodents.** *International journal of obesity* 2015, **39**(3):424-429.
144. Carvalho BM, Guadagnini D, Tsukumo DM, Schenka AA, Latuf-Filho P, Vassallo J, Dias JC, Kubota LT, Carnevali JB, Saad MJ: **Modulation of gut microbiota by antibiotics improves insulin signalling in high-fat fed mice.** *Diabetologia* 2012, **55**(10):2823-2834.

145. Gruber L, Kisling S, Lichti P, Martin FP, May S, Klingenspor M, Lichtenegger M, Rychlik M, Haller D: **High fat diet accelerates pathogenesis of murine Crohn's disease-like ileitis independently of obesity.** *PloS one* 2013, **8**(8):e71661.
146. Stenman LK, Waget A, Garret C, Klopp P, Burcelin R, Lahtinen S: **Potential probiotic *Bifidobacterium animalis* ssp. lactis 420 prevents weight gain and glucose intolerance in diet-induced obese mice.** *Beneficial microbes* 2014, **5**(4):437-445.
147. Lam YY, Ha CW, Campbell CR, Mitchell AJ, Dinudom A, Oscarsson J, Cook DI, Hunt NH, Caterson ID, Holmes AJ *et al*: **Increased gut permeability and microbiota change associate with mesenteric fat inflammation and metabolic dysfunction in diet-induced obese mice.** *PloS one* 2012, **7**(3):e34233.
148. West DB, Boozer CN, Moody DL, Atkinson RL: **Dietary obesity in nine inbred mouse strains.** *The American journal of physiology* 1992, **262**(6 Pt 2):R1025-1032.
149. Flores CA, Cid LP, Sepulveda FV: **Strain-dependent differences in electrogenic secretion of electrolytes across mouse colon epithelium.** *Experimental physiology* 2010, **95**(6):686-698.
150. Hamilton MK, Boudry G, Lemay DG, Raybould HE: **Changes in Intestinal Barrier Function and Gut Microbiota in High-Fat Diet Fed Rats Are Dynamic and Region-Dependent.** *American journal of physiology Gastrointestinal and liver physiology* 2015:ajpgi 00029 02015.
151. Suzuki T, Hara H: **Dietary fat and bile juice, but not obesity, are responsible for the increase in small intestinal permeability induced through the suppression of tight junction protein expression in LETO and OLETF rats.** *Nutrition & metabolism* 2010, **7**:19.
152. Benoit B, Laugerette F, Plaisancie P, Geloën A, Bodennec J, Estienne M, Pineau G, Bernalier-Donadille A, Vidal H, Michalski MC: **Increasing fat content from 20 to 45 wt% in a complex diet induces lower endotoxemia in parallel with an increased number of intestinal goblet cells in mice.** *Nutrition research* 2015.
153. Progatzky F, Sangha NJ, Yoshida N, McBrien M, Cheung J, Shia A, Scott J, Marchesi JR, Lamb JR, Bugeon L *et al*: **Dietary cholesterol directly induces acute inflammasome-dependent intestinal inflammation.** *Nature communications* 2014, **5**:5864.
154. Serino M, Luche E, Gres S, Baylac A, Berge M, Cenac C, Waget A, Klopp P, Iacovoni J, Klopp C *et al*: **Metabolic adaptation to a high-fat diet is associated with a change in the gut microbiota.** *Gut* 2012, **61**(4):543-553.
155. Luche E, Cousin B, Garidou L, Serino M, Waget A, Barreau C, Andre M, Valet P, Courtney M, Casteilla L *et al*: **Metabolic endotoxemia directly increases the proliferation of adipocyte precursors at the onset of metabolic diseases through a CD14-dependent mechanism.** *Molecular metabolism* 2013, **2**(3):281-291.
156. Sagher FA, Dodge JA, Johnston CF, Shaw C, Buchanan KD, Carr KE: **Rat small intestinal morphology and tissue regulatory peptides: effects of high dietary fat.** *The British journal of nutrition* 1991, **65**(1):21-28.
157. Jin X, Zimmers TA, Zhang Z, Pierce RH, Koniaris LG: **Interleukin-6 is an important in vivo inhibitor of intestinal epithelial cell death in mice.** *Gut* 2010, **59**(2):186-196.

158. Neyrinck AM, Van Hee VF, Piront N, De Backer F, Toussaint O, Cani PD, Delzenne NM: **Wheat-derived arabinoxylan oligosaccharides with prebiotic effect increase satietogenic gut peptides and reduce metabolic endotoxemia in diet-induced obese mice.** *Nutrition & diabetes* 2012, **2**:e28.
159. Benoit B, Plaisancie P, Geloën A, Estienne M, Debard C, Meugnier E, Loizon E, Daira P, Bodennec J, Cousin O *et al*: **Pasture v. standard dairy cream in high-fat diet-fed mice: improved metabolic outcomes and stronger intestinal barrier.** *The British journal of nutrition* 2014, **112**(4):520-535.
160. Sakar Y, Duca FA, Langelier B, Devime F, Blottiere H, Delorme C, Renault P, Covasa M: **Impact of high-fat feeding on basic helix-loop-helix transcription factors controlling enteroendocrine cell differentiation.** *International journal of obesity* 2014, **38**(11):1440-1448.
161. Everard A, Geurts L, Caesar R, Van Hul M, Matamoros S, Duparc T, Denis RG, Cochez P, Pierard F, Castel J *et al*: **Intestinal epithelial MyD88 is a sensor switching host metabolism towards obesity according to nutritional status.** *Nature communications* 2014, **5**:5648.
162. de La Serre CB, Ellis CL, Lee J, Hartman AL, Rutledge JC, Raybould HE: **Propensity to high-fat diet-induced obesity in rats is associated with changes in the gut microbiota and gut inflammation.** *American journal of physiology Gastrointestinal and liver physiology* 2010, **299**(2):G440-448.
163. Marchiando AM, Shen L, Graham WV, Weber CR, Schwarz BT, Austin JR, 2nd, Raleigh DR, Guan Y, Watson AJ, Montrose MH *et al*: **Caveolin-1-dependent occludin endocytosis is required for TNF-induced tight junction regulation in vivo.** *The Journal of cell biology* 2010, **189**(1):111-126.
164. Bianchini F, Caderni G, Dolara P, Fantetti L, Kriebel D: **Effect of dietary fat, starch and cellulose on fecal bile acids in mice.** *The Journal of nutrition* 1989, **119**(11):1617-1624.
165. Hughes R, Kurth MJ, McGilligan V, McGlynn H, Rowland I: **Effect of colonic bacterial metabolites on Caco-2 cell paracellular permeability in vitro.** *Nutrition and cancer* 2008, **60**(2):259-266.
166. Munch A, Strom M, Soderholm JD: **Dihydroxy bile acids increase mucosal permeability and bacterial uptake in human colon biopsies.** *Scandinavian journal of gastroenterology* 2007, **42**(10):1167-1174.
167. Stenman LK, Holma R, Gylling H, Korpela R: **Genetically obese mice do not show increased gut permeability or faecal bile acid hydrophobicity.** *The British journal of nutrition* 2013, **110**(6):1157-1164.
168. Greenwood J, Adu J, Davey AJ, Abbott NJ, Bradbury MW: **The effect of bile salts on the permeability and ultrastructure of the perfused, energy-depleted, rat blood-brain barrier.** *Journal of cerebral blood flow and metabolism : official journal of the International Society of Cerebral Blood Flow and Metabolism* 1991, **11**(4):644-654.
169. Raimondi F, Santoro P, Barone MV, Pappacoda S, Barretta ML, Nanayakkara M, Apicella C, Capasso L, Paludetto R: **Bile acids modulate tight junction structure and barrier function of Caco-2 monolayers via EGFR activation.** *American journal of physiology Gastrointestinal and liver physiology* 2008, **294**(4):G906-913.
170. Everard A, Belzer C, Geurts L, Ouwerkerk JP, Druart C, Bindels LB, Guiot Y, Derrien M, Muccioli GG, Delzenne NM *et al*: **Cross-talk between Akkermansia muciniphila and intestinal epithelium controls diet-induced obesity.** *Proceedings of the National Academy of Sciences of the United States of America* 2013, **110**(22):9066-9071.

171. Buffie CG, Bucci V, Stein RR, McKenney PT, Ling L, Gobourne A, No D, Liu H, Kinnebrew M, Viale A *et al*: **Precision microbiome reconstitution restores bile acid mediated resistance to *Clostridium difficile***. *Nature* 2015, **517**(7533):205-208.
172. Pfeiffer N, Desmarchelier C, Blaut M, Daniel H, Haller D, Clavel T: **Acetatifactor muris gen. nov., sp. nov., a novel bacterium isolated from the intestine of an obese mouse**. *Archives of microbiology* 2012, **194**(11):901-907.
173. Johansson ME, Gustafsson JK, Holmen-Larsson J, Jabbar KS, Xia L, Xu H, Ghishan FK, Carvalho FA, Gewirtz AT, Sjovall H *et al*: **Bacteria penetrate the normally impenetrable inner colon mucus layer in both murine colitis models and patients with ulcerative colitis**. *Gut* 2014, **63**(2):281-291.
174. Mastrodonato M, Mentino D, Portincasa P, Calamita G, Liquori GE, Ferri D: **High-fat diet alters the oligosaccharide chains of colon mucins in mice**. *Histochemistry and cell biology* 2014, **142**(4):449-459.
175. Jia L, Betters JL, Yu L: **Niemann-pick C1-like 1 (NPC1L1) protein in intestinal and hepatic cholesterol transport**. *Annual review of physiology* 2011, **73**:239-259.
176. Huang X, Yang C, Luo Y, Jin C, Wang F, McKeenan WL: **FGFR4 prevents hyperlipidemia and insulin resistance but underlies high-fat diet induced fatty liver**. *Diabetes* 2007, **56**(10):2501-2510.
177. Henkel AS, Anderson KA, Dewey AM, Kavesh MH, Green RM: **A chronic high-cholesterol diet paradoxically suppresses hepatic CYP7A1 expression in FVB/NJ mice**. *Journal of lipid research* 2011, **52**(2):289-298.
178. Goodwin B, Jones SA, Price RR, Watson MA, McKee DD, Moore LB, Galardi C, Wilson JG, Lewis MC, Roth ME *et al*: **A regulatory cascade of the nuclear receptors FXR, SHP-1, and LXR-1 represses bile acid biosynthesis**. *Molecular cell* 2000, **6**(3):517-526.
179. Lehmann JM, Kliewer SA, Moore LB, Smith-Oliver TA, Oliver BB, Su JL, Sundseth SS, Winegar DA, Blanchard DE, Spencer TA *et al*: **Activation of the nuclear receptor LXR by oxysterols defines a new hormone response pathway**. *The Journal of biological chemistry* 1997, **272**(6):3137-3140.
180. Kerr TA, Saeki S, Schneider M, Schaefer K, Berdy S, Redder T, Shan B, Russell DW, Schwarz M: **Loss of nuclear receptor SHP impairs but does not eliminate negative feedback regulation of bile acid synthesis**. *Developmental cell* 2002, **2**(6):713-720.
181. Fang Q, Li H, Song Q, Yang W, Hou X, Ma X, Lu J, Xu A, Jia W: **Serum fibroblast growth factor 19 levels are decreased in Chinese subjects with impaired fasting glucose and inversely associated with fasting plasma glucose levels**. *Diabetes care* 2013, **36**(9):2810-2814.
182. Barutcuoglu B, Basol G, Cakir Y, Cetinkalp S, Parildar Z, Kabaroglu C, Ozmen D, Mutaf I, Bayindir O: **Fibroblast growth factor-19 levels in type 2 diabetic patients with metabolic syndrome**. *Annals of clinical and laboratory science* 2011, **41**(4):390-396.
183. Fu L, John LM, Adams SH, Yu XX, Tomlinson E, Renz M, Williams PM, Soriano R, Corpuz R, Moffat B *et al*: **Fibroblast growth factor 19 increases metabolic rate and reverses dietary and leptin-deficient diabetes**. *Endocrinology* 2004, **145**(6):2594-2603.
184. Winzell MS, Ahren B: **The high-fat diet-fed mouse: a model for studying mechanisms and treatment of impaired glucose tolerance and type 2 diabetes**. *Diabetes* 2004, **53** Suppl 3:S215-219.

185. Alssema M, Rijkeljkhuizen JM, Holst JJ, Teerlink T, Scheffer PG, Eekhoff EM, Gastaldelli A, Mari A, Hart LM, Nijpels G *et al*: **Preserved GLP-1 and exaggerated GIP secretion in type 2 diabetes and relationships with triglycerides and ALT.** *European journal of endocrinology / European Federation of Endocrine Societies* 2013, **169**(4):421-430.
186. Brons C, Jensen CB, Storgaard H, Hiscock NJ, White A, Appel JS, Jacobsen S, Nilsson E, Larsen CM, Astrup A *et al*: **Impact of short-term high-fat feeding on glucose and insulin metabolism in young healthy men.** *The Journal of physiology* 2009, **587**(Pt 10):2387-2397.
187. Nauck MA, Baller B, Meier JJ: **Gastric inhibitory polypeptide and glucagon-like peptide-1 in the pathogenesis of type 2 diabetes.** *Diabetes* 2004, **53 Suppl 3**:S190-196.
188. Nauck MA, Vardarli I, Deacon CF, Holst JJ, Meier JJ: **Secretion of glucagon-like peptide-1 (GLP-1) in type 2 diabetes: what is up, what is down?** *Diabetologia* 2011, **54**(1):10-18.
189. Wadden D, Cahill F, Amini P, Randell E, Vasdev S, Yi Y, Church J, Sun G: **Circulating glucagon-like peptide-1 increases in response to short-term overfeeding in men.** *Nutrition & metabolism* 2013, **10**(1):33.
190. Nakajima S, Hira T, Hara H: **Postprandial glucagon-like peptide-1 secretion is increased during the progression of glucose intolerance and obesity in high-fat/high-sucrose diet-fed rats.** *The British journal of nutrition* 2015:1-12.
191. Drucker DJ, Nauck MA: **The incretin system: glucagon-like peptide-1 receptor agonists and dipeptidyl peptidase-4 inhibitors in type 2 diabetes.** *Lancet* 2006, **368**(9548):1696-1705.
192. Topping DL, Clifton PM: **Short-chain fatty acids and human colonic function: roles of resistant starch and nonstarch polysaccharides.** *Physiological reviews* 2001, **81**(3):1031-1064.
193. Le Poul E, Loison C, Struyf S, Springael JY, Lannoy V, Decobecq ME, Brezillon S, Dupriez V, Vassart G, Van Damme J *et al*: **Functional characterization of human receptors for short chain fatty acids and their role in polymorphonuclear cell activation.** *The Journal of biological chemistry* 2003, **278**(28):25481-25489.
194. Ichimura A, Hasegawa S, Kasubuchi M, Kimura I: **Free fatty acid receptors as therapeutic targets for the treatment of diabetes.** *Frontiers in pharmacology* 2014, **5**:236.
195. Tang C, Ahmed K, Gille A, Lu S, Grone HJ, Tunaru S, Offermanns S: **Loss of FFA2 and FFA3 increases insulin secretion and improves glucose tolerance in type 2 diabetes.** *Nature medicine* 2015, **21**(2):173-177.
196. Katsuma S, Hirasawa A, Tsujimoto G: **Bile acids promote glucagon-like peptide-1 secretion through TGR5 in a murine enteroendocrine cell line STC-1.** *Biochemical and biophysical research communications* 2005, **329**(1):386-390.
197. Adrian TE, Ballantyne GH, Longo WE, Bilchik AJ, Graham S, Basson MD, Tierney RP, Modlin IM: **Deoxycholate is an important releaser of peptide YY and enteroglucagon from the human colon.** *Gut* 1993, **34**(9):1219-1224.
198. Wu T, Bound MJ, Standfield SD, Jones KL, Horowitz M, Rayner CK: **Effects of taurocholic acid on glycemic, glucagon-like peptide-1, and insulin responses to small intestinal glucose infusion in healthy humans.** *The Journal of clinical endocrinology and metabolism* 2013, **98**(4):E718-722.

199. Carey MC: **Bile acids and bile salts: ionization and solubility properties.** *Hepatology* 1984, **4**(5 Suppl):66S-71S.
200. Richards P, Pais R, Habib AM, Brighton CA, Yeo GS, Reimann F, Gribble FM: **High fat diet impairs the function of glucagon-like peptide-1 producing L-cells.** *Peptides* 2015.
201. Goddard AD, Watts A: **Regulation of G protein-coupled receptors by palmitoylation and cholesterol.** *BMC biology* 2012, **10**:27.
202. Adrian TE, Gariballa S, Parekh KA, Thomas SA, Saadi H, Al Kaabi J, Nagelkerke N, Gedulin B, Young AA: **Rectal taurocholate increases L cell and insulin secretion, and decreases blood glucose and food intake in obese type 2 diabetic volunteers.** *Diabetologia* 2012, **55**(9):2343-2347.
203. Sonne DP, Hansen M, Knop FK: **Bile acid sequestrants in type 2 diabetes: potential effects on GLP1 secretion.** *European journal of endocrinology / European Federation of Endocrine Societies* 2014, **171**(2):R47-65.
204. Harach T, Pols TW, Nomura M, Maida A, Watanabe M, Auwerx J, Schoonjans K: **TGR5 potentiates GLP-1 secretion in response to anionic exchange resins.** *Scientific reports* 2012, **2**:430.
205. Suzuki T, Oba K, Igari Y, Matsumura N, Watanabe K, Futami-Suda S, Yasuoka H, Ouchi M, Suzuki K, Kigawa Y *et al*: **Colestimide lowers plasma glucose levels and increases plasma glucagon-like PEPTIDE-1 (7-36) levels in patients with type 2 diabetes mellitus complicated by hypercholesterolemia.** *Journal of Nippon Medical School = Nippon Ika Daigaku zasshi* 2007, **74**(5):338-343.
206. Beyesen C, Murphy EJ, Deines K, Chan M, Tsang E, Glass A, Turner SM, Protasio J, Riiff T, Hellerstein MK: **Effect of bile acid sequestrants on glucose metabolism, hepatic de novo lipogenesis, and cholesterol and bile acid kinetics in type 2 diabetes: a randomised controlled study.** *Diabetologia* 2012, **55**(2):432-442.
207. Marina AL, Utzschneider KM, Wright LA, Montgomery BK, Marcovina SM, Kahn SE: **Colesevelam improves oral but not intravenous glucose tolerance by a mechanism independent of insulin sensitivity and beta-cell function.** *Diabetes care* 2012, **35**(5):1119-1125.
208. Schwartz SL, Lai YL, Xu J, Abby SL, Misir S, Jones MR, Nagendran S: **The effect of colesevelam hydrochloride on insulin sensitivity and secretion in patients with type 2 diabetes: a pilot study.** *Metabolic syndrome and related disorders* 2010, **8**(2):179-188.
209. Sakanaka T, Inoue T, Yorifuji N, Iguchi M, Fujiwara K, Narabayashi K, Kakimoto K, Nouda S, Okada T, Kuramoto T *et al*: **The effects of a TGR5 agonist and a dipeptidyl peptidase IV inhibitor on dextran sulfate sodium-induced colitis in mice.** *Journal of gastroenterology and hepatology* 2015, **30** Suppl 1:60-65.
210. Cipriani S, Mencarelli A, Chini MG, Distrutti E, Renga B, Bifulco G, Baldelli F, Donini A, Fiorucci S: **The bile acid receptor GPBAR-1 (TGR5) modulates integrity of intestinal barrier and immune response to experimental colitis.** *PloS one* 2011, **6**(10):e25637.

6.4 List of publications

Kless C, Müller VM, Schüppel VL, Lichtenegger M, Rychlik M, Daniel H, Klingenspor M, Haller D., Diet-induced obesity causes metabolic impairment independent of alterations in gut barrier integrity. *Molecular nutrition & food research* 2015, 59(5):968-978.

Müller VM, Zietek T, Rohm F, Fiamoncini J, Lagkouvardos I, Haller D, Clavel T, Daniel H: Gut barrier impairment by high-fat diet in mice depends on housing conditions. *Molecular nutrition & food research* 2015. DOI 10.1002/mnfr.201500775.